Analysis of FOXC1 Function During Somite Formation and Chondrogenesis of the Axial Skeleton

by

Rotem Lavy

A thesis submitted in partial fulfillment of the requirements for the degree of

Doctorate in Philosophy

in

Experimental Surgery

Department of Surgery
University of Alberta

ABSTRACT

Development of the axial skeleton in vertebrates begins with the segmentation of the paraxial mesoderm into somites. Somites are transient structures in the embryos that ultimately give rise to the skeletal muscle, dermis, tendons, cartilage, and bony structures of the axial skeleton. Once somite-derived sclerotome migrates to the appropriate position within the embryo body, it undergoes chondrogenesis and ossification, giving rise to the ribs and vertebrae through endochondral ossification. Defects in the formation of the somites or the generation or ossification of the cartilage template of the skeleton can lead to abnormal skeletal development. While the molecular mechanisms driving somitogenesis and skeletal development and differentiation have been extensively studied much is still unknown.

FOXC1 is a forkhead box transcription factor with an essential role in skeletal development. *Foxc1* is expressed in the mesodermal tissues giving rise to the axial skeleton. Disruptions in *Foxc1* are associated with abnormalities in somitogenesis as well as in the formation of the ribs, vertebrae, long bones, and bones of the skull vault. Here I assess the role of FOXC1 in somitogenesis and chondrogenesis, two of the critical developmental process crucial for proper formation of the axial skeleton.

Loss of *foxc1a* function in zebrafish results in reduced expression of *mesp-ba* and a lack of formation of the anterior somites. The transcription factor *mesp-ba* has an important role in determining somite boundary formation. The expression of

mesp-ba in the presomitic mesoderm is regulated by the *ripply1-tbx6* negative feedback network. I examined how *foxc1a* interacts with the *ripply1-tbx6* network to regulate the expression of *mesp-ba* in the presomitic mesoderm and anterior somite formation. The results herein demonstrate that *foxc1a* interacts with the *ripply1-tbx6* regulatory network to regulate the expression gradient of *raldh2*, a member of the retinoic acid signaling network. The interaction between the opposing gradients of *raldh2* and *fgf8a* in the presomitic mesoderm is critical for somite boundary formation and the expression of *mesp-ba*. When Foxc1a is absent establishment of these gradients is disrupted resulting in reduced *mesp-ba* expression. Anterior somite formation is more sensitive to fluctuations in retinoic acid expression, and they are therefore more severely affected in the *foxc1a* morphants.

Chondrogenic differentiation is highly dependent on the expression of *Sox9*, a SRY-related transcription factor. Using published ChIP-Seq data I have identified a *Foxc1* enhancer region responsive to SOX9 activation. I have also demonstrated that FOXC1 overexpression in the initial stages of chondrogenesis leads to acceleration of the chondrogenic differentiation and elevation of chondrogenic marker expression. Finally, I have shown that while FOXC1 and SOX9 do not appear to be physically interacting with one another, they do come in close vicinity, suggesting they have cooperative function regulating downstream targets in chondrogenesis and endochondral bone formation.

My results demonstrate that FOXC1 has a crucial role in correct development of the axial skeleton and that it is directly involved in the regulation of many processes during skeletal growth. These observations shed some light on the complexities and tight regulation involving embryonic development and help gain better understanding of the role that FOXC1 plays in many of these events.

This thesis is an original work by Rotem Lavy. The research project, of which this thesis is a part, received research ethics approval from the University of Alberta Research Ethics Board, No. AUP00000077. No part of this thesis has been previously published.

מוקדש באהבה לסבא צבי, שתמיד אמר לי "ילדתי, אף פעם אל תפסיקי ללמוד"

ACKNOWLEDGEMENTS

My years in the doctorate program at the Department of Surgery have had many ups and downs, successes and failures, happy dances and frustrations. I would not have made it through without help and support from many people - in the lab, at the university, and at home. I would like to offer my sincere gratitude to the following people:

First and foremost, to my supervisor, Dr. Fred Berry, for giving me the opportunity and the support I needed to learn, practice and grow under his supervision. I came in to the lab as a young graduate student and I am leaving as a capable scientist. Thank you.

To our beloved lab technician, Freda Mirzayans. Freda's patience, guidance, technical proficiency, and the much-needed occasional hug helped me in more ways than I could ever express. Freda was essentially my lab-momma, happy to assist whenever I needed her. I am so lucky to have had Freda's help in the first confusing years of my graduate school adventure.

To my graduate committee members – Dr. Ted Allison and Dr. Alan Underhill. Thank you for the guidance, the feedback, for helping me steer my research in the right directions, and for always being available to answer my questions or give words of encouragement.

To all members of the Allison lab, especially Michele DuVal, Phil Oel, Trish Leighton and Richard Kanyo – for all your help, for letting me rant endlessly, for the beers and friendship.

To Drs. Ordan Lehmann and Paul Chrystal for letting me play with your zebrafish mutants, and to Drs. David Eisenstat, Andrew Waskiewicz and Sarah Hughes for allowing me to use your lab equipment.

To my lab-sister, Dr. Leiah Luoma. I am extremely grateful for all the help, for finishing my experiments when I couldn't, for putting up with my good days and bad, the cheers and the tears, for the beers, fries and dips, and constant friendship. I would not have survived this without you.

To my extended family, who have always supported me in every way they could. Saba Yonatan, Aviram & Tova, and everyone else, I never would have made it this far without you.

To all of my wonderful, amazing friends, and especially Sarah and Catherine. For always being there at the drop of a hat with a bottle of wine and pizza, for the dances, the laughs, the hugs, the cries, the weekends away, the long walks, the love and support.

To Roman. You are my rock, my Trekkie monster, my shoulder to lean on. I am incredibly lucky to have you in my life. Thank you for all that you are.

Most importantly – to my family. I owe them everything I have, everything I am, everything I have become. I have always known that I can succeed in anything I put my heart into, and that if I fall it will be a soft landing. You are the best parents, the best siblings, the best *friends* I could have ever wished for. I love you so, so much.

TABLE OF CONTENTS

LIST OF TABLES

LIST OF FIGURES

LIST OF SYMBOLS AND ABBREVIATIONS

°C	degrees Celsius
AD	activation domain
aei	after eight
ANOVA	a factorial analysis of variance
AP	alkaline phosphatase
ARS	Axenfeld-Rieger Syndrome
BCIP	5-bromo-4-chloro-3’-indolyphsohate p-toluidine salt
bHLH	basic helix loop helix
BMP	bone morphogenetic protein
BS	binding site
BSA	bovine serum albumin
C-terminal	carboxyl terminal
$CaCl_2$	calcium chloride
cAMP	cyclic adenosine monophosphate
CD	campomelic dysplasia
cDNA	complementary DNA
ChIP	chromatin immunoprecipitation
CNS	central nervous system
CO_2	carbon dioxide

Col	collagen
CRISPR	clustered regulatory interspaced short palindromic repeats
CS	chondroitin sulfate
Cy3	cyanine 3
DAPI	4',6'-diamidine-2-phenylindole
DBD	DNA binding domain
ddH_2O	double distilled water
des	deadly seven
DIG	digoxigenin
Dll	drosophila distal-less, transcription factor
DMEM	Dulbecco's modified Eagle's medium
dMO	double morpholino
DNA	deoxyribonucleic acid
dpc	days post coitum
DTT	dithiothreitol
E	embryonic age
E. coli	*Escherichia coli*
EB	embryoid body
ECM	extracellular matrix
EDTA	ethylenediaminetetraacetic acid

EMSA	electrophoretic mobility shift assay
EMT	epithelial to mesenchymal transition
Eph	ephrin
ES	embryonic stem
ESC	embryonic stem cells
EtBr	ethidium bromide
EtOH	ethanol
EV	Empty vector
FBS	fetal bovine serum
FGF	fibroblast growth factor
FHD	Forkhead domain
FIMO	Find individual motif occurrences
FLR	fluorescein
FOX	Forkhead box
FOXC1	Forkhead Box C1
FOXC2	Forkhead Box C2
GAPDH	glyceraldehyde 3-phosphate dehydrogenase
gBlock	genomic block
gDNA	genomic DNA
GFP	green fluorescent protein

Gli	glioma associated, transcription factor
h	hour
H1, H2, H3, H4	helix 1, 2, 3, or 4
H_2O	Water
H3K4me2	di-methylation of histone 3 lysine 4
HCl	hydrochloric acid
HDAC4	histone deacetylase 4
HES1	hairy and enhancer of split transcription factor 1
HES7	hairy and enhancer of split transcription factor 7
HEY1	Hairy/enhancer-of-split related with YRPW motif protein 1
HEY5	Hairy/enhancer-of-split related with YRPW motif protein 5
HMG	high mobility group
HPF	hours post fertilization
HPRT	Hypoxanthine Phosphoribosyltransferase
HRM	high resolution melt analysis
HS	homosapien
ID	inhibitory domain
IgG	immunoglobulin G
IHH	indian hedgehog, transcription factor
KCl	potassium chloride

LD	lymphedema distichiasis
Lfng	lunatic fringe
LiCl	lithium chloride
Lif	leukemia inhibitory factor
MAPK	mitogen activated protein kinase
MESP2	Mesoderm posterior protein 2
MET	mesenchymal to epithelial transition
$MgSO_4$	magnesium sulfate
MMP13	metalloproteinase 13
MO	morpholino
mRNA	messenger RNA
MS222	tricaine methanesultonate
MSB	modified sample buffer
MSCs	mesenchymal stem cells
MSX	Msh homeobox, transcription factor
N-CAM	neural cell adhesion molecule
N-terminal	amino-terminal
Na_2EDTA	disodium ethylenediaminetetraacetate
Na_2HPO_4	sodium phosphate
NaCl	sodium chloride

NaOH	sodium hydroxide
NBT	nitro-blue tetrazolium chloride
NEB	New England biolabs
NLS	nuclear localization signal
O_2	oxygen
Osx	osterix
Pax	paired box, transcription factor
PBS	phosphate buffered saline
PBST	phosphate buffered saline + 0.1% Tween 20
PCR	polymerase chain reaction
PFA	paraformaldehyde
PIC	protease inhibitor cocktail
PITX2	paired-like homeodomain transcription factor 2
PMSF	phenylmethanesulfonyl fluoride
PORD	progressive oscillatory reaction-diffusion
PSM	presomitic mesoderm
PTHrP	parathyroid hormone related protein
PTU	phenylthiourea
PWM	position weight matrix
qPCR	quantitative polymerase chain reaction

RA	retinoic acid
RNA	ribonucleic acid
RPM	revolutions per minute
RT	reverse transcription
Runx2	runt-related transcription factor 2
S1, S2, S3	β-strand 1, 2, or 3
SDS	sodium dodecyl sulphate
SDS-PAGE	sodium dodecyl sulfate polyacrylamide gel electrophoresis
sGAG	sulfated glycosaminoglycan
SOX	Sry-related HMG-box, transcription factor
TBX	T-box, transcription factor
TC	tissue culture
TGF-β	transforming growth factor β
Uncx	UNC homeobox, transcription factor
UTR	untranslated region
UV	ultraviolet
VT	vestigial tail
W1, W2	wing 1, wing 2
WB	western blot
WT	wild type

CHAPTER 1. INTRODUCTION

The vertebrate skeleton is composed of cartilage and bone and is derived from three different cell lineages: neural crest cells, paraxial mesoderm, and lateral plate mesoderm (Bronner-Fraser, 1994; Cohn and Tickle, 1996; Noden, 1991; Tam and Trainor, 1994). The development of these tissues begins as mesenchymal cells form condensations which later differentiate into chondrocytes or osteoblasts, giving rise to cartilage and bone (Hall and Miyake, 1992). The developmental process leading from the condensation of mesenchymal tissue to the formation of a fully formed skeletal structure is complex and includes many stages of differentiation. Anomalies in any of these highly regulated processes can lead to potentially debilitating defects in the formation of the craniofacial, axial or limb skeleton. Skeletal deformities can be congenital or acquired and can result from genetic or environmental causes or trauma (Ingalls and Curley, 1957; Murakami et al., 1963; O'Rahilly et al., 1980). Among these malformations are conditions such as scoliosis, arthritis, cancers of the blood and/or bone and fractures (Rawls, 2009). Congenital skeletal defects include abnormally shaped or fused ribs and vertebrae, scoliosis and dysostosis (axial); cleft lip and/or palate, abnormal jaw formation and defective formation of the skull vault (craniofacial); supernumerary or missing digits, incomplete, disproportional or missing limbs or dwarfism (limb) (Olsen et al., 2000; Rawls, 2009). The biological events leading to formation of the skeleton involve many finely tuned processes and developmental pathways. Defects can

arise in any stage of development and have significant effects on the health and quality of life of the individual. While many of the processes and genetic pathways regulating the formation of the skeleton have been studied extensively, much is still unknown. In the work presented here, I explore the role of the transcription factor FOXC1 in the development of the axial skeleton and long bones.

Development of the axial skeleton begins with the segmentation of the paraxial mesoderm into somites. The somites contain the precursors to the ribs, vertebrae and intervertebral disks. Proper formation of the somites is therefore vital for subsequent development. The ossification of the bony elements of the axial skeleton proceeds primarily through endochondral ossification via an intermediate cartilage template. Mutations in *Foxc1* in mouse and zebrafish animal models can lead to defects in the formation of the somites (Hsu et al., 2015; Kume et al., 1998; Kume et al., 2001; Li et al., 2015; Sun et al., 2013; Topczewska et al., 2001a), as well as abnormalities in the formation of the cartilage template that gives rise to the endochondral bones (Hsu et al., 2015; Kume et al., 2001; Li et al., 2015; Sun et al., 2013; Topczewska et al., 2001a; Winnier et al., 1997; Yoshida et al., 2015).

SOMITOGENESIS

The axial skeleton consists of the bones of the skull, ribs, and vertebrae as well as the intervertebral disks. In humans, the hyoid bone and ear ossicles are also considered part of the axial skeleton. The vertebral column fulfills three main, essential functions: it protects the spinal cord and the spinal nerves, it supports the weight of the body and it provides a flexible axis for the movement of the head and the torso. The spinal column is capable of extension, flexion, lateral flexion and rotation (Rawls, 2009). It consists of four regions, forming four curvatures: the cervical curvature, the thoracic curvature, the lumbar curvature and the sacrococcygeal curvature. The thoracic and sacrococcygeal curvatures develop during gestation while the cervical and lumbar curvatures develop in infancy. The cervical curvature develops when the newborn begins to hold its head upright and the lumbar curvature develops when it begins to sit upright and walk (Rawls, 2009).

Development of the axial skeleton begins with the formation of the paraxial mesoderm, occurring when cells of the epiblast migrate through the primitive streak during gastrulation and differentiate into mesodermal cells. Later, as the primitive streak undergoes differentiation with the closure of the neural tube, a progenitor cell population situated at the tailbud - the posterior-most end of the embryo - differentiates into the mesoderm of the posterior presomitic mesoderm (PSM) (Tam and Tan, 1992). Premature exhaustion or ablation of this progenitor pool leads to embryo truncation (Goldman et al., 2000). It is unclear how the switch from gastrulation formation of the PSM to its generation from tailbud progenitors is

regulated at the genetic level.

While the PSM is continuously formed, the cells in its rostral end segment into repeating units known as somites. Somitogenesis is the reiterated process by which the paraxial mesoderm subdivides into paired, epithelial spheres of cells (somitocoels) on either side of the neural tube (Figure 1.1). It is the earliest developmental segmentation event and is a feature shared by all vertebrate embryos (Giampietro et al., 2009; Sawada et al., 2001). In mammals, the somites contain the precursors to four cell lineages and eventually contribute to the (1) sclerotome-derived vertebrae and ribs, (2) myotome derived skeletal muscle, (3) dermomyotome derived dermis and skeletal muscles of the back, and (4) syndetome derived tendons (Brand-Saberi et al., 1996; Brent et al., 2003; Dubrulle and Pourquie, 2003; Kato and Aoyama, 1998; Ordahl and Le Douarin, 1992). There are four processes fundamental to somite formation: (1) an oscillating clock controlling the timing of somitogenesis, (2) positional identity of the somites (rostral/caudal, dorsal/ventral), (3) the formation of intersomitic boundaries, and (4) mesenchymal to epithelial transition (Figure 1.1A, B). Disruption to any of these processes or to subsequent somite resegmentation can result in malformations of the vertebral column. The progression of somite formation, boundary determination and positional identity definition and maintenance are tightly regulated by many regulatory pathways, including the NOTCH, WNT, and FGF signaling pathways (Biris et al., 2007; Campanelli and Gedeon, 2010; Cinquin, 2007; Kawamura et al., 2005; Morimoto et al., 2007; Rawls, 2009). While the roles of many of the genes and

pathways involved in somitogenesis have been established and analyzed thoroughly, the roles of others are still poorly understood.

Figure 1.1 Schematic Representation of Somitogenesis and Resegmentation

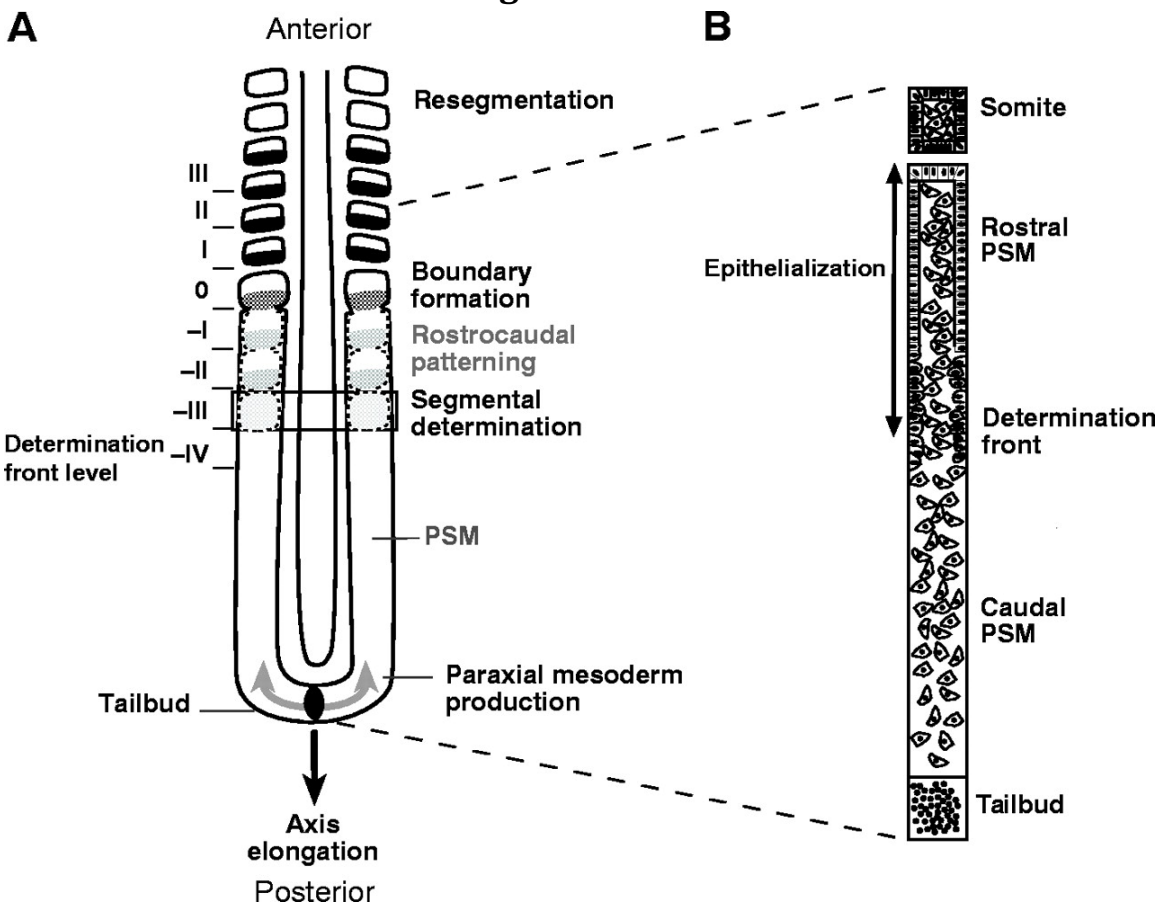

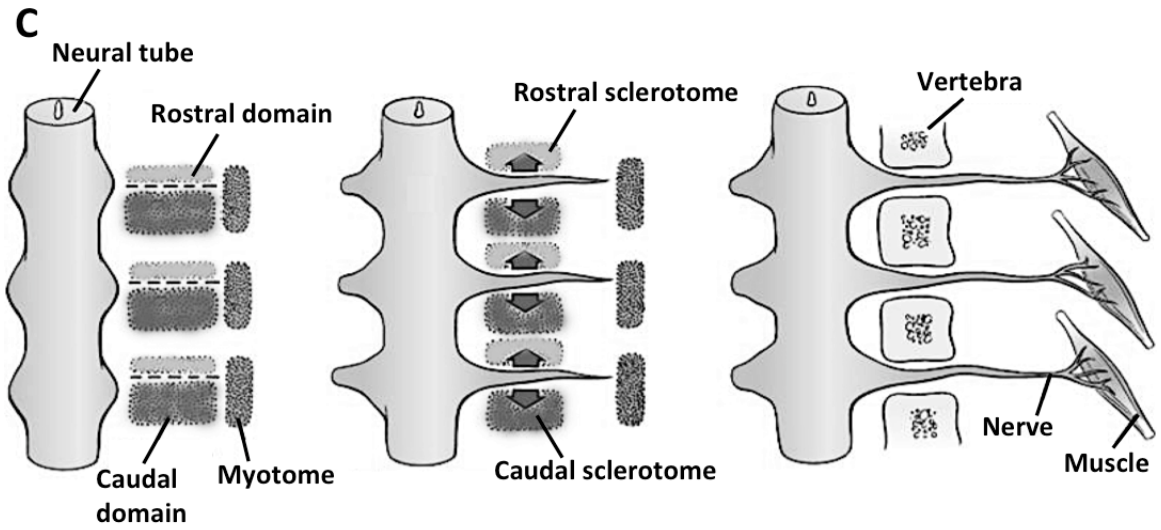

Figure 1.1 Schematic Representation of Somite Formation and Resegmentation. Mesenchymal progenitor cells originating in the tailbud differentiate into presomitic mesodermal cells as the embryo elongates along the anterior-posterior axis. Waves of gene expression sweep through the PSM anteriorly until they reach the boundary determination front in the pre-patterned anterior PSM and form an intersomitic boundary **(A)** Ventral view. **(B)** Parasagittal view. **(C)** Resegmentation. The rostral domain of one somite, together with the caudal domain of the immediately preceding somite, give rise to one vertebral body. Spatial cues also guide the branching of the peripheral nerves and formation of trunk muscles. The currently forming somite is designated S0. Segmented somites are numbered SI, SII, etc. starting with the newest fully segmented somite. The unsegmented PSM is divided into prospective somites beginning with S-I, S-II, and so on (Ordahl, 1993; Pourquie and Tam, 2001). Figure adapted from (Dubrulle and Pourquie, 2004a) and (Schoenwolf and Larsen, 2009).

The Oscillating Clock

A clock and wavefront segmentation model was proposed by Cooke and Zeeman in 1976 to regulate the timing of somite segmentation and the size of the formed somites (Cooke and Zeeman, 1976). According to this model, a wave of gene expression originates at the posterior end of the PSM and proceeds anteriorly. Once the wave of expression reaches the anterior end of the PSM a new somite buds off. The oscillating wave of gene expression 'switches' cells of the PSM into a susceptible mode for somite formation. Since it was first proposed, there has been accumulating experimental evidence supporting the idea that vertebral segmentation involves a molecular oscillator which triggers the cyclic activation of the NOTCH, WNT and FGF signaling pathways, as well as other genes (Cooke and Zeeman, 1976; Oginuma et al., 2008; Rawls, 2009; Sawada et al., 2001). More recent evidence suggests that the oscillator controls the ability of the cells in the PSM to respond to external signals that regulate the mesenchymal-to-epithelial transition of the PSM cells (Goldbeter et al., 2007). However, regulation of these molecular oscillations is still not entirely understood. The three main mechanisms that have been brought forth as controlling the generation of oscillations are the Notch pathway and lunatic fringe (*Lfng*), *Hes*/*Her* autorepression, and *Axin2* and the *Wnt* pathway.

The Notch pathway appears to have a central role in driving the oscillation in the PSM. The glycosyltransferase *Lunatic fringe* (*Lfng*) and the basic helix-loop-helix genes *Hes1, Hes7, Hey5, and Hey1* have all been identified as having cyclical

expression in the PSM (Aulehla and Johnson, 1999; Bessho et al., 2001; Forsberg et al., 1998; Leimeister et al., 2000; McGrew et al., 1998; Palmeirim et al., 1997). A key component of the oscillating machinery is *Hes7*. *Hes7* regulates its own expression and that of *Lfng* through a negative feedback loop, thus establishing the oscillating wave sweeping through the PSM (Bessho et al., 2003). Loss of regulation in either *Lfng* or *Hes7* leads to ubiquitous Notch activation in the PSM and severe vertebral malformations (Morales et al., 2002; Shifley et al., 2008). Interestingly, the vertebral defects observed in the *Lfng*-null mouse model appear to be restricted to the posterior somites while the anterior ones form normally (Shifley et al., 2008), suggesting that somitogenesis regulation is different in the anterior vs. posterior PSM.

Another pathway involved in oscillatory regulation of the PSM is the Wnt signaling pathway. The expression of *Axin2*, a negative regulator of the Wnt pathway, oscillates in the mouse PSM (Aulehla et al., 2003). Additionally, in a mouse model with a hypomorphic form of *Wnt3a, vestigial tail* (*vt*), the oscillation of *Lfng* and *Axin2* are disrupted, suggesting that the Wnt pathway is involved in the regulation of both signaling pathways (Aulehla et al., 2003).

Positional Identity

Strict temporal and spatial regulation of gene expression is paramount during somitogenesis and determines the metamerism of all somite-derived tissues. Even before the morphological somites are formed, their rostral-caudal domains are

predetermined in the unsegmented PSM (Figures 1.1A, 1.2A). Once the somites have formed, the positional identity within each somite is retained and continues to define those rostral and caudal domains (Figure 1.2A) (Aoyama and Asamoto, 1988). Loss of spatial properties prior to segmentation or within the somites leads to defects in resegmentation (see below) and can result in multiple skeletal disorders such as fused vertebrae, fused ribs, incomplete formation of the vertebrae, as well as anomalies in the segmental pattern of peripheral nerves (Sawada et al., 2001). The Notch pathway is crucial for the determination of spatial identity. Disruptions in *Notch1*, *Dll1* and *Dll3*, or *Presenilin-1* can result in loss of specific spatial gene expression (Figure 1.2A) (Barrantes et al., 1999; Conlon et al., 1995; de la Pompa et al., 1997; Dunwoodie et al., 2002; Hrabe de Angelis et al., 1997; Koizumi et al., 2001; Kusumi et al., 1998; Oka et al., 1995; Rawls, 2009; Saga and Takeda, 2001; Schuster-Gossler et al., 2009; Swiatek et al., 1994). Additionally, the expression of *Mesp2*, which is transcribed broadly in the presumptive somite -1 and becomes restricted to the rostral domain of somite 0 (Figure 1.2A), is critical for maintenance of the spatial identity in the rostral domain of the somites. Mesp2 has been shown to activate the expression of the rostral markers *Epha4* and *Lfng* and to suppress the expression of the caudal markers *Dll1* and *Uncx4.1* in the rostral domain of the presumptive somite, promoting positional identity within the somite (Morimoto et al., 2007; Saga et al., 1997; Saga and Takahashi, 2008; Takahashi et al., 2000; Yasuhiko et al., 2006).

Boundary Formation

Formation of morphological intersomitic boundaries occurs as somitic cells pull apart from the adjacent PSM. It is an intrinsic activity of the PSM and it occurs in explants in the absence of the adjacent endoderm (Cinquin, 2007; Palmeirim et al., 1998; Saga and Takeda, 2001). The process of boundary formation varies in different species. In *Xenopus* and zebrafish, intersomitic boundaries are formed through simple cleavage fissures whereas in chicks and mice it involves a more dynamic reshuffling of cells (Henry et al., 2000; Kulesa and Fraser, 2002; Kulesa et al., 2007; Wood and Thorogood, 1994). Intersomitic boundaries are formed when the waves of gene expression originated by the oscillator in the tailbud reach a boundary determination front in the anterior PSM (Figure 1.1A) (Sawada et al., 2001). PSM cells can only be induced to become boundary cells if they are reached by the wavefront at a specific phase of their oscillation (Cinquin, 2007).

The transcription factor Mesp2 is considered to be the main boundary-determining gene. Loss of Mesp2 in mice results in lack of boundary formation and fused somites and subsequently, in fused ribs and vertebrae (Morimoto et al., 2007; Takahashi et al., 2010). Mutations in human *MESP2* cause spondylocostal dysostosis, a syndrome characterized by misshapen and fused ribs and vertebrae, as well as scoliosis (Whittock et al., 2004). The expression of *Mesp2* in the PSM is temporally regulated by Notch and spatially regulated by Tbx6 (Morimoto et al., 2007; Oginuma et al., 2008). Once activated by Tbx6, Mesp2 induces the expression of *Ripply2*, a Groucho co-repressor. In a negative-feedback loop, RIPPLY then binds

to Tbx6, converting it into a repressor as well as promoting the degradation of Tbx6, further preventing *Mesp2* induction (Morimoto et al., 2007; Oginuma et al., 2008). When Tbx6 expression is missing in mice and zebrafish embryos, the expression of Mesp2 is not detected and severe defects in somite formation are observed (Kume et al., 2001; Zhao et al., 2015). When *Ripply2* expression is missing in mice, or its orthologue *ripply1* in zebrafish, intersomitic boundaries fail to form and the expression of both Mesp2 and Tbx6 are upregulated and extend anteriorly in the PSM (Kawamura et al., 2005; Zhao et al., 2015). The expression of *Mesp2* is also highly dependent on the balance between the opposing Fibroblast growth factor-8 (FGF8) and retinoic acid (RA) gradients in the PSM (Figure 1.2B).

Fgf8 mRNA expression is highest at the caudal end of the PSM and is gradually decreased rostrally (Dubrulle et al., 2001; Dubrulle and Pourquie, 2004a; Sawada et al., 2001). When the FGF gradient was disrupted, the expression of caudal molecules such as *T/Brachyury* was increased in the rostral PSM whereas the expression of rostral markers such as *paraxis* and *Mesp2* was decreased (Delfini et al., 2005; Dubrulle et al., 2001). While *Fgf8* mRNA is detected in the tailbud and is terminated in the caudal PSM, the expression of the FGF8 protein continues until the mRNA is decayed when the cells in the caudal PSM shift anteriorly, producing a gradient of FGF8 expression. The reduced expression of FGF8 in the anterior PSM allows the determination front to shift anteriorly and *Mesp2* to be expressed, leading to proper formation of the somites. FGF8 expression, therefore, is coupling embryonic elongation and somite formation (Dubrulle et al., 2001; Dubrulle and Pourquie, 2004a; Sawada et al., 2001).

The retinoic acid gradient, on the other hand, established through *Retinaldehyde dehydrogenase-2* (*Raldh2*) expression, is restricted to the rostral PSM (Diez del Corral et al., 2003; Moreno and Kintner, 2004; Niederreither et al., 2002a; Niederreither et al., 2002b; Sirbu and Duester, 2006; Vermot and Pourquie, 2005). *Raldh2* and *Fgf8* negatively regulate one another, leading to the establishment of two opposing gradients in the PSM: a caudal-rostral FGF8 expression gradient and a rostral-caudal *Raldh2* gradient (Abu-Abed et al., 2001; Diez del Corral et al., 2003; Vermot and Pourquie, 2005). RA signaling does not appear to be necessary for segmentation as somites can still form in its absence (Niederreither et al., 2002a; Niederreither et al., 2002b). The interaction between RA and FGF signaling however appears to be crucial for the localization of the determination front and intersomitic boundary formation (Diez del Corral et al., 2003). While it is known that FGF signaling can promote degradation of *Raldh2* (Abu-Abed et al., 2001; Vermot and Pourquie, 2005), normal *Raldh2* expression has been detected in mice with an *Fgfr1* mutation (Wahl et al., 2007), suggesting that RA signaling in the PSM can be regulated by other molecular mechanisms.

Figure 1.2 Molecular Networks Regulating Positional Identity and Boundary Determination in the PSM

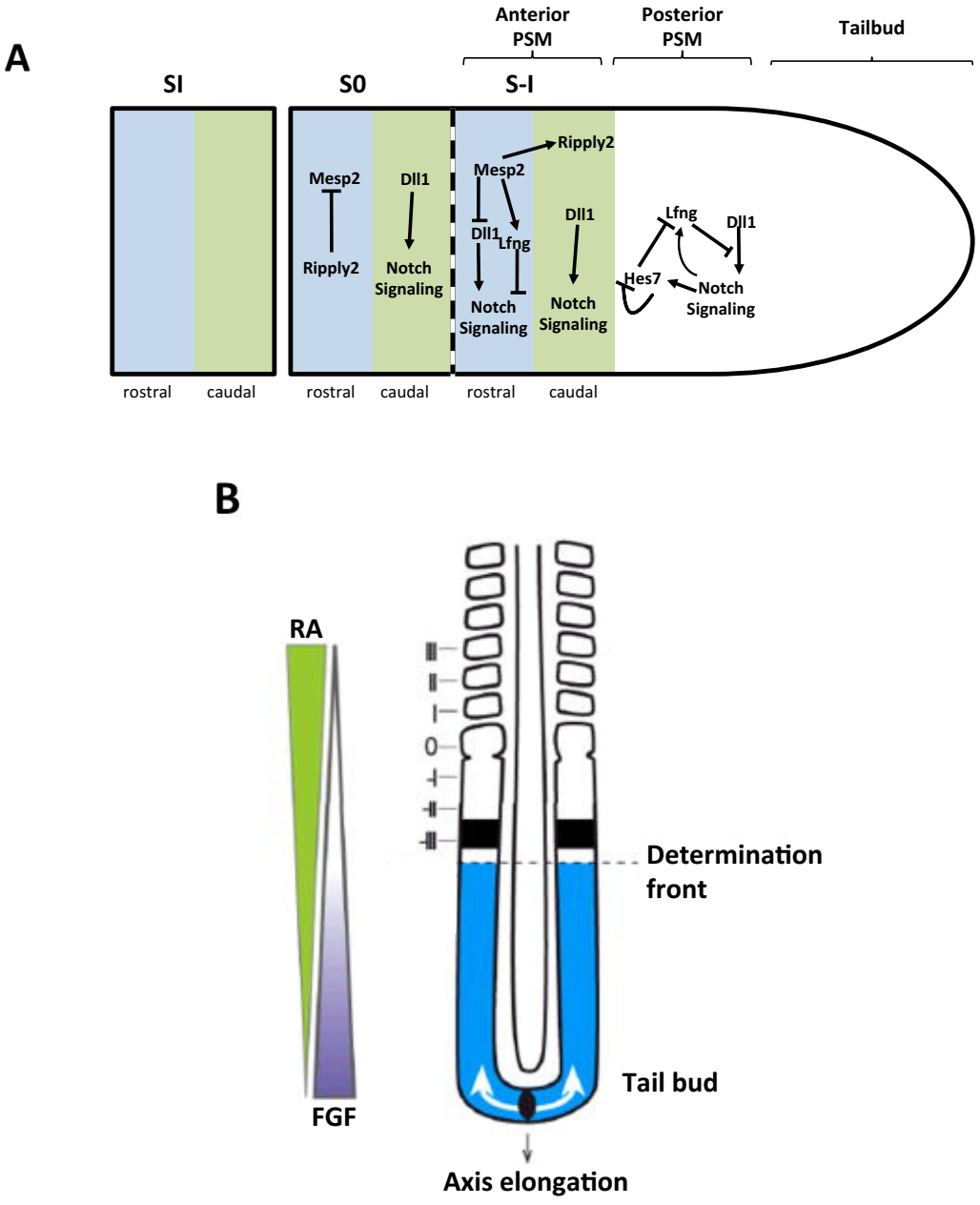

Figure 1.2 Molecular networks regulating positional identity and boundary determination in the PSM. Mesenchymal progenitor cells originating in the tailbud differentiate into presomitic mesodermal cells as the embryo elongates along the anterior-posterior axis. Waves of gene expression sweep through the PSM anteriorly until they reach the boundary determination front in the pre-patterned anterior PSM and form an intersomitic boundary **(A)** Regulation of somite formation at the molecular level is complex and involves several different regulatory networks at the various stages of somitogenesis, from differentiation of progenitor cells in the tailbud to formation of cyclical gene expression in the posterior PSM, determination of positional identity in the anterior PSM, and maintenance of rostral and caudal domains in the newly formed somites. **(B)** The opposing retinoic acid and FGF signalling gradients determine the position of the boundary determination front in the anterior PSM. (B) Adapted with permission from (Gomez and Pourquie, 2009)

Mesenchymal to Epithelial Transition

Once the intersomitic boundaries start forming, cells of the somites proliferate, condense and undergo mesenchymal to epithelial transition (MET) (Figure 1.1B). The anterior PSM is made up of loose mesenchyme, but once the oscillatory gene expression reaches the determination front, which is marked by the caudal boundary of *Mesp2* expression, they become epithelialized (Delfini et al., 2005). This results in the formation of an epithelial ball surrounding a mesenchymal core, the somitocoel. Epithelialization of the somite is complete with the formation of the next intersomitic boundary. The epithelialization process is characterized by an increase in expression of cell adhesion molecules, mainly of the cadherin family (Duband et al., 1987; Dubrulle and Pourquie, 2004a; Tam and Trainor, 1994). MET and intersomitic boundary formation are temporally linked, most likely through the function of the transcriptional repressors *Snai1* and *Snai2* (Dale et al., 2006). These *Snail* genes are expressed in an oscillatory manner in the PSM and prevent epithelialization of the mesoderm by blocking the expression of *paraxis*, integrins, and cadherins (Dale et al., 2006; Horikawa et al., 1999; Linask et al., 1998; Peinado et al., 2004). In mice with a homozygous null *paraxis* mutation, PSM cells failed to epithelialize, leading to the formation of gaps between mesenchymal somites and defects in the formation of somite-derived skeletal tissues (Burgess et al., 1996).

Other Models of Somite Formation

Experimental evidence supporting the oscillatory clock and wavefront somitogenesis model also increases its complexity. Recently, a new somitogenesis model has been proposed in which somite formation results from a local reaction-diffusion mechanism rather than long-range morphogen gradients (Cotterell et al., 2015; Maini et al., 2015). In this model, which is called the progressive oscillatory reaction-diffusion (PORD) system, anterior-to-posterior formation of the somites is controlled not by a shift in the gradient position coupled to embryo elongation but by local self-organization. The PORD system also involves molecular oscillations in the PSM and a travelling wavefront, but postulates that positional determination of this wavefront is not dependent on global positional information in the PSM but rather that the distance between the stripes of gene expression is determined by local diffusion of a repressor molecule from the last formed stripes (Figure 1.2) (Cotterell et al., 2015). This more recent mathematical model is attempting to improve the integration of current knowledge yet the basic concepts of the genetic regulation of somite formation remain unchanged.

Figure 1.3 PORD Model vs. Clock & Gradient Model of Somitogenesis

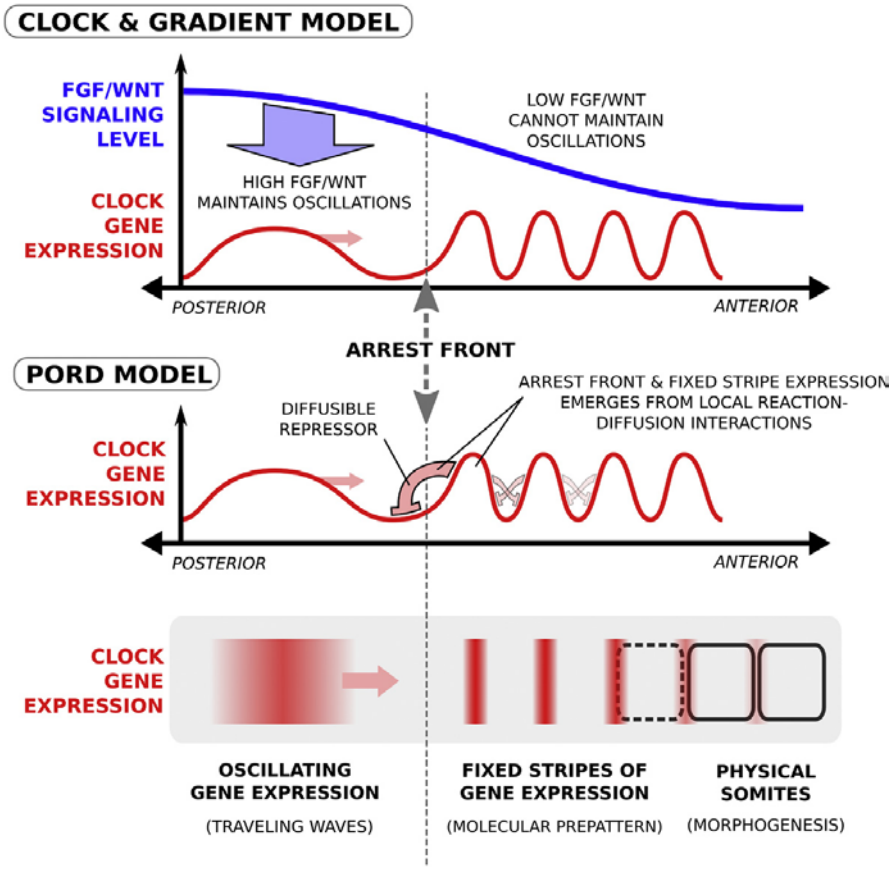

Figure 1.3 PORD Model vs. Clock & Gradient Model of Somitogenesis. Based on the Clock & Gradient model, oscillatory gene expression proceed anteriorly through the PSM until they pass a threshold of lower levels FGF/Wnt signaling that cannot sustain the oscillations, leading to formation of fixed stripes of gene expression in the anterior, unsegmented PSM. The PORD model postulates that a repressor molecule is diffused from the last fixed stripe of gene expression, leading to arrest of the oscillations. Figure reproduced with permission from (Cotterell et al., 2015).

Resegmentation and Sclerotome Migration

Once the formation of the new somite is complete, the cells in the ventral/medial portion of the somite undergo an epithelial-to-mesenchymal transition (EMT) and, together with the mesenchymal cells of the somitocoel, form the sclerotome (Christ and Ordahl, 1995; Huang et al., 1994; Ostrovsky et al., 1988; Pourquie et al., 1993). The cells of the sclerotome migrate ventrally to surround the notochord and neural tube and will eventually undergo endochondral ossification and form the vertebrae and the ribs (Aoyama and Asamoto, 2000; Goldstein and Kalcheim, 1992; Karaplis, 2008).

Prior to sclerotome migration, immediately following their formation, the somites undergo a rearrangement process called resegmentation in which the rostral compartment of one somite together with the caudal compartment of its immediately preceding somite give rise to one vertebral body (Saga and Takeda, 2001). As a result, the vertebral bodies are comprised of sclerotome from two adjacent somites, whereas the neural arches are derived from the caudal domain of one somite and the spinous processes are derived from the rostral domain of another somite (Figure 1.1C). Maintenance of spatial identity early in somitogenesis is therefore crucial for this subsequent rearrangement and for vertebral formation. The caudal domain of the somite is characterized by expression of *Uncx4.1* and *Dll1* whereas *Tbx18* and *Mesp2* are restricted to the rostral region (Biris et al., 2007; Giampietro et al., 2009; Kume et al., 2001; Sawada et al., 2001; Topczewska et al., 2001a). Inactivation of *Mesp2* results in somite caudalization and formation of fused

vertebral bodies and neural arches (Saga et al., 1997), while disruption of Notch signaling leads to rostralization, fusion of the vertebral bodies and a complete absence of the neural arches (Cordes et al., 2004).

CARTILAGE AND BONE FORMATION

The vertebrate skeleton is composed mainly of cartilage and bone. Skeletogenesis begins when mesenchymal cells migrate to the site of future bone and form high-density condensations outlining the shape of the future bones. The bony elements of the skeleton are formed via one of two processes: intramembranous or endochondral ossification. The bones of the skull base, the posterior part of the skull, and the appendicular skeleton are formed via endochondral ossification, whereas intramembranous ossification gives rise to the flat bones of the skeleton, the clavicle and calvarial bones, the mandible and the maxilla (Olsen et al., 2000; Ornitz and Marie, 2002).

Intramembranous Ossification

In intramembranous ossification, mesenchymal progenitor cells directly differentiate into osteoblasts (committed bone precursor cells) that promote the secretion and mineralization of bone matrix. The mesenchymal cells committed to become osteoblasts proliferate and condense into compact nodules that then differentiate into capillaries or osteoblasts. Once a cell has differentiated into an osteoblast, it secretes a collagen-proteoglycan matrix called an osteoid. The osteoid is able to bind calcium salts promoting calcification of the bone. The osteoblasts are usually separated from the calcification zone by a layer of the osteoid matrix. Occasionally however, osteoblasts can become trapped in the calcified matrix and differentiate into osteocytes (bone cells). As calcification proceeds, bony spicules

radiate out from the region where ossification began, and the entire region of calcified spicules becomes surrounded by compact mesenchymal cells that form the periosteum (a membrane that surrounds the bone). The cells on the inner surface of the periosteum also become osteoblasts and deposit osteoid matrix parallel to that of the existing spicules, producing many layers of bone matrix (Gilbert, 2000; Olsen et al., 2000).

Bone morphogenetic proteins (BMPs) and *Runx2* (Runt-related transcription factor 2) (also known as *Cbfa1* or *Osf2*) have important regulatory roles in the initiation of intramembranous ossification (Karaplis, 2008). BMP2, BMP4, BMP7 from the head epidermis drive the direct formation of bone cells from the neural crest-derived mesenchymal cells through the Wnt pathway. They activate *RUNX2* in mesenchymal cells, leading to an increase in *β-catenin* levels. RUNX2 then induces the expression of *Osterix* (Osx), causing the cells to produce collagen I and other non-collagenous extracellular matrix proteins (Gilbert, 2000; Karaplis, 2008).

Endochondral Ossification

Endochondral ossification involves the formation of cartilage tissue from condensed mesenchymal cells that generate a cartilage model of the future bone and the subsequent replacement of cartilage tissue by bone (Kronenberg, 2003). The advantage of the cartilage skeletal model over intramembranous ossification is in the unique capacity of cartilage to grow interstitially through the division of its chondrocytes, allowing for very rapid growth. Like intramembranous ossification,

endochondral ossification begins with the formation of condensed aggregates of mesenchymal cells (Thorogood and Hinchliffe, 1975). However, while these mesenchymal condensations are an important prerequisite for subsequent chondrogenesis, current understanding of the molecular mechanisms driving their formation is still lacking. Both N-CAM (Neural Cell Adhesion Molecule) and N-cadherin have been implicated in mediating cell-to-cell adhesion in these condensations (Oberlender and Tuan, 1994; Tavella et al., 1994), although their roles are unclear. Mice deficient in N-CAM (Neural Cell Adhesion Molecule) had no apparent defects in chondrogenic differentiation (Cremer et al., 1994), and N-cadherin deficient mice die at an early embryonic age, preventing investigation of their mesenchymal condensations (Radice et al., 1997). *Hoxa13* and *Hoxd13* also have important roles in the regulation of cell adhesion in mesenchymal condensations (Fromental-Ramain et al., 1996; Stadler et al., 2001). Mouse embryos that are deficient in Hoxa13 and Hoxd13 have defects in cell-to-cell adhesion that is mediated through Ephrin (Eph) signaling in the condensing mesenchyme (Lu et al., 2008; Wada et al., 1998). Finally, *Sox9* (discussed below) has been shown to be important for maintaining the mesenchymal condensations. In the absence of *Sox9* the mesenchyme will initially condense but the condensations fail to remain aggregated (Barna and Niswander, 2007).

Once formed, the mesenchymal cells in the condensation core start differentiating into chondrocytes (cartilage-committed cells). This differentiation is marked by the secretion of a cartilaginous matrix composed mainly of types II, IX and XI collagen as well as proteoglycans such as aggrecan (Figure 1.4) (Caplan and

Pechak, 1987). The cells at the periphery of the condensation secrete type I collagen, forming the perichondrium surrounding the mesenchyme which demarcates the boundaries of the forming skeletal element (Caplan and Pechak, 1987). Next, the chondrocytes undergo rapid proliferation, driving the linear growth of the skeletal element. The chondrocytes in the center eventually begin a maturation process, stop dividing, and dramatically increase their volume. Ultimately, these cells exit the cell cycle, become hypertrophic, and begin to secrete collagen type X, collagen type XI and collagen type IX as well as aggrecan and other extracellular matrix molecules (Figure 1.4) (de Crombrugghe and Schmidt, 1987; Gibson et al., 1986; Leboy et al., 1988; Matsui et al., 1991; Schmid and Linsenmayer, 1985). These hypertrophic markers induce the differentiation of cells in the inner perichondrium into osteoblasts, thus directing mineralization of the ECM (Caplan and Pechak, 1987). Hypertrophic chondrocytes also secrete metalloproteinase 13 (MMP13), an enzyme that cleaves the ECM within the hypertrophic cartilage, facilitating vascular invasion (Figure 1.4) (Inada et al., 2004; Stickens et al., 2004). Once the matrix is vascularized, osteoblast precursor cells begin to migrate in and establish the primary ossification center in the cartilaginous model, initiating new bone formation on the matrix scaffolding (Maes et al., 2010). The hypertrophic chondrocytes eventually die by apoptosis or transdifferentiate into osteoblasts and osteocytes (Yang et al., 2014).

The clear formation of chondrocyte maturation zones within the growth plate, proceeding from proliferation to hypertrophy and bone formation, allows for the linear growth of the long bones from the articular ends (epiphysis) to the

midshaft (diaphysis). Chondrocytes in the epiphysis center proliferate and shift distally, undergoing hypertrophy and maturation and eventually getting replaced by bone near the diaphysis, resulting in longitudinal growth of the endochondral skeletal element (Figure 1.5) (Kronenberg, 2003).

Figure 1.4 Differential Gene Expression at Various Stages of Endochondral Differentiation

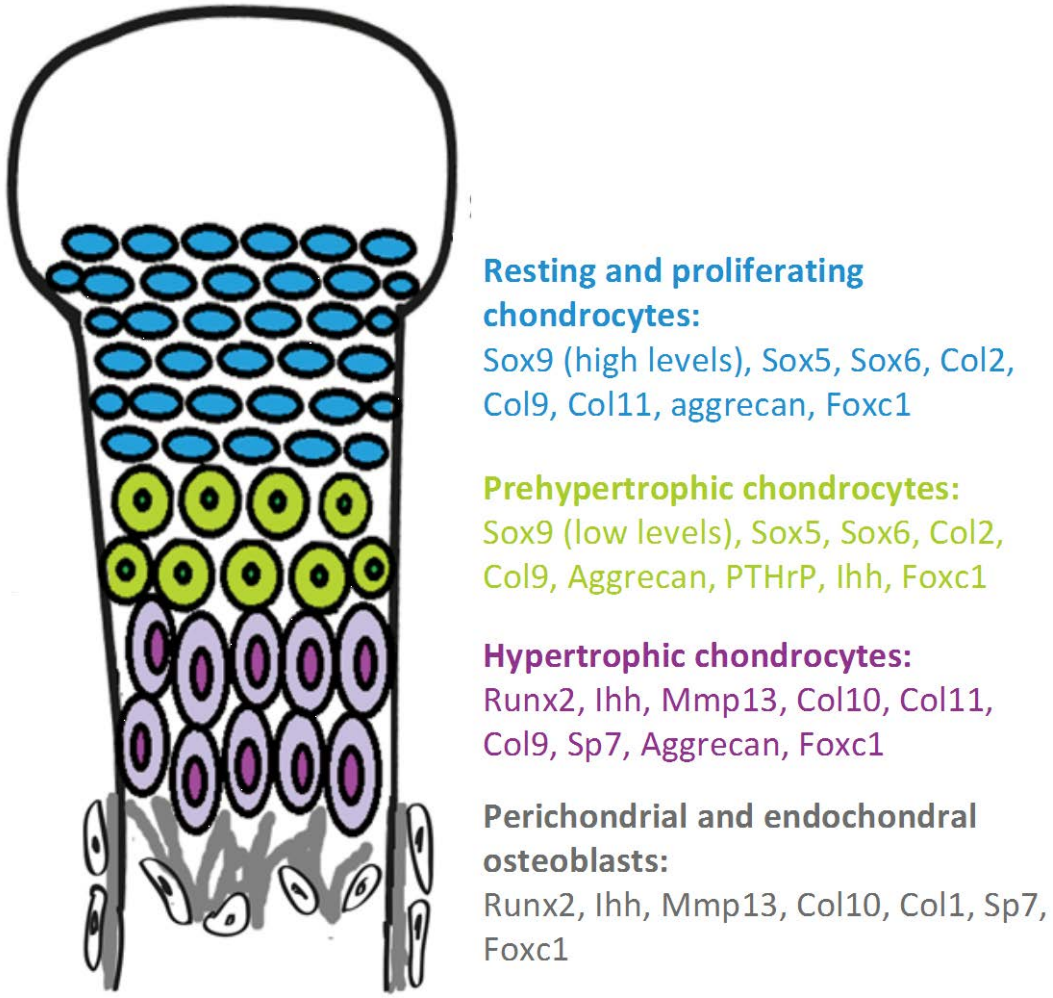

Figure 1.4 Differential gene expression at various stages of endochondral differentiation. As mesenchymal cells undergo endochondral differentiation, they secrete different extracellular matrix proteins and gene regulatory proteins depending on their stage of differentiation. The expression is detected throughout chondrogenesis. Adapted from (Gomez-Picos and Eames, 2015).

Figure 1.5 Illustration of Endochondral Ossification

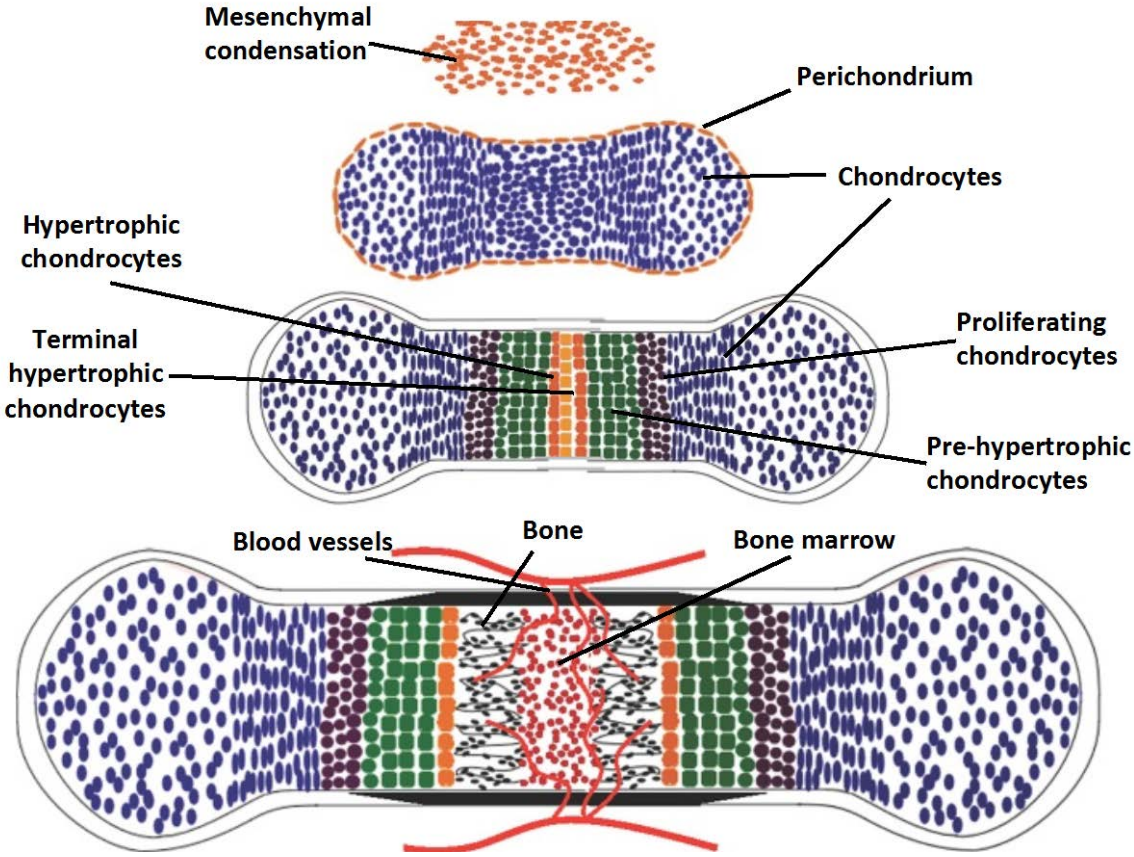

Figure 1.5 Illustration of Endochondral Ossification. Endochondral ossification begins with mesenchymal condensations (brown); the cells in the center differentiate into chondrocytes (blue) surrounded by a mesenchymal perichondrium (brown). As the chondrocytes mature they proliferate (purple), become pre-hypertrophic (green), and finally acquire hypertrophic properties (orange). Terminal hypertrophic chondrocytes are replaced by invading blood vessels (red lines) and bone-forming osteoblasts (black). The space left by the apoptotic chondrocytes fills with hematopoietic bone marrow (red). Adapted with permission from (Long and Ornitz, 2013).

SOX9 Has a Critical Role in Cartilage and Bone Formation

SOX proteins are Sry-related (sex-determining region Y) HMG (high-mobility-group) transcription factors whose role in bone formation is crucial (Lefebvre et al., 1998; Olsen et al., 2000; Yoon and Lyons, 2004). *SOX9* is considered to be a master regulator of chondrogenesis, regulating the specification and differentiation of chondrocytes (Lefebvre et al., 1998; Yoon and Lyons, 2004). *Sox9* is the earliest known factor that is required for chondrogenic differentiation. *Sox9* transcripts are first detected in condensing mesenchymal cells at 8.5-9.5 days post coitum (dpc) in mice, and reach peak expression in the cartilage primordia at 11.5-14.5 dpc (Bi et al., 1999). While Sox9 is not required for the formation of mesenchymal condensations, it is required for their maintenance, and subsequent differentiation does not occur in its absence (Barna and Niswander, 2007). In humans, heterozygous mutations in *SOX9* cause campomelic dysplasia (CD), a severe form of chondrogenic dysgenesis (Foster et al., 1994; Wagner et al., 1994). Similarly, haploinsufficiency of *Sox9* in mice also leads to chondrodysplasia. Loss of *Sox9* in the prechondrogenic mesenchyme results in complete lack of chondrogenic differentiation (Akiyama et al., 2002; Bi et al., 1999; Kist et al., 2002). *Sox9*-null mice had no chondrocyte-specific markers, and their cells did not differentiate into chondrocytes but instead remained in the perichondrium (Bi et al., 1999). *L-Sox5* and *Sox6*, two other Sry-related genes, are believed to form a complex with *Sox9* and other nuclear proteins in chondrocytes, and are co-expressed in all chondrogenic sites (Akiyama et al., 2002; Han and Lefebvre, 2008; Lefebvre et al., 1998; Olsen et al., 2000; Smits et al., 2001). Loss of *SOX9*, *L-SOX5* or *SOX6*, or mutations in these genes, result in missing

skeletal elements, absent chondrogenic condensations and loss of cartilage-specific markers (Han and Lefebvre, 2008; Lefebvre et al., 1998; Yoon and Lyons, 2004). Bone morphogenetic proteins (BMPs) help to maintain *SOX* gene expression during chondrocyte differentiation, and are potentially involved in the regulation of *SOX9* expression, although the molecular mechanisms linking BMP signaling and *SOX9* expression are still unknown (Yoon and Lyons, 2004). The critical requirement for Sox9 in chondrogenesis is well established, however not all *Sox9* downstream targets have been identified and it is not completely understood how it functions to drive chondrogenesis.

Other Regulators of Chondrogenesis

Another important regulator of chondrogenic differentiation is the paracrine factor PTHrP (parathyroid hormone-related peptide). *PTHrP* is highly expressed by chondrocytes in the perichondrium and has low expression in proliferating chondrocytes (Lee et al., 1995). Similarly, its receptor, PTHR1, is expressed at high levels in chondrocytes immediately before they begin hypertrophy (pre-hypertrophic chondrocytes), and only at low levels in proliferating ones (Lanske et al., 1996; St-Jacques et al., 1999; Vortkamp et al., 1996). PTHrP acts to suppress the onset of hypertrophy in two main ways: (1) activating cAMP-dependent signaling, leading to an increase in the activity of Sox9, and (2) dephosphorylation of HDAC4, leading to reduced Runx2 activity (Guo et al., 2002; Huang et al., 2001; Kozhemyakina et al., 2009; Vega et al., 2004). Targeted inactivation of the PTHrP

protein or its receptor results in premature hypertrophy of chondrocytes and embryo lethality, while misexpression results in delayed hypertrophy and a cartilaginous endochondral skeleton at birth (Karaplis et al., 1994; Kronenberg et al., 1996; Lanske et al., 1996; Weir et al., 1996). In humans, loss of function mutations in *PTHR1* lead to Blomstrand chondrodysplasia, a syndrome characterized with shortened bones, increased bone density and advanced skeletal maturation (Jobert et al., 1998; Karaplis et al., 1998; Karperien et al., 1999). Gain of function mutations, on the other hand, lead to Jansen metaphyseal chondrodysplasia in both humans and mice (Schipani et al., 1995; Schipani et al., 1996; Schipani et al., 1997; Soegiarto et al., 2001). The expression of *PTHrP* in chondrogenesis is regulated by Indian hedgehog (IHH). *Ihh* is expressed in pre-hypertrophic and early hypertrophic chondrocytes (Lanske et al., 1996; St-Jacques et al., 1999; Vortkamp et al., 1996). Embryos lacking *Ihh* expression had severe reduction of chondrocyte proliferation and premature hypertrophy (Long et al., 2001; St-Jacques et al., 1999). These chondrocyte hypertrophy defects appear to be secondary to *Ihh* and result from disregulation of *PTHrP* expression, induced by IHH (Karp et al., 2000; Long et al., 2001; St-Jacques et al., 1999).

FGF signaling also has an important regulatory role in endochondral differentiation. Disruption in the expression of the FGF receptor *Fgfr1* in chondrocytes resulted in delayed hypertrophic maturation (Jacob et al., 2006). Disruption of *Fgfr2* expression in mesenchymal condensation led to skeletal dwarfism and decreased bone density (Yu et al., 2003). Additionally, null-*Fgfr3* mice had increased chondrocyte proliferation and expanded hypertrophic zone (Colvin et

al., 1996; Deng et al., 1996; Eswarakumar and Schlessinger, 2007). Overexpression of FGFR3 resulted in decreased proliferation and reduced number of cells in the pre-hypertrophic and hypertrophic zones (Chen et al., 2001; Iwata et al., 2001; Naski et al., 1998). While FGFr3 appears to be inhibiting chondrocyte proliferation and hypertrophy by regulating IHH/PTHrP expression, the mechanisms through which it functions are not clearly understood.

THE FORKHEAD BOX TRANSCRIPTION FACTOR C1

The transcription factor family known as Forkhead Box, or FOX, is characterized by a conserved 110 amino acid monomeric DNA binding motif that folds into a variant of the helix-turn-helix motif and gives these proteins their characteristic winged helix, or "Forkhead", appearance. A large portion of the forkhead domain is highly conserved among its family members and contains the same chain of amino acids, suggesting there is a similarity in the 3D structure of this transcription factors class and in their DNA recognition. Outside of the 110 amino-acid chain that characterizes this protein class, all other portions of the FOX proteins are highly divergent (Carlsson and Mahlapuu, 2002). FOX proteins activate the transcription of target genes by binding the Forkhead response elements in promoter and enhancer regions. The binding sites usually span 15-17 basepairs and are asymmetrical, allowing for monomeric binding of DNA (Carlsson and Mahlapuu, 2002). Over 100 FOX family members have been identified in animals and fungi. Nineteen *FOX* subgroups have been identified and classified based on homology, FOXA to FOXS (Kaestner et al., 2000). Members of the Forkhead transcription factors family are remarkably diverse functionally and take part in various biological processes. FOX proteins can either inhibit or activate gene expression. They are associated with development and embryonic patterning as well as angiogenesis, stem cell proliferation, cardiovascular injury, neurodegeneration, metabolism, cancer, immune surveillance, aging and cell longevity (Maiese, 2009). FOX proteins regulate major signaling pathways, including the transforming growth

factor β (TGF-β) and mitogen activated protein kinase (MAPK) pathways, and are thought to be molecular integrators of extracellular signals (Benayoun et al., 2011).

The *FOXC* subclass contains two closely related members: *FOXC1* (formerly *FREAC3, FKHL7* or *Mf1*) and *FOXC2*. Human *FOXC1 and FOXC2* are single exonic genes located on chromosomes 6 (6p25) and 16 (16q22-q24), respectively. Their DNA binding domains are 97% identical and 99% similar, differing only in two positions: *FOXC1* has an aspartic acid at residues 90 and 110, whereas *FOXC2* has glutamic acid in those positions (Berry et al., 2005b). The N- and C- terminal flanking regions of the two transcription factors are somewhat diverse, with 56% shared homology at the N-terminal and only 30% homology at the C-terminal (Kume, 2009). Many vertebrate species, such as the frog, mouse, chicken and humans possess both *FOXC* genes (Berry et al., 2005b; Koster et al., 1998; Kume et al., 1998; Topczewska et al., 2001b).

FOXC1 and *FOXC2* act as monomers and are expressed in embryonic and adult tissues in endothelial and in mesenchymal cells, and play an essential role in arterial cell specification, lymphatic vessel formation, angiogenesis and cardiac outflow tract development (Fatima et al., 2016; Gripp et al., 2013; Hayashi et al., 2008; Hollier et al., 2013; Ivanov et al., 2013; Kume, 2009; Kume et al., 1998; Kume et al., 2001; Winnier et al., 1999). Their expression domains overlap in certain regions, such as neural crest derivatives, pharyngeal arches and endocardial cushions of the cardiac flow tract (Hiemisch et al., 1998a; Hiemisch et al., 1998b; Koster et al., 1998). The similarities in their structure and expression domains

suggest that FOXC1 and FOXC2 might act in redundancy to regulate mutual downstream targets. Both FOXC1 and FOXC2 are important regulators of skeletal development. The FOXC transcription factors are crucial for proper human development and there are many anomalies and abnormalities associated with mutations in the *FOXC* subclass family in addition to skeletal defects, ranging from mild clinical manifestations such as lymphedema-distichiasis to severe, life-threatening conditions like highly metastatic cancer.

Structure of FOXC1

The FHD of FOX family members is made up of 3 N-terminal α-helices (H1, H2, H3) and three antiparallel β-strands (S1, S2, S3) (Figure 1.6) (Clark et al., 1993). Certain FOX proteins, including FOXC1, also have a fourth, smaller α-helix (H4) located between H2 and H3 (van Dongen et al., 2000). The β strands form a β sheet, providing the protein with a tight hydrophobic core (Clark et al., 1993; van Dongen et al., 2000; Weigelt et al., 2001). The regions between S2 and S3 and between S3 and the C-terminal fold into loop-like wings (W1, W2, respectively) giving the FHD its characteristic "winged-helix" motif. The wings appear to be involved in bending the DNA double helix at an angle of 80-90° to facilitate and stabilize the protein-DNA interaction. This function renders them essential for the ability of FOX proteins to bind DNA as monomers, providing them a functional advantage since a single molecule could act to regulate downstream targets (Pierrou et al., 1994). H3 is predicted to be the DNA recognition helix and is the region of the molecule that

provides the various FOX members their DNA-binding capabilities and specificities. H3 binds to the major groove of the DNA by recognizing the FHD core target sequence RTAAAYAAA (Clark et al., 1993; Pierrou et al., 1994). Wing 2 is predicted to bind to the minor groove of the DNA molecule (Clark et al., 1993; Pierrou et al., 1994).

The FHD in FOXC1 is located between residues 69 and 178. The FHD contains two nuclear localization signals (NLS) in the N- and C-termini of the FHD (residues 77-93 and 168-176, respectively), enabling the FOXC1 protein to localize to the nucleus where DNA binding can occur (Berry et al., 2002). The N-terminal NLS is necessary but not sufficient to promote nuclear localization of the molecule and is considered to be an accessory domain (Berry et al., 2002). The C-terminus NLS appears to be sufficient on its own to promote nuclear localization (Berry et al., 2002). The FOXC1 protein also contains two transcriptional activation domains (AD) located outside of the FHD, between residues 1-51 (AD1) and 466-553 (AD2) (Berry et al., 2002). Lastly, a phosphorylated inhibitory domain (ID) is located between residues 215 and 366 (Berry et al., 2002). Missense mutations in the FHD disrupt the function of FOXC1 and are often associated with Axenfeld-Rieger syndrome in humans. Mutations in α-helix 1 or that lie N-terminal to it impede the ability of FOXC1 to bind to DNA and activate transcription, and interfere with nuclear localization of the protein (Berry et al., 2005a; Fetterman et al., 2009; Murphy et al., 2004). Mutations in α-helix 3 affect nuclear localization and grossly impair DNA binding and specificity. Mutations in these loci also appear to reduce the amount of FOXC1 protein produced (Murphy et al., 2004). Mutations in α-helix 2

impair transcriptional activation, but nuclear localization and DNA binding capacities remain intact. Interestingly, mutations in wing 2 seem to be tolerated and do not disrupt the NLS (Murphy et al., 2004), however they do affect DNA binding and transactivation (Berry et al., 2005a).

The most common mutations in *FOXC1* are point mutations, with over 40 different mutations identified. Two nonsense mutations and 2 deletions resulting in frame-shift mutation and truncated protein have also been identified (Nishimura et al., 1998a; Tumer and Bach-Holm, 2009) .

Figure 1.6 Structure and Domains in FOXC1

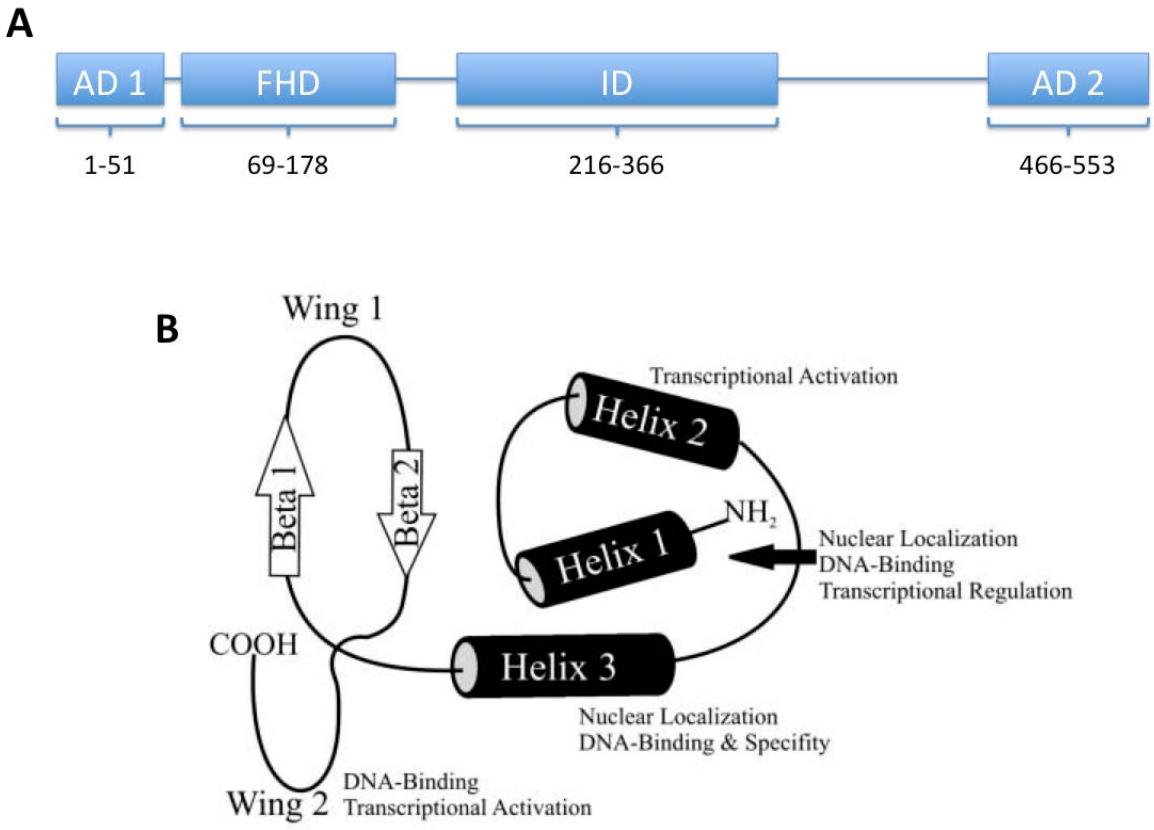

Figure 1.6 Structure and Domains in FOXC1. **(A)** The FOXC1 protein contains an N-terminus activation domain lying between amino acid residues 1-51 and a C-terminus activation domain at residues 466-553. The Forkhead domain is located between residues 69-178 and the inhibitory domain is between residues 216-366. **(B)** The FOXC1 protein is made up of 3 α-helices and 2 β sheets. A fourth, smaller α-helix, H4, is located between H2 and H3. AD, activation domain; FHD, Forkhead domain; ID, inhibitory domain. Figure adapted from Berry et al., 2005b.

The Role Of The *FOXC* Subclass In Disease

Human *FOXC*1 mutations are predominantly associated with Axenfeld-Rieger Syndrome (ARS), a dominantly inherited birth abnormality in the anterior chamber of the eye causing early onset glaucoma (Mears et al., 1998; Nishimura et al., 1998a). ARS patients often also suffer from craniofacial anomalies such as a prominent forehead, flat nasal bridge, hypertelorism and dental abnormalities. Cardiac defects, abnormalities of the pituitary gland, anal stenosis and excess periumbilical skin have also been reported (Bakayoko and Guirou, 2015; Brooks et al., 1989; Childers and Wright, 1986; Dressler and Gramer, 2006; Gripp et al., 2013; Meyer-Marcotty et al., 2008; Ozeki et al., 1999; Shields et al., 1985). ARS has been linked to mutations in both the *FOXC1* and *PITX2* (paired-like homeodomain transcription factor 2) genes. A variety of mutations in chromosome 6p25 have been mapped in ARS patients, including nonsense and missense mutations and partial duplications of chromosome 6p25 (Gripp et al., 2013; Ito et al., 2009; Ito et al., 2007; Kim et al., 2013; Kobayashi et al., 2004; Lehmann et al., 2002; Mears et al., 1998; Mirzayans et al., 2000; Mortemousque et al., 2004; Nishimura et al., 2001; Nishimura et al., 1998b; Suzuki et al., 2001). Only approximately 18% of patients with ARS-related glaucoma have responded positively to surgical correction or medical therapy (Strungaru et al., 2007).

Mice with *Foxc1* null mutations suffer from hydrocephalus and multiple skeletal anomalies and die pre- or perinatally (Grüneberg, 1943; Hong et al., 1999; Kume et al., 1998; Rice et al., 2003). Some of the major skeletal anomalies seen in these mice include lack of formation of the calvarial and sternal bones and

malformation of the meningeal layer (Green, 1970; Long, 2011; Ornitz, 2005). Many of these mutants also develop kidney and urinary tract abnormalities, including duplex kidneys and double ureters (Komaki et al., 2013; Kume et al., 2000).

Mutations in human *FOXC*2 are associated with Lymphedema-distichiasis (LD) syndrome, an autosomal dominant anomaly. Lymphedema, which manifests in obstructed lymphatic drainage of the limbs, defective lymphatic valves and impaired formation of microvessels, usually appears in late childhood or early puberty and is often asymmetric (Brice et al., 2002; Dale, 1987; Erickson et al., 2001; Finegold et al., 2001). Distichiasis, an eyelash abnormality ranging from an extra full set of eyelashes to a single hair, can be detected at birth and is often associated with corneal irritation, recurrent conjunctivitis and photophobia (Bakayoko and Guirou, 2015; Brice et al., 2002; Mansour et al., 1993). Varicose veins, congenital heart disease and skeletal anomalies are also often associated with this syndrome (Brice et al., 2002; Mellor et al., 2007; Rosbotham et al., 2000). *FOXC2* is the only known gene associated with LD, and 90% of its genetic mutations are small deletions or insertions, with only a few missense mutations and nonsense mutations detected in patients with LD (Bell et al., 2001; Brice et al., 2002; Itoh et al., 2016; Kovacs et al., 2003; Ogura et al., 2013; Petrova et al., 2004; Ridderstrale et al., 2002; Sargent et al., 2014; Sholto-Douglas-Vernon et al., 2005; Tavian et al., 2016; van Steensel et al., 2009; Zhu et al., 2014).

Null mutations in mouse *Foxc2* are embryonic lethal due to severe cardiovascular, skeletal, craniofacial, and vertebral abnormalities (Gozo et al., 2013;

Iida et al., 1997; Park et al., 2011; Winnier et al., 1997). The kidneys of null-*Foxc2* mice show hypoplasia, disorganized glomerular mesangium and abnormal glomerular capillary formation (Takemoto et al., 2006).

FOXC1 and FOXC2 have functional redundancy in the development of several systems and organs and double *Foxc1*/*Foxc2* heterozygous mice die perinatally (Kume et al., 2001; Seo and Kume, 2006; Winnier et al., 1999). In the developing skeleton, *Foxc1* and *Foxc2* have distinct but overlapping expression patterns in the paraxial mesoderm of the head and trunk (Iida et al., 1997; Winnier et al., 1997). Complete deletion of *Foxc1* and *Foxc2* results in lack of somite segmentation (Kume et al., 1998), and double *Foxc1*/*Foxc2* heterozygous mice had abnormal ossification centers, anomalies in arch formation, deformed skull and sphenoid bones, and absent exoccipital bones (Motojima et al., 2016). Mice with compound homozygous *Foxc1*/*Foxc2* mutations do not proceed through gestation. No individuals with homozygous mutations in human *FOXC*1 or *FOXC*2 have been identified (Kume, 2009).

FOXC1 Regulates Skeletal Formation and Differentiation

Both FOXC1 and FOXC2 are important regulators of axial skeletal development and somitogenesis (Carlsson and Mahlapuu, 2002). Mice with homozygous null mutations in *Foxc1* or *Foxc2* have defects in axial skeleton development such as fused ribs, incomplete formation of the dorsal neural arches, small lateral neural arches and reduced centra of the vertebrae (Kume et al., 1998;

Winnier et al., 1997). Mice with homozygous *Foxc1* mutations often have hemorrhagic hydrocephalus, and multiple skeletal, ocular, genitourinary and cardiovascular defects (Carlsson and Mahlapuu, 2002; Kume, 2009). In addition, these mice often lack the frontal bones of the skull vault which are derivatives of cranial neural crest cells. Severe defects in ossification are also seen in the rib cage and sternum and many of the ribs are fused, fragile or irregularly formed (Kume et al., 1998).

Loss of Foxc1 function in zebrafish results in somite segmentation defects (Topczewska et al., 2001a). In mice where both *Foxc1* and *Foxc2* were absent or dysfunctional, segmented paraxial mesoderm and somites are completely absent (Kume et al., 2001). Additionally, in zebrafish mutants with a partial deletion of chromosome 2, including the complete *foxc1a* gene, formation of the anterior somites was defective, although the posterior somites did form (Hsu et al., 2015). The expression of *foxc1a* was not detected at all stages examined indicating it is only essential for anterior somitic cell fate specification and not required for later somite specification (Hsu et al., 2015). These observations suggest that FOXC1 and FOXC2 have important regulatory roles during somite formation and skeletogenesis.

Foxc1 Has an Important Regulatory Role in Somitogenesis

As mentioned above, FOXC1 has an important role during somite formation. Previous studies reveal that reduced *Foxc1* expression leads to defects in the formation of the somites in both mice and zebrafish models (Kume, 2009; Kume et

al., 2001; Topczewska et al., 2001a). Similarly, the expression of *Mesp2,* the boundary determination factor, was reduced in both animal models (Kume et al., 2001; Topczewska et al., 2001a). In zebrafish, due to genome deletion/duplication events, there is no *Foxc2* orthologue, and 2 *Foxc1* paralogues: *foxc1a* and *foxc1b* (Topczewska et al., 2001b). However, it appears that only Foxc1a has a role in somitogenesis, and *foxc1a-foxc1b* double knockdowns have similar phenotypes to single *foxc1a* knockdowns (Topczewska et al., 2001b). Knockdown of *foxc1a* in zebrafish leads to defects in the formation of the anterior somites and loss of spatial polarity within the PSM. The expression of *mesp-ba*, a zebrafish *Mesp2* orthologue, was lost in the absence of Foxc1a, resembling the mouse *Foxc1* phenotype (Topczewska et al., 2001b). This suggests that FOXC1 has a conserved and important role in *Mesp2* regulation. Additionally, a zebrafish mutant with a partial chromosomal deletion encompassing *foxc1a, mib*^{nn2002}*,* also has defects in anterior somite formation that are potentially linked to the absence of *foxc1a* (Hsu et al., 2015). Another *foxc1a* mutant model, *foxc1a*^{nju18} also displayed irregular formation of the anterior somites (Li et al., 2015). Taken together, these findings suggest that Foxc1 is necessary for proper formation of the anterior somites, and that it has a differential role in early stages of somitogenesis versus late stages since posterior somites are less affected by reduced or absent *foxc1a* expression. How *Foxc1* functions to regulate somitogenesis is still unclear.

Foxc1 Regulates Endochondral and Intramembranous Ossification

The transcription factor *Foxc1* appears to have an important role in both endochondral and intramembranous ossification as well as in the formation of the cartilaginous structures of the skeleton. *Foxc1* is expressed in the mesenchyme of the cranium, and in mice lacking *Foxc1* the skull fails to form and the meninges show abnormal development (Kume et al., 1998). Further, *Foxc1* mouse mutants often develop bony syngnathia, in which the upper and lower jaws are fused together by atypical bone formation, the maxillary and mandibular structures show irregular development, and the temporomandibular joint is absent (Inman et al., 2013). Osteoblasts derived from the neural crest develop ectopically in the maxillary prominence, causing a bony fusion with the dentary bone (Inman et al., 2013). As described before, homozygous null *Foxc1* mice had several defects in the bony elements of the vertebrae and axial skeleton (Kume et al., 1998). The rib cage and sternum display severe ossification defects, with many fused, misshapen and fragile ribs. There is a complete absence of the skull vault and defects to the base of the skull, the basio-occipital bone and the hyoid bone (Kume et al., 1998).

Recently, there have been some new insights into how *Foxc1* exerts its regulatory role during osteogenic differentiation and intramembranous ossification. In the skulls of homozygous *Foxc1* mutants apical growth did not progress beyond the primordium stage and the rudiments were mineralized by E15 with little or no further growth, indicating a reduction in cell proliferation (Rice and Rice, 2008; Rice et al., 2003). Analysis of skull vault growth and development beyond E15 in *Foxc1* mutants is prevented by their hydrocephalus, but the lack of apical extension

of the frontal and parietal bones does not appear to be caused by a failure of osteogenic precursor cells to migrate into position in the supraorbital ridge. Instead, FOXC1 functions through *Msx2* to set a threshold level of BMP activity, and to control the differentiation of osteogenic precursor cells and the development of the calvarial bones. FOXC1 directly regulates the expression of *Msx2* by binding to the promoters of both mouse and human *MSX2* (Mirzayans et al., 2012). Interestingly, it has also been shown that FOXC1 can negatively regulate *Msx2* activity in the early stages of osteoblast differentiation by inhibiting the BMP responsiveness of *Msx2* (Sun et al., 2013). FOXC1 directly interacts with a BMP-responsive element that lies 560bp upstream of the *Msx2* enhancer and acts as a negative regulator of the Bmp responsiveness of *Msx2* (Sun et al., 2013). In this way, FOXC1 restricts the occupancy of P-Smad1/5/8 on the *Msx2* BMP responsive element and limits *Msx2* expression to the osteogenic zone that will become the developing frontal bone (Sun et al., 2013). This suggests that the role of FOXC1 in early osteogenic differentiation is context dependent, potentially through the recruitment of co-factors to target promoters.

FOXC1 appears to have a role in several stages of endochondral ossification and chondrogenesis. FOXC1 is expressed in the cartilage of the sternum and ribs as well as in the developing limb buds and in distal chondrocytes (Yoshida et al., 2015). FOXC1 was detected in mesenchymal condensations that give rise to chondrogenic cells, and in resting, proliferating, and hypertrophic chondrocytes, as well as in perichondrial cells (Hsu et al., 2015; Kume et al., 1998; Kume et al., 2001; Li et al., 2015; Sun et al., 2013; Topczewska et al., 2001a; Winnier et al., 1997; Yoshida et al.,

2015). These expression patterns suggest that FOXC1 has an important role in regulating early- to late-stage chondrogenesis and endochondral ossification (Yoshida et al., 2015). Mice with a *Foxc1* mutation had no ossification center in the sternum, impaired ossification of the vertebrae, significantly shorter limbs, as well as smaller ossification center in the limbs (Kume et al., 1998). The sternum had disorganized rib fusion and a complete absence of hypertrophic chondrocytes and ossification(Kume et al., 1998). Additionally, the hypertrophic zone in the tibial growth plate was significantly longer than in WT mice (Yoshida et al., 2015). These data suggest that FOXC1 is vital for endochondral ossification. It has recently been shown that FOXC1 directly regulates the expression of *PTHrP* and *Col10a1* by interacting with the IHH-GLI2 signaling network. As mentioned above, both PTHrP and COL10A1 are important markers of hypertrophic chondrocytes, and this interaction elucidates some of the roles of FOXC1 during late-stage chondrogenesis. However, the molecular mechanisms by which FOXC1 regulates early-stage endochondral formation remain largely unknown.

HYPOTHESES AND RATIONALE

Foxc1 has an important role in skeletal development. It is expressed during many stages of skeletal patterning and differentiation such as somitogenesis, chondrogenesis and intramembranous ossification. Animal models deficient in or missing FOXC1 display a range of skeletal defects, including patterning and segmentation defects as well as reduced formation of the bony elements of the skeleton. However, the molecular mechanisms underlying the functions of *Foxc1* in these various events are not yet understood.

Mice with *Foxc1/Foxc2* mutation show defects in the formation of the anterior somites and a decrease in *Mesp2* expression (Kume, 2009). Similarly, *mesp-ba* is reduced in zebrafish embryos when *foxc1a* is knocked down (Topczewska et al., 2001a). These effects on somite formation and *mesp-ba* expression are similar to what is seen in zebrafish embryos lacking Tbx6. These embryos also show a complete lack of somite formation, and the expression of *mesp-ba* is reduced. When *ripply1*, a zebrafish *Ripply2* orthologue, is reduced, embryos show complete lack of somite formation. The expression pattern of *mesp-ba* in these fish is opposite to what is seen when Foxc1a is reduced – an anterior expansion of the *mesp-ba* expression domain (Kawamura et al., 2005). The similarities in *mesp-ba* expression seen in the *foxc1a* and *tbx6* morphants and the reverse effect seen in the *ripply1* morphants suggest that Foxc1 might be interacting with or acting upstream of *tbx6.* I therefore hypothesized that *foxc1a* is controlling *mesp-ba* expression through an interaction with the *tbx6-ripply* regulatory network.

Furthermore, endochondral ossification and cartilage formation are severely affected in FOXC1 mutants. And yet, while there have been recent insights into the roles of *Foxc1* in intramembranous ossification and osteogenic differentiation, its function in chondrogenesis is still largely unknown. Recently, a ChIP-Seq study examined transcriptional programs within mammalian chondrocytes, attempting to characterize SOX9 binding and chromatin organization (Ohba et al., 2015). Their findings demonstrated the existence of four SOX9 peaks in distal elements of *FOXC1,* suggesting that FOXC1 might be a target of SOX9. It has also been suggested that there is an enrichment of SOX9 binding in the vicinity of FOXC1 binding motifs, raising the idea that FOXC1 and SOX9 have similar downstream targets (Liu and Lefebvre, 2015). These results led us to speculate that *Foxc1* might be a target of Sox9 regulation during chondrogenesis and that it interacts with SOX9 to regulate common downstream targets.

Here, I will examine how *foxc1a* regulates axial skeleton development by controlling the formation of the somites in zebrafish embryos, and how it interacts with SOX9 to control the formation of the bony elements of the skeleton later in development.

CHAPTER 2. MATERIALS AND METHODS

Animal Care and Ethics Statement

Zebrafish husbandry and experimental procedures complied with the University of Alberta Animal Care and Use Committee guidelines under directives of the Canadian Council on Animal Care. Approval granted to T. Allison #AUP00000077.

Microinjections and Morpholino-Mediated Gene Knockdown

Danio rerio embryos were collected 15-20 minutes post fertilization and arranged on an E3-agarose plate. Previously characterized translation blocking antisense morpholino oligonucleotides (MOs) were obtained from Gene Tools, LLC (Table 2.1). 10-20 nl of the morpholino solutions containing the target morpholino, 0.5 M KCl, and 0.05% Phenol Red were injected into the yolk of a 1-2 cell embryo. The *foxc1a* MO was injected at a concentration of 6.5 ng/embryo and the *ripply1* MO was injected at a concentration of 3.25 ng/embryo. When a single gene was targeted for knockdown, the injection solution also contained the standard control MO such that all embryos were injected with a total MO concentration of 9.75 ng/embryo. Embryos were then incubated in embryonic media (3 mM NaCl, 0.17 mM KCl, 0.33 mM $CaCl_2$, 0.33 mM $MgSO_4$, 1% Methylene Blue) at 28.5°C until euthanization. All embryos were euthanized using MS222 (tricaine methanesultonate) and fixed in 4% paraformaldehyde (PFA) overnight at 4°C.

TABLE 2.1 MORPHOLINO OLIGONUCLEOTIDES USED

Target Gene	Sequence	Mode of Action
foxc1a-MO2	5'-CCTGCATGACTGCTCTCCAAAACGG-3'	Translation blocking
ripply1-MO	5'-CATCGTCACTGTGTTTTTCGTTTTG-3'	Translation blocking

RNA Probe Generation

cDNAs for *foxc1a, ripply1, mesp-ba,* and *tbx6* were used as PCR-based templates for antisense probes synthesis whereby a T7 or T3 binding site was juxtaposed to the 3' end of the reverse primer sequence (Thisse, 2005) (Table 2.2). Templates for *raldh2* and *fgf8a* riboprobes were obtained as a plasmid containing an Sp6 binding site, courtesy of Dr. Waskiewicz, and linearized.

Riboprobes were synthesized using either a DIG- or a FLR-RNA labeling kit (Roche). 2 µg plasmid or PCR template were incubated with transcription buffer, labeling mix, T7 or T3 RNA polymerase, and RNase inhibitor for 2 hour at 37°C. An additional 1 µl RNA inhibitor was added after the first hour. Reaction was then incubated with 1 µl DNase I for 5 minutes at 37°C and 2 µl 0.25 M EDTA pH 8.0 to stop the reaction. Riboprobes were purified using SigmaSpin Post-Reaction Clean-up columns, after which 2 µl 0.25 M EDTA pH 8.0 and 2 µl RNase inhibitor were added. Probes were stored as stocks in -80°C. Prior to hybridization probes were diluted 1:200 in hybridization solution.

Table 2.2 Primers Used for mRNA Probe Preparation

Target Gene	Sequence	Probe Size (bp)
mesp-ba	5'-GCAAACCTCAAGCAAGAACC-3'	549
	5'-gaaattaatacgactcactataggTACCGCTCCCTGTATTGTCC-3'	
foxc1a	5'-GAGACATTGGCCATCTAGGC-3'	437
	5'- *gaaattaatacgactcactatagg*CTGACGCATTTCAACACAGC-3'	
ripply1	5'-CTGTGTGCTTTGCCACTCC-3'	467
	5'- gaaattaatacgactcactataggCATCATCTTCATCACAGCTTTCC-3'	
*tbx6**	5'-CAATCAATCCCTGCTTGTC-3'	1067
	5'- gaaattaatacgactcactataggCGAGGATCCTGGCAAAG-3'	
fgf8a	5'-TCTTCGTATTGCTGCTCAAGGG-3'	453
	5'- gaaattaatacgactcactataggTATCCTAAGGTAAATTTATTA-C-3'	

* Previously characterized in (Thisse, 2005)

Lower case: T7-binding site sequence. Upper case: Gene specific sequence.

Whole-Mount *in-situ* Immunohistochemistry

Single or double whole mount *in-situ* hybridization was performed as described in Gongal and Waskiewicz (2008). Briefly, zebrafish embryos at the selected time points were euthanized with MS222 and fixed in 4% PFA overnight at 4°C. Embryos were then washed 5 x 5 minutes in PBST at room temperature and permeabilized with 10 µg/µl Proteinase K in PBST for 30-seconds, 1- or 3-minutes (12.5, 14 or 22 hpf, respectively). Embryos were then fixed in 4% PFA for an additional 20 minutes at room temperature and washed 5 x 5-minutes in PBST at room temperature. Next, embryos were pre-hybridized in hybridization solution (50% formamide, 5X SSC, 50 µg/ml heparin, 500 µg/ml tRNA, 0.1% Tween-20) for 1 hour at 65°C followed an overnight hybridization at 65°C with the appropriate RNA probe. Serial washes followed next: (1) 66% hybridization solution and 33% 2X SSC

for 5 minutes at 65°C; (2) 33% hybridization solution and 66% 2X SSC for 5 minutes at 65°C; (3) 2X SSC for 5 minutes at 65°C; (4) 0.2X SSC and 0.1% Tween-20 for 20 minutes at 65°C; (5-6) 0.1X SSC and 0.1% Tween-20 for 20 minutes at 65°C, repeated twice; (7) 66% 0.2X SSC and 33% PBST for 5 minutes at room temperature; (8) 33% 0.2X SSC and 66% PBST for 5 minutes at room temperature; and (9) PBST for 5 minutes at room temperature.

Following the washes, embryos were blocked with 2% lamb serum and 2 mg/ml BSA in PBST for 1 hour at room temperature before an overnight incubation with anti-digoxigenin (1:5000) or anti-fluorescin (1:10000) in block solution at 4°C. Finally, embryos were washed 5 x 15 minutes in PBST and incubated in NBT/BCIP. Coloration reaction was stopped with PBST, pH 5.5.

Messenger RNA Preparation and Rescue Injections

Zebrafish *foxc1a* was inserted into a pCS2+ vector and grown in DH5α cells. Plasmid was purified using Qiagen Plasmid *Plus* Midi kit (Qiagen) and linearized using NEB *Not*I restriction enzyme (R0189S). Linearized DNA was then purified using 0.5 M EDTA and 3 M sodium acetate pH 5.2 in 100% EtOH and chilled in -80°C overnight. DNA was then pelleted and RNA was transcribed and purified using Ambion mMessage mMachine T7 transcription kit (AM1344). mRNA was aliquoted and stored at -80°C. For rescue experiments, 20 pg mRNA were co-injected with 6.25 ng *foxc1a* MO2 into embryos at the 1-2 cell stage. This injected *foxc1a* mRNA was inert to its cognate MO because the injected mRNA lacked the 5'UTR of the

natively expressed *foxc1a* mRNA, and this is principally where this MO binds to affect gene knockdown. Following injections, embryos were grown and euthanized as described above.

Embryonic Growth

Embryonic growth was analyzed by measuring the angle created between embryonic poles (i.e. head and tailbud) using CorelDraw 16. Observer was blinded to treatment groups when acquiring measurements.

Genomic DNA Extraction

Genomic DNA was extracted from fish embryos as per Meeker et al. 2007 (Meeker et al., 2007). Embryos were incubated in 50mM NaOH at 95°C for 20 minutes. Embryos were then cooled down to 4°C and 10% 1M Tris HCl, pH 8.0 was added. Tubes were then centrifuged at high speed to pellet debris and supernatant was collected and used directly for subsequent processing.

Fish Genotyping of *foxc1a* Mutants

Genomic DNA was used as template in PCR reaction using *foxc1a* sequencing primers. PCR amplicons were then digested with *Bst*XI (Thermo Scientific, FastDigest) or *Alw*NI (Thermo Scientific, FastDigest) 1% agarose gel was used to visualize digested DNA. WT amplicons contain the *Bst*XI restriction site whereas the mutation leads to a deletion of this restriction site and the creation of the *Alw*NI

restriction site. As a result, WT embryos are cleaved by *Bst*XI (resulting in a cleaved band around 200bp, whereas uncleaved, mutated fragment is detected around 400bp), homozygous mutants are cleaved by *Alw*NI (resulting in a 200bp band whereas uncleaved WT DNA is detected at around 400bp), and heterozygous mutants are cleaved by either, resulting in the formation of two bands, cleaved and uncleaved, at 200bp and 400bp, respectively) (Figure 2.1).

Figure 2.1 Restriction Enzyme Genotyping of Zebrafish Mutants

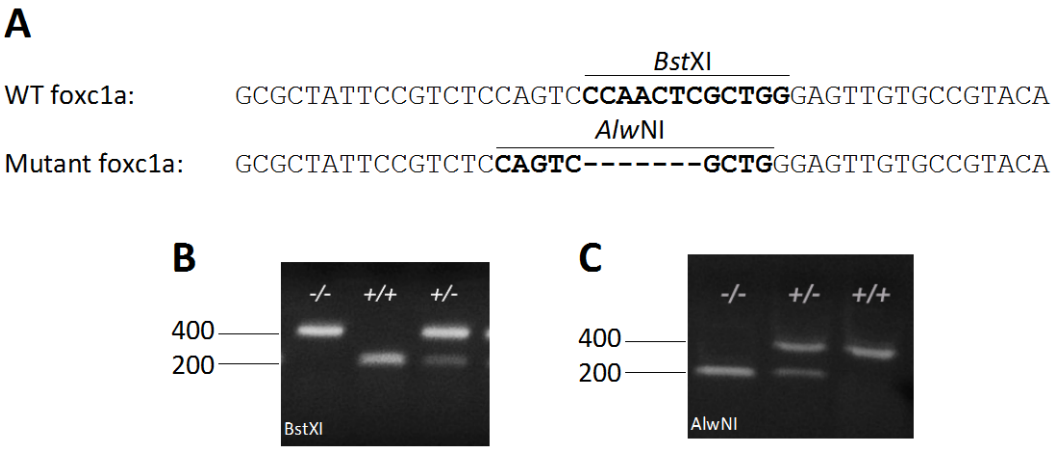

Figure 2.1 Restriction Enzyme Genotyping of Zebrafish Mutants. The genotypes of zebrafish embryos were successfully identified using PCR and restriction enzyme digestions. **(A)** The 7bp deletion in the foxc1a gene leads to a loss of the *Bst*XI restriction site found in the WT gene and the creation of a *Alw*NI restriction site instead. **(B)** The restriction enzyme *Bst*XI does not cleave the homozygous mutant DNA, homozygous WT DNA is cleaved, and heterozygous DNA is partly cleaved. **(C)** The DNA of homozygous mutants is cleaved by the restriction enzyme *Alw*NI, whereas that of heterozygous mutants is only partially cleaved and that of homozygous mutants is not digested.

Table 2.3 Primers Used for Zebrafish Genotyping

Primer Name	Sequence
foxc1a Seq-Fwd	5'-GAAAGAGGTGGCCAGTACG -3'
foxc1a Seq-Rev	5'-GAGCGCAATGTAGCTGTACG -3'

U2OS Cell Culture and Transfections

For all experiments utilizing U2OS, cells were grown in high-glucose Dulbecco's modified eagle medium (Gibco) with supplemented 10% fetal calf serum (FBS). Cells were grown in 5% CO_2 at 37°C. Transfections were carried out with Mirus LT-1 transfection reagent according to manufacturer's suggestions. Briefly, 3:1 (µl:µg) Mirus *Trans*IT-LT1 transfection reagent (Mirus Bio LLC) to DNA were added to serum free DMEM and incubated at room temperature for 30 minutes before being added drop-wise to experimental plate. Cells were then allowed to grow for 24-48 hours before further processing.

Embryonic Stem Cells Growth Conditions

To maintain pluripotency, TT2 mouse embryonic stem cells (Yagi et al., 1993) were grown in leukemia inhibitory factor (Lif) (+) ES media (High Glucose DMEM, L-Glutamine, β mercaptoethanol, 0.1 mM MEM non-essential amino acids solution (100X), 15% FBS (Fetal bovine serum, ESC-qualified), Pen/Strep, 0.1 µl/ml Lif) on gelatin-coated 100 mm TC plates at 37°C and 5% CO_2. ES cells were passaged or cryopreserved in 20% FBS, 20% DMSO every 2 days to prevent spontaneous differentiation. Transfections were carried out as described above.

Differentiation of Embryonic Stem Cells

Hanging droplet ESC differentiation assay was developed from (Kawaguchi et al., 2005; Yu et al., 2015) (Figure 2.2). TT2 cells were suspended in Lif (-) ES media at a concentration of 100,000 cells/ml and plated as hanging droplets on the lids of 100 mm tissue culture plate containing 10 ml PBS. Fifty-six droplets were used in each plate. Cells were then incubated at 37°C and 5% CO_2 for 2 days. On day 3, embryoid bodies (EBs) were transferred into 60 mm low-adherence plates containing 5 ml Lif (-) ES media with or without 0.1 μM retinoic acid (RA) and incubated at 37°C and 5% CO_2. On day 5, EBs were collected and washed twice in PBS before being re-suspended in Lif (-) ES media and getting returned to their original 60mm plates for incubation. On day 7, EBs were plated on gelatin-coated plates and cultured in Lif (-) ES media with or without 10 ng/μl TGFβ3. Media was changed every 2 days throughout the differentiation assay. Cells were harvested on days 0, 2, 5 and 13. For overexpression studies, cells were plated as monolayer at $5x10^5$ cells/ml on day -2 in Lif (+) ES media, transfected on day -1, and plated as hanging droplets as described above.

Figure 2.2 Embryonic Stem Cell Differentiation

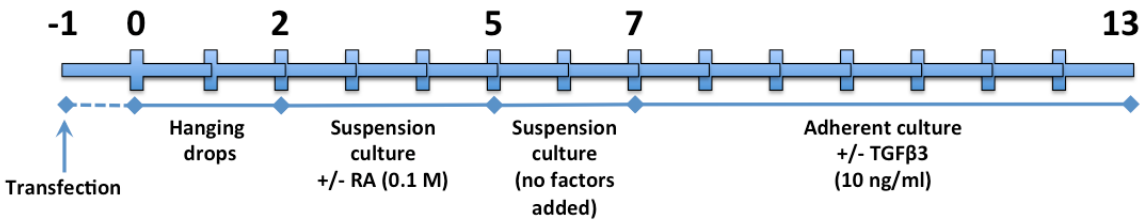

Figure 2.2 Embryonic Stem Cell Differentiation. Embryonic stem cells were differentiated into chondrogenic cells using the hanging droplet assay. Cells at a concentration of 100,000 cells/ml were plated in 25 µl droplets onto the lid of a 100mm tissue culture dish containing 10 ml PBS and cultured for 2 days to allow for formation of embryoid bodies. On day 2 EBs were transferred to 60 mm low adherence plates with or without 0.1 µM RA. On day 5, RA was removed from media. EBs were transferred to gelatin-coated plates on day 7 and were cultured with or without 10 ng/ml TGFβ3 until day 13.

Reverse Transcription Quantitative Polymerase Chain Reaction

Total RNA was extracted and purified using RNeasy Mini Kit (Qiagen). RNA quality and quantity were assessed using a Nanodrop 1000. Reverse transcription was performed using a QuantiTect Reverse Transcription Kit (Qiagen), in which 500-1000 ng RNA were used per reaction and ddH_2O was added to a total volume of 12 µl per reaction. Two microliters gDNA Wipeout solution were added to each tube and reactions were incubated at 42°C for 2 minutes. Four microliters of the RT buffer, 1 µl of a RT primer mix containing 2 µM of each primer and 1 µl of the reverse transcriptase were added to each tube and reactions were incubated at 42°C for 15 minutes. Reactions were then inactivated at 95°C for 3 minutes. Finally, reactions were diluted 1:20 and cDNAs were analyzed using qPCR.

qPCR reactions were set up using Kapa Sybr Fast universal qPCR kit (Kapa Biosystems). Each 10 µl reaction consisted of 5µl 2X QuantiFast Sybr Green master mix, 1 µl Primer mix (2 µM each) and 4 µl cDNA. Reactions were quantitated and analyzed on a Bio-rad CFX Manager version 3.0.125.0601. For analysis, ΔΔCq was calculated compared to the housekeeping genes *Gpdh*, *Hprt*, and *β-actin*.

Table 2.4 Primers Used for qPCR

Target Gene	Sequence	Target Gene	Sequence
Col2	5'-ACTGGTAAGTGGGGCAAGAC-3'	*Runx2*	5'-ACCATGGTGGAGATCATCG-3'
	5'-CCACACCAAATTCCTGTTCA-3'		5'-TAACAGCGGAGGCATTTCG-3'
ColX	5'-CTTTGTGTGCCTTTCAATCG-3'	*Sox2*	5'-GTACAACTCCATGACCAGCTC-3'
	5'-GTGAGGTACAGCCTACCAGTTTT-3'		5'-CTTGACCACAGAGCCCAT-3'
Foxc1	5'-CAAGACGGAGAACGGTACGTG-3'	*Sox5*	5'-CAGCATGCTTACTGACCCTG-3'
	5'-GGCTCTCGATTTTGGGCACT-3'		5'-TCTCCTCCTCTTCCACTTTC-3'
Gapdh	5'-AGGTCGGTGTGAACGGATTTG-3'	*Sox6*	5'-GGTCATGTTTCCCACCCACAA-3'
	5'-TGTAGACCATGTAGTTGAGGTCA-3'		5'-TTCAGAGGGGTCCAAATTCCT-3
Hprt	5'-AACAAAGTCTGGCCTGTATCC-3'	*Sox9*	5'-GAGTGTCCCTTAGCCTTCCTTG-3'
	5'-CCCCAAAATGGTTAAGGTTGC-3'		5'-CCTTCCTTCCTTCCTTCCTTCC-3'
Hs. FOXC1	5'-AGAACTTCCACTCGGTGCG-3'	*β-Actin*	5'-GGCTGTATTCCCCTCCATCG-3'
	5'- CCCGTTCACTGGAGAGTTGT-3'		5'-CCAGTTGGTAACAATGCCATGT-3'
Oct4	5'-CCTCCTCTGAGCCCTGT-3'		
	5'-AACTGTTCTAGCTCCTTCTGC-3'		

Plasmid Generation

BioID-Foxc1

BirA(R118G)-HA destination vector was acquired from Addgene (catalogue #53581). pDonr-ms-Foxc1 was recombined into the destination vector using the LR Gateway kit (Invitrogen). Briefly, 150 ng of the destination vector were mixed with 150 ng of the entry vector, along with 2 µl of the LR Clonase II and the reaction was topped with TE buffer to a total volume of 10 µl. Recombination reaction was incubated overnight at room temperature. 1 µl Proteinase K was added to the reaction, and incubated at 37°C for 10 minutes. DH5α cells were transformed with reaction mix, and selected for ampicillin resistance. Recombination was confirmed using a WB blotted against Foxc1 and HA.

Distal Element Reporter Vectors

Genomic blocks (gBlocks) containing the sequences corresponding to the Foxc1 distal elements were designed and ordered from IDT by Fred Berry. Serial deletions of distal element B gBlocks were designed by Rotem Lavy. The gBlocks contained regions overlapping vector sequence in pGL4.23. gBlocks were dissolved at 10 ng/µl in sterile H_2O. One microgram of pGL4.23 vector was digested with EcoRV and linearized vector was purified on 1% agarose gel using the Qiagen gel purification kit (Qiagen). Distal element gBlocks were recombined into the linearized vector using the Gibson Assembly kit (NEB). Fifty nanograms vector and 150 ng insert were mixed with 10µl 2X Gibson Assembly Master Mix and reaction was topped up to 20 µl with deionized H_2O and incubated at 50°C for 1 hour. NEB 5α Competent *E. coli* cells were chemically transformed and selected for ampicillin resistance. The Halo-FOXC1 plasmid was purchased from Promega.

Dual-Luciferase Reporter Assays

Reporter assays were performed using Promega Dual-Luciferase Reporter Assay System (Promega). In this protocol, U2OS cells were plated at 10^4 cell/ml in 24 well plates and allowed to grow for 24 hours. Cells were then transfected using Mirus with 100 ng reporter, 100 ng affector and 0.1 ng RL-hTK in DMEM. 48 hours post transfection cell were lysed using the supplied passive lysis buffer for 30 minutes at room temperature. Twenty microliters lysate were added to the provided 100 µl Luciferase assay reagent and luminescence was measured. 100 µl

Stop-n-Glo buffer was added and Renilla luminescence was measured using a Promega Glomax 20/20 luminometer. All experiments contained 3 technical replicates and were repeated 3 times.

Protein Isolation

For protein isolation, culture media was aspirated from the cells followed by two washes with 1X PBS. Cells were scraped in fresh PBS and collected in 15 ml falcon tubes pre-chilled on ice. Samples were centrifuged at 2700 RPM for 5 minutes at 4°C and supernatant was discarded. Cells were then re-suspended in cell lysis buffer (10 mM NaCl, 1.5 mM $MgCl_2$, 0.2 mM EDTA, 20 mM Hepes pH 7.6, 20% Glycerol, 0.1% Triton X-100, 1 mM DDT, 1 mM PMSF, 0.5% protein inhibitor cocktail) and sonicated 3 times for 5 seconds on, 5 seconds off at 30% intensity using Sonic Dismembrator ultrasonic processor FB-120 (Fisher Scientific). Following sonication samples were incubated on a rocker at 4°C for 30 minutes and then centrifuged at 14000 RPM for 10 minutes at 4°C to pellet cellular debris. Protein concentration was determined using the Bradford Assay (Bio-Rad), compared to standards containing 0, 2, 5, 10, 20 and 30 µg/µl bovine serum albumin (BSA) and measured on a Promega Glomax 20/20 luminometer.

Immunoblotting

Proteins were prepared for immunoblotting with either 2X or 6X sodium dodecyl sulfate (SDS) loading dye and boiled at 95°C for 5 minutes. Samples were then loaded onto a 10% polyacrylamide gel for size separation. Proteins were transferred onto nitrocellulose membrane for 1 hour at 100 volts or overnight at 30mA at 4°C. Membranes were blocked for 1 hour at room temperature in 5 ml Licor Odyssey Blocking Buffer (Licor Biosciences) and incubated with the appropriate primary antibodies for 1 hour at room temperature or overnight at 4°C (for list of primary antibodies used see Table 2.7). The primary antibodies were diluted 1:500 in 2.5 ml PBST and 2.5 ml Licor Odyssey Blocking Buffer. Membrane was then washed four times in PBST for 5 minutes at room temperature. Secondary antibodies were incubated at 1:5000-10000 in 2.5 ml PBST and 2.5 ml Licor Odyssey Blocking Buffer and incubated for 1 hour at room temperature (Table 2.8), followed 4X PBST washes for 5 minutes at room temperature. Membrane was rinsed briefly with PBS and scanned using the Licor Odyssey Infrared Imager (Licor).

Table 2.5 List of Primary Antibodies Used

Name	Species	Company	Catalogue no.	Lot no.
αFlag	Mouse	Genscript	A00187	5A8E5
αHA	Mouse	Santa Cruz	sc-7392	H1413
αHA	Rabbit	Santa Cruz	sc-805	B2615
αXP	Mouse	Invitrogen	46-0528	1710348
αV5	Mouse	Invitrogen	46-0705	1821026
αFoxc1	Goat	Santa Cruz	sc-21396	K0415
αSox9	Rabbit	Santa Cruz	sc-20095	G0710
αHalo	Mouse	Promega	G9211	0000222397
αDIG-AP	Sheep	Roche	11093274910	12486522
αFLR	Sheep	Roche	11426338910	14973500

Table 2.6 List of Secondary Antibodies Used

Name	Species	Company	Catalogue no.	Lot no.
αMouse IRDye 680	Donkey	Life Technologies	610-730-124	24338
αRabbit IRDye 800	Donkey	Life Technologies	611-732-127	25342
αGoat IRDye 700	Donkey	Rockland	605-730-125	21244

Polymerase Chain Reaction

Polymerase Chain Reaction (PCR) was performed using the GoTaq Master Mix (Promega). Each reaction contained 4 µl 5X GoTaq buffer, 0.5 µl10 mM dNTPs, 1µl 10 µM forward primer, 1µl 10 µM reverse primer, 0.1 µl GoTaq polymerase and 2-5 µl gDNA. Reactions were topped up to 20 µl with ddH_2O. PCR conditions were as follows: activation of enzyme at 95°C for 2 minutes, 35 cycles of denaturation at 95°C for 30 seconds, annealing at 58°C for 30 seconds and extension at 72°C for 30 seconds, followed by a final extension step at 72°C for 5 minutes. PCR products

were run on 1% agarose gel containing 1% Ethidium bromide (EtBr) and visualized under UV light. Sequences used can be found in Tables 2.2 (*in-situ* probe generation), 2.4 (ChIP), and 2.5 (zebrafish genotyping).

Activin A Treatment of ES Cells

This differentiation protocol is derived from (Wang et al., 2003). ES cells were grown as a monolayer (10^5 cells/ml) on 100 mm gelatin-coated TC plates in Lif (+) ES media for 24 hours to facilitate adherence. After 24 hours, media was replaced with Lif (-) ES media with or without 30 ng/ml Activin A (Day 0). Lif (-) ES media +/- Activin A was replaced every day. Cells were harvested for protein analysis or ChIP on day 4. For RT-qPCR analysis cells were harvested on day 5.

Chromatin Immunoprecipitation

Cells were plated in duplicates on 100 mm TC plates as per experimental design. At the selected time point, one 100 mm plate was trypsinized and cells were counted to determine cell concentration. One million cells were used for each reaction. Cells were cross-linked for 10 minutes at room temperature with 1% formaldehyde. The reaction was quenched by the addition of 1 ml 1.125 M glycine and incubated for 5 minutes at room temperature. Cells were then washed twice in ice-cold 1X PBS and harvested in 2 ml ice-cold 1X PBS. Samples were centrifuged at 800 X g at 4°C for 5 minutes. Cell pellets were re-suspended in 0.5 ml ChIP cell lysis buffer per 10^7 cells (5 mM Pipes, 85 mM KCl, 0.5% Igepal, 0.5% PIC, 1% PMSF, 0.1%

DTT) and incubated on ice for 15 minutes, with brief vortexing every 5 minutes. Samples were again centrifuged at 800g for 5 minutes at 4°C and pellets were re-suspended in 0.5 ml ChIP nuclei lysis buffer per 10^7 cells (50 mM Tris-HCl pH 8.0, 10 mM EDTA pH 8.0, 1% SDS, 0.5% PIC, 1% PMSF, 0.1% DTT) and sonicated 6 times for 30 seconds on, 30 seconds off, at 50% intensity using Sonic Dismembrator ultrasonic processor FB-120 (Fisher Scientific) (number of cycles was empirically optimized with a shear centered around 500bp, Figure 2.2). Following sonication samples were centrifuged at 15,000 X g for 10 minutes at 4°C and the supernatant was divided into individual reactions containing 10^6 nuclear equivalents per tube. Fifty microliters Protein A Dynabeads were used per reaction. Using a magnetic rack, the supernatant was removed from the beads, and replaced with an equal volume of ChIP dilution buffer (0.01% SDS, 1.1% Triton X-100, 1.2 mM EDTA pH 8.0, 16.7 mM Tris-HCl pH 8.0, 167 mM NaCl, 0.5% PIC, 1% PMSF, 0.1% DTT). Twenty-five microliters beads were added to protein lysates and samples were incubated on a rotator at 4°C for 1 hour to pre-clear. Using a magnetic rack lysates were then moved to fresh, clean tubes. The appropriate antibody for the reaction was added to each lysate and allowed to bind for 1 hour at 4°C on a rotator (5 µg α-SOX9, 1 µg αH3ac and 1 µg rabbit IgG were used per reaction). To collect the antibody-protein/chromatin complexes, 25 µl beads were add to each lysate and allowed to bind for 1 hour at 4°C on a rotator. Protein A-antibody-protein/chromatin complexes were collected using a magnetic rack, and incubated for 5 minutes at room temperature in each of the following buffers: low salt buffer (0.1% SDS, 1% Triton X-100, 2 mM EDTA pH 8.0, 150 mM NaCl, 20 mM Tris-HCl pH 8.0), high salt

buffer (0.1% SDS, 1% Triton X-100, 2 mM EDTA pH 8.0, 500 mM NaCl, 20 mM Tris-HCl pH 8.0), LiCl buffer (0.25M LiCl, 1% Igepal, 1% Sodium deoxycholate, 1 mM EDTA pH 8.0, 10 mM Tris-HCl pH 8.0) and TE buffer (1 mM EDTA pH 8.0, 10 mM Tris-HCl pH 8.0). Samples were eluted in elution ChIP reversal buffer (10 mM Tris pH8.0, 1 mM EDTA, 300 mM NaCl) overnight at 62°C. Eluted lysates were transferred to fresh tubes and heat shocked for 5 minutes and 95°C, cooled to room temperature and analyzed using PCR.

Figure 2.3 Empirical Determination of ChIP Sonication Cycles

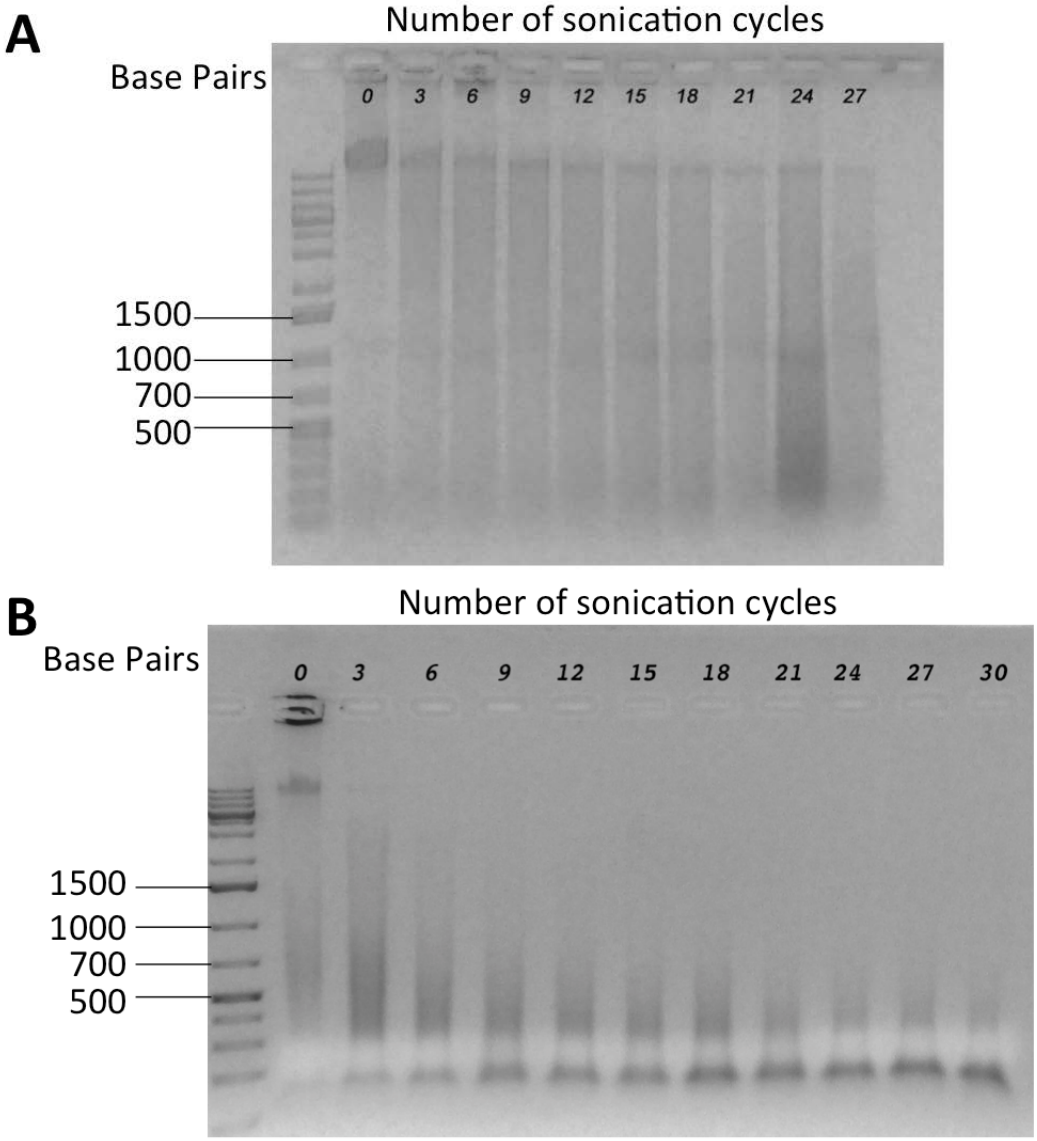

Figure 2.3 Empirical Determination of ChIP Sonication Cycles. ChIP sonication was empirically determined to be optimal around 6 cycles of 30 seconds on/ 30 seconds off at 50% intensity using Sonic Dismembrator ultrasonic processor FB-120 (Fisher Scientific). **(A)** U2OS cells transfected with Flag-SOX9. **(B)** TT2 cells stimulated with 30 ng/ml Activin A.

Table 2.7 Primers Used for ChIP

Target Gene	Sequence	Probe Size (bp)
Distal A	5'-GCCCTGAATCCAGAAACTTG-3'	249
	5'-GCGAATTCATATGGTTTTTCC-3'	
Distal B	5'-GGCCATCATGTCTAGGGGAA-3'	239
	5'-GTTGCTCTGAACTTGGGGTG-3'	
Distal C	5'-TGTGAAATCGCCTGTGAGAG-3'	297
	5'-CCCCATATCCTCTTTGAGAGC-3'	
Distal D	5'-TGTCAGGAGAACTGCTGTAAGAA-3'	340
	5'-CTCTAGGCTGACCACGCTGT-3'	
Col2a Intron 1*	5'-TGAAACCCTGCCCGTATTTATT-3'	100
	5'-GCCTTGCCTCTCATGAATGG-3'	
Sox6-1	5'- GTGCTGGAAAACATGAGGCA-3'	217
	5'-GTCCAGAGTGAAGTCAGAGTCT-3'	
Sox6-2	5'-AGCCTGCCTTTCATTCTCTT-3'	318
	5'-AACCACATTTGTCTCAGCTAGA-3'	

* Previously characterized in (Oh et al., 2010)

Table 2.8 Antibodies Used for ChIP Reactions

Antibody	Species	Company	Catalogue no.
αSOX9	Rabbit	Santa Cruz	sc-20095
H3ac	Rabbit	Millipore	06-599B
Rabbit IgG	Rabbit	Jackson Labs	N/A

Sulfated Glycosaminoglycan Measurement

To measure the amount of sulfated glycosaminoglycan (sGAG) produced by the embryoid bodies in the various conditions, embryoid bodies were collected and pelleted in PBS. Pellets were stored at -20°C until processing time. Pellets were then re-suspended in 250 µl proteinase K solution (1 mg/ml proteinase K, 50 mM Tris pH 7.6, 1 mM EDTA, 1 mM Iodoacetamide, 10 µg/ml pepstatin A) and incubated overnight at 56°C. Samples were then diluted 1:20 and 10 µl of each samples were

added to 250 µl DMMB dye (16 µg/ml DMMB in glycine/NaCL, pH 3). Absorbance was read at a wavelength of 530 nm using CytoFluor II (PerSeptive Biosystems) and analyzed using SOFTmax PRO and Microsoft Excel. Readings were compared to a standard curve composed of different concentrations of chondroitin sulfate (CS) in PBE buffer (100 mM Na_2HPO_4, 10 mM Na_2EDTA, pH 6.5).

Clustered Regulatory Interspaced Short Palindromic Repeats (CRISPR) Mediated Gene Knockout

A plasmid consisting of 3 Foxc1-specific guide RNA (gRNAs) sequences as well as green fluorescent protein (GFP) under the same promoter as the Cas9 was obtained from Santa Cruz Biotechnology (catalogue number sc-421637). This plasmid allows for utilization of the GFP for visualization of transfection efficiency and cell selection. One µg/µl of the CRISPR/Cas9 knockout plasmid was transfected into TT2 cells as per the transfection protocol outlined herein. Control cells were transfected with PBS and treated similarly to the CRISPR-transfected cells. Transfected cells were isolated through serial dilutions to ensure single-cell derived colonies and then expanded over a period of 3 weeks. Five individual knockdown cell lines were selected based on proliferation rates and cell appearances to ensure cell health.

High Resolution Melt Analysis

High resolution melt analysis (HRM) was performed using the Qiagen Type-it PCR kit (Qiagen). Briefly, 12.5 µl of the 2X HRM PCR master mix were mixed with

1.75 µl primer mix (10 µM), 5 µl DNA template and 5.75 µl RNase-free water. HRM-PCR was run using the following conditions: 5 minutes activation at 95°C followed by 45 cycles of 10 second denaturation at 95°C, 30 second annealing at 55°C and 10 second extension at 72°C. Melt data was acquired for 2 seconds at 0.1°C increments from 55°C to 95°C. Data was analyzed using the Bio-Rad Precision Melt Analysis software.

BioID Pull-Down

BioID protocol was developed based on (Roux et al., 2012). U2OS cells were transfected with Flag-SOX9 and either BioID-Foxc1 or empty BioID. Biotin (50 µM) was added at time of transfection. 48 hours post transfection cells were washed twice with 1X PBS. 800 µl BioID lysis buffer (50 mM Tris HCl pH7.5, 500 mM NaCl, 0.2% SDS, 2% Triton-X, 1% PMSF, 0.5% PIC and 0.1% DTT) were added, and plates were incubated on rocker at room temperature for 10 minutes. Lysates were then transferred to 1.5 ml microcentrifuge tubes and placed on ice. Samples were sonicated 3X for 5 seconds at 30% intensity using Sonic Dismembrator ultrasonic processor FB-120 (Fisher Scientific). Samples were allowed to rest for 5 seconds between sonications. Following sonication, samples were spun at 16,500 X g at 4°C for 10 minutes. Lysates were filtered using Amicon Ultra Centrifugal units. Thirty microliters of the filtered lysate were removed and stored as input. Thirty microliters Sterptavidin-conjugated Dynabeads (MyOne C1) (Invitrogen) per reaction were incubated in 200 µl BioID lysis buffer and 200 µl 50 mM Tris-HCl pH 7.5 and allowed to equilibrate at room temperature for 3 minutes. Using a magnetic

rack, supernatant was removed from the beads and filtered lysate was added. Samples were incubated on a rotator at 4°C overnight. Lysate was then removed from the tubes using a magnetic rack and stored as unbound fraction. Beads were incubated with 750 µl wash buffer 1 (2% SDS in MQ water) on a rotator at room temperature for 8 minutes. Wash buffer 1 was removed using a magnetic rack and samples were incubated in 750 µl wash buffer 2 (0.1% deoxycholic acid, 1% Triton-X, 1 mM EDTA, 500 mM NaCl, 50 mM Hepes pH 7.5) on a rotator at room temperature for 8 minutes. Wash buffer 2 was replaced with 750 µl wash buffer 3 (0.5% deoxycholic acid, 0.5% Igepal, 1 mM EDTA, 250 mM LiCl, 10 mM Tris HCl pH 7.5) on a rotator at room temperature for 8 minutes. Beads were then re-suspended in 30 µl 50 mM Tris-HCl , 30 µl 2X MSB (20% glycerol, 4% SDS, 0.13 M Tris-HCl) and 5 µl 1 mM Biotin and boiled at 95°C for 5 minutes. Samples were analyzed using SDS-PAGE western blots.

Halo-Tag Pull-Down

Halo-Tag pull down was performed using the Promega HaloTag Mammalian Pull-Down and Labeling System according to manufacturer protocol (Promega). U2OS cells were transfected with Flag-SOX9 and either Halo-FOXC1 or empty Halo vector. Forty-eight hours post-transfection, cells were washed in ice-cold 1X PBS and then harvested in 2 ml ice-cold 1XPBS. Cells were centrifuged at 2500 X g for 5 minutes at 4°C and PBS was removed. Cell pellets were stored at -80°C overnight. Next, 100 µl HaloLink resin per reaction was equilibrated in 400 µl wash buffer (1X TBS, 1% Igepal). Tubes were centrifuged at 800 X g for 2 minutes and supernatant

was removed. Wash/equilibration was repeated for a total of 3 washes. Cell pellets were thawed on ice for 5 minutes and re-suspended in 300 µl of Mammalian Lysis Buffer (Promega). Six microliters of 50X Protease inhibitor cocktail (Promega) was added, and cells were homogenized using a 25-gauge needle. Samples were centrifuged at 14,000 X g for 5 minutes at 4°C, and lysates were transferred to new tubes. Lysates were diluted with 700µl 1X TBS and 30 µl of the diluted lysate was removed and stored as input. Remainder of lysate was added to the resin and incubated on a rotator for 30 minutes at room temperature. Samples were then centrifuged for 2 minutes at 800 X g and supernatant was removed and stored as unbound fraction. Resin was washed five times with 1 ml wash buffer (1X TBS, 1% Igepal) followed by centrifugation for 2 minutes at 800 X g. Last wash was incubated on rotator for 5 minutes prior to centrifugation. Samples were eluted in 50 µl SDS Elution Buffer (1% SDS, 50 mM Tris-HCl, pH 7.5) and incubated for 30 minutes with shaking at room temperature. Tubes were spun for 2 minutes at 800 X g and elute collected in new tubes. Samples were analyzed using SDS-PAGE western blots.

Statistical Analysis

Statistical analysis (Student's T-Test, Fisher's exact test or one way ANOVA) was performed using SigmaPlot v13, Microsoft Excel v14.7.2, StatPlus v6.2.21, or Bio-Rad CFX Manager v3.0.125.0601.

CHAPTER 3. FOXC1 IS IMPORTANT FOR PRESOMITIC DEVELOPMENT

Somite formation is an important segmentation process occurring early in embryonic development that is common to all vertebrate species (Biris et al., 2007; Giampietro et al., 2009; Kawamura et al., 2005; Pourquie, 2003). This multifaceted differentiation process lays the foundation for the development of the axial skeleton. The somites - epithelial condensations surrounding mesenchymal cores - contain the precursors to the bony and cartilage elements of the axial skeleton as well as the tendons, muscles and skin of the back (Brand-Saberi et al., 1996; Brent et al., 2003; Dubrulle and Pourquie, 2003; Kato and Aoyama, 1998; Ordahl and Le Douarin, 1992). Defects in somite formation lead to abnormal development of the skeleton and can manifest in fused ribs and vertebrae, pebble-like vertebral formation and scoliosis (Cooke and Zeeman, 1976, Sawada et al., 2001 Morales et al., 2002; Shifley et al., 2008, Kume et al., 1998).

Several regulatory pathways and networks drive and regulate somitogenesis. The clock and wavefront segmentation model postulates that cyclic waves of gene expression sweep through the presomitic mesoderm (PSM) in a posterior to anterior manner until they reach a boundary determination front in the anterior PSM (Biris et al., 2007; Campanelli and Gedeon, 2010; Cinquin, 2007; Rawls, 2009; Takahashi et al., 2000). The cells in the anterior PSM, where the wavefront meets the boundary determination front, must be in a permissive state for subsequent

differentiation and mesenchymal to epithelial transformation, allowing the formation of intersomitic boundaries (Cinquin 2007, Sawada et al. 2001). The spatial and temporal expression of the regulatory components involved in somitogenesis are thus crucial for proper somite formation and subsequent skeletal development.

The transcription factor MESP2 has an indispensable role in somitogenesis. *Mesp2* regulates boundary formation and rostro-caudal patterning of the sclerotome (Morimoto et al., 2007). The spatial expression of MESP2 is regulated by the Notch pathway whereas its temporal expression is regulated via the TBX6-RIPPLY regulatory network (Morimoto et al., 2007; Oginuma et al., 2008). *Ripply1* and *Ripply2* are Groucho co-repressors required for somite boundary formation. MESP2 directly binds to the *Ripply2* promoter to activate expression (Morimoto et al., 2007). RIPPLY2 then regulates *Mesp2* expression via a negative feedback loop (Morimoto et al., 2007). In *Ripply2*-null mice the expression of *Mesp2* was prolonged (Morimoto et al., 2007). Similarly, when the zebrafish *Ripply2* orthologue *ripply1* was knocked down, the expression of *mesp-ba*, a *Mesp2* zebrafish orthologue, was expanded (Kawamura et al., 2005). FOXC1 also has a crucial, dose-dependent role in somitogenesis. Loss of *Foxc1* and *Foxc2* expression in mice led to complete lack of somite segmentation and the expression of *Mesp2* was reduced (Kume et al., 2001). When only *Foxc1* was missing the formation of somite-derived axial skeletal structures was abnormal (Kume et al., 2001). When *foxc1* expression in zebrafish was lost, the expression of *mesp-ba* was significantly reduced (Topczewska et al., 2001a). Moreover, zebrafish embryos with a chromosomal deletion encompassing

the complete *foxc1a* loci had lack of formation of the anterior somites and reduced expression of *mesp-ba* (Hsu et al., 2015). These findings suggest that FOXC1 has an important regulatory role of MESP2 expression and somitogenesis.

My goal was to analyze the role of Foxc1 in the regulation of *mesp-ba* expression and somite formation. We hypothesized that this regulation is achieved through a genetic interaction between *foxc1a* and *ripply1*.

RESULTS

To gain insight into the role of Foxc1a in somitogenesis, a well-characterized antisense morpholino-modified oligonucleotide (MOs) was injected into zebrafish embryos at the 1-2 cell stage (Thisse, 2005; Topczewska et al., 2001a). This MO targets the *foxc1a* mRNA translation start site, leading to a reduced expression of the Foxc1a protein in these embryos. The optimal morpholino dose for these injections was determined by injecting WT embryos with 1.63-9.8 ng/embryo *foxc1a* MO and comparing the resulting phenotype to previously published results (Thisse, 2005; Topczewska et al., 2001a). The optimal concentration for an efficient *foxc1a* knockdown that would also result in the least amount of embryo lethality was determined to be 6.5 ng/embryo. As shown previously, injections with the *foxc1a* MO resulted in lack of somite formation at 12.5 hours post fertilization (hpf), compared with control-injected embryos which were at the 3-somite stage at this time point (Figure 3.1A, B). Similarly, no morphological segmentation was observed at 14 hpf, when control embryos were at the 9-somite stage (Figure 3.1A', B'). At 22 hpf posterior somites did form in both the *foxc1a* morphants and the control injected embryos (Figure 3.1A", B"). The expression of *mesp-ba* in the control-injected embryos was detected as 1-3 bands in the anterior PSM at 12.5, 14, and 22 hpf (Figure 3.1D, E, F, respectively). In the *Foxc1*-MO-injected embryos, the expression of *mesp-ba* was reduced at all tested time points (Figure 3. 1D', E', F'). These results suggest that loss of *foxc1a* expression results in defects in early somitogenesis and reduced expression of the boundary determination gene *mesp-ba*.

In order to validate the specificity of the knockdown effect, zebrafish embryos were co-injected with *foxc1a* MO and 20 pg *foxc1a* mRNA which is resistant to the morpholino. In these embryos somite formation proceeded normally and at a comparable rate to that of the control-injected embryos at 14 hpf (Figure 3.2A, C). In the control-injected embryos, *mesp-ba* expression was detected in 1-3 bands in the anterior PSM throughout somitogenesis (Figure 3.2A'). In the *foxc1a*-morphants, the expression of *mesp-ba* was reduced in the anterior PSM (Figure 3.2B'). When *foxc1a*-mRNA was injected in addition to the *foxc1a* MO, the *mesp-ba* expression pattern was rescued to the level observed in the control embryos (Figure 3.2C').

Figure 3.1 *Foxc1a* Knockdown Results in Lack of Anterior Somite

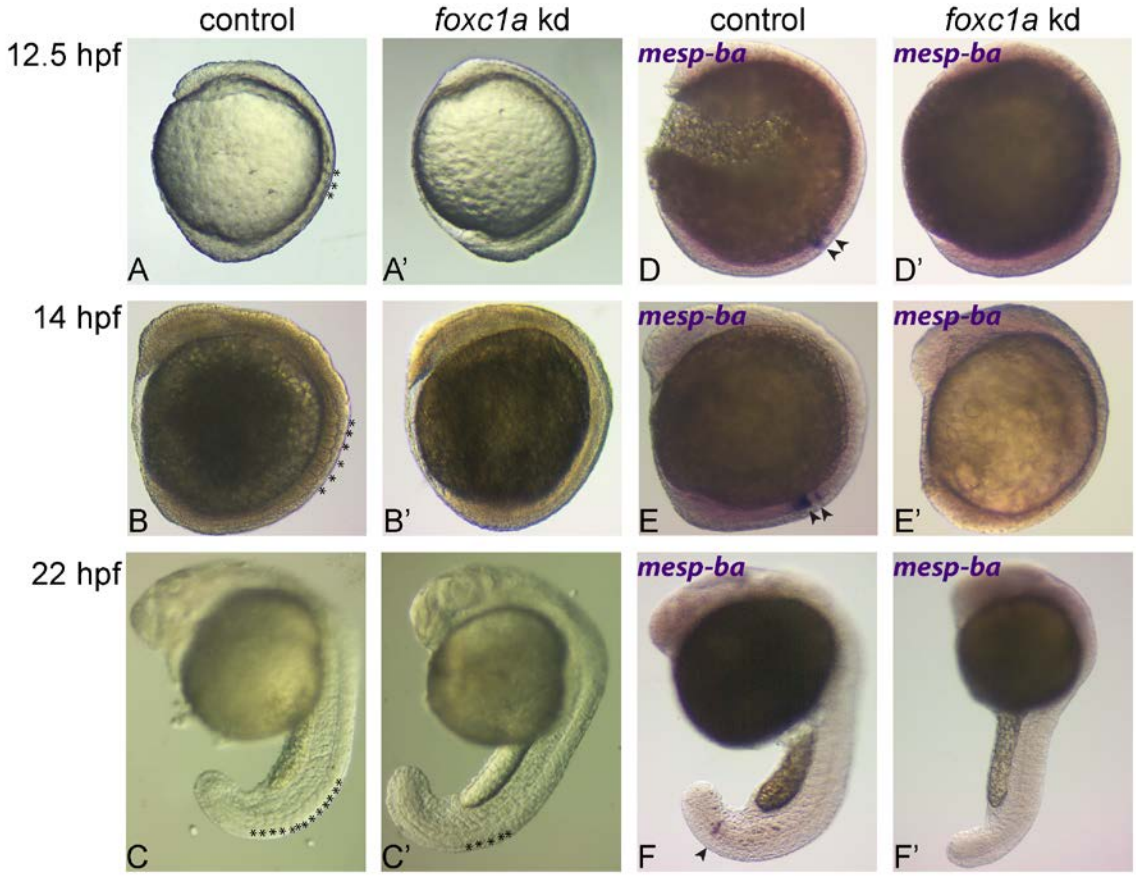

Figure 3.1 *foxc1a* Knockdown Results in Lack of Anterior Somite Formation and Reduced *mesp-ba* Expression. In control-injected embryos, morphological somite formation was apparent at 12.5, 14, and 22 hpf (asterisks denote morphological somites) **(A, B, C)**. In the *foxc1a* morphants, development of the anterior somites was halted at 12.5 and 14 hpf, whereas posterior somites were observed at 22 hpf **(A', B', C')**. The expression of *mesp-ba* in control embryos was observed as one or two bands in the anterior PSM (black arrowheads) **(D, E, F)**, but was reduced in the *foxc1a* morphants at all time points tested **(D', E', F')**. Images are representative of multiple replications. n>100 in all groups.

Figure 3.2 Co-injecting *foxc1a* mRNA with the *foxc1a* Morpholino Rescues Somite Formation and *mesp-ba* Expression

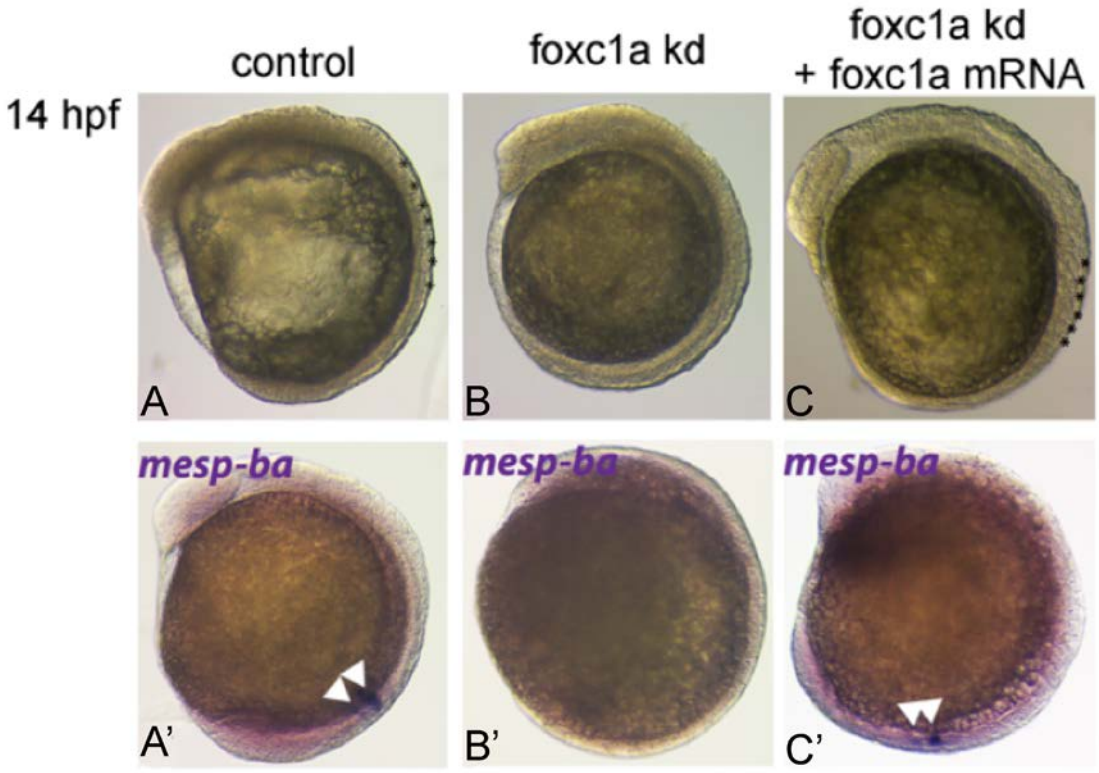

Figure 3.2 Co-injecting *foxc1a* mRNA with the *foxc1a* Morpholino Rescues Somite Formation and *mesp-ba* Expression. In the control embryos 7-9 somites formed at 14 hpf (asterisks) **(A)** and 1-2 stripes of *mesp-ba* expression were observed in the anterior PSM (white arrowheads) **(A')**. In the *foxc1a* morphants no somites were observed **(B)** and *mesp-ba* expression was reduced or missing **(B')**. Co-injections of *foxc1a* mRNA with the *foxc1a* morpholino resulted in 7-9 somites (asterisks) **(C)** and rescue of the *mesp-ba* expression (white arrowheads) **(C')**.

The similarities between the published *ripply1* knockdown morphological phenotype, notably the lack of segmentation of the PSM and expanded expression of *mesp-ba* and *tbx6* (Kawamura et al., 2005), and the opposite effect seen on *mesp-ba* expression in the *foxc1a* morphants led us to hypothesize that Foxc1a might be interacting with the Tbx6-Ripply network to regulate *mesp-ba* expression. To analyze this potential interaction, the expression of *tbx6* in the *foxc1a* morphants was assessed first (Figure 3.3). In the control-injected embryos, *tbx6* was detected throughout the PSM, but not in the tailbud (Figure 3.3A, B, C). In *foxc1a* morphants the expression domain of *tbx6* appeared smaller and more anteriorly shifted compared to control embryos (Figure 3.3A', B', C'). Next, a previously characterized translation-blocking *ripply1* morpholino (Kawamura et al., 2005) was utilized in order to determine whether *foxc1a* genetically interacts with *ripply1* to regulate the expression of *tbx6* and its downstream target *mesp-ba*. When *ripply1* was knocked down in zebrafish embryos a complete lack of somite formation was observed both at 12.5 hpf and 22 hpf (Figure 3.4A", B"). The expression domains of *tbx6* and *mesp-ba* in the *ripply1* morphants extended anteriorly into the somitic mesoderm (Figure 3.4C"-F"). Interestingly, when *ripply1* and *foxc1a* were knocked down together, anterior somites failed to form (Figure 3.4A'"), while posterior somites did form (Figure 3.4B'"), resembling the morphological phenotype seen in the *foxc1a* single morphants (Figure 3.4A', B', respectively). However, *mesp-ba* was detected in 2-3 bands in the anterior PSM (Figure 3.4C, D, C'", D'"), and the *tbx6* expression domain was also restored in the PSM (Figure 3.4E, E'", F, F'"). These results suggest that

mesp-ba and *tbx6* expression were both rescued throughout somitogenesis in the *foxc1a-ripply1* double morphants.

Figure 3.3 The Expression Domain of *tbx6* is Altered When *foxc1a* is Knocked Down

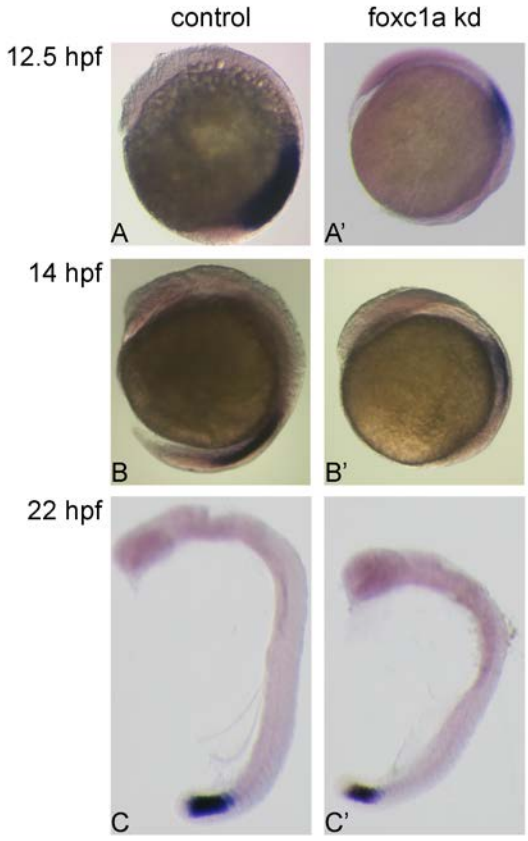

Figure 3.3 The expression domain of *tbx6* is altered when *foxc1a* is knocked down. In control-injected embryos, *tbx6* expression begins near the tailbud and expands anteriorly up to the boundary determination front at 12.5, 14 and 22 hpf **(A, B, C)**. In *foxc1a* morphants, the expression domain of *tbx6* was smaller and was shifted more anteriorly at all time points tested **(A', B', C')**. Images are representative of multiple experiments. n>50 in all groups.

Figure 3.4 The Expression of *mesp-ba* and *tbx6* is Restored in *foxc1a-ripply1* Double Morphants

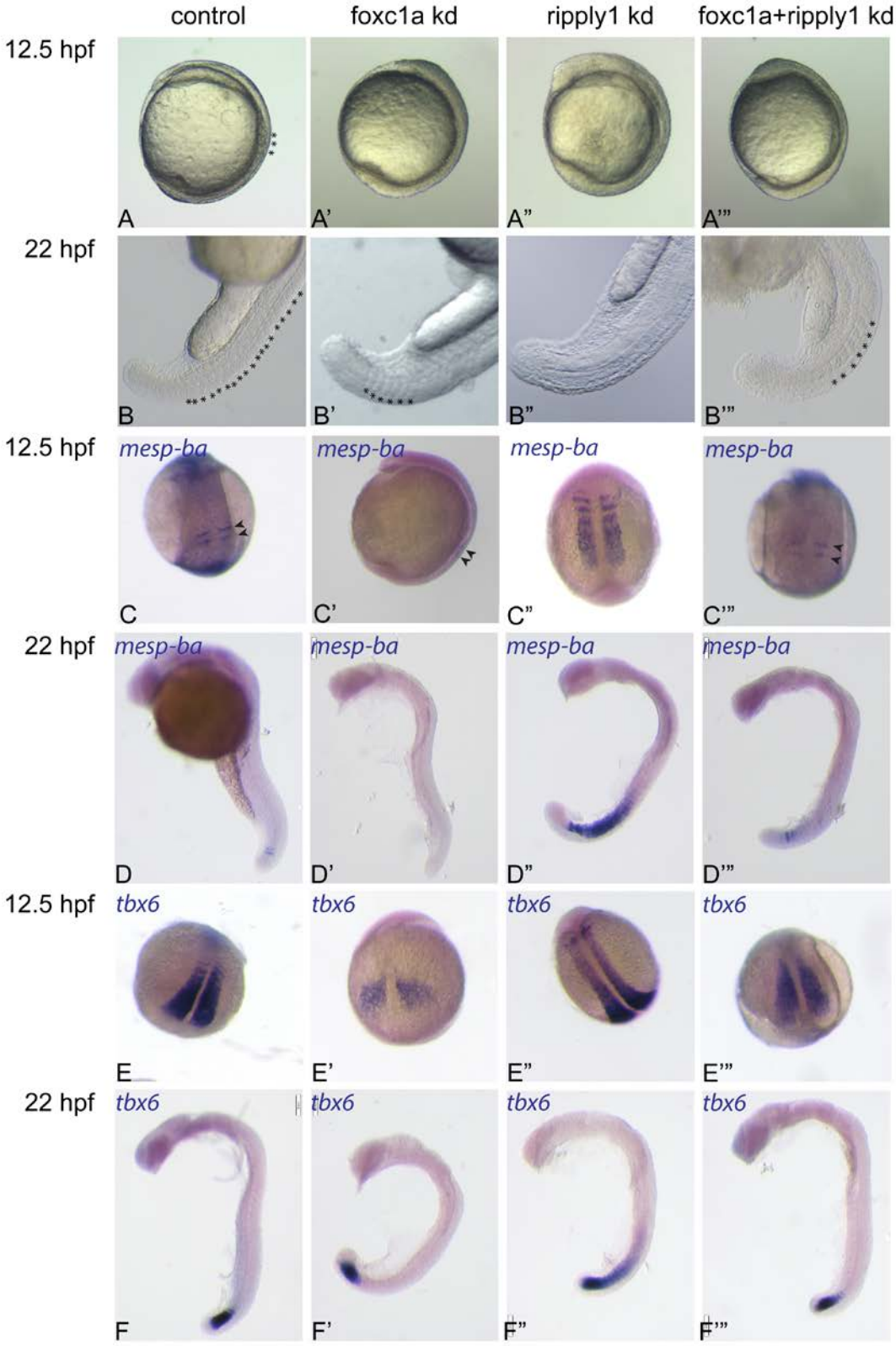

Figure 3.4 The Expression of *mesp-ba* and *tbx6* is Restored in *foxc1a-ripply1* Double Morphants. In control embryos at 12.5 hpf, 3 somites developed **(A)**, whereas no somites were observed in age-matched *foxc1a* morphants **(A')**, *ripply1* morphants **(A")**, or *foxc1a-ripply1* double morphants **(A'")**. At 22 hpf, 17-18 segmented somites were seen in control embryos **(B)**, whereas only 6-9 somites were observed in the *foxc1a* morphants **(B')**. No segmented somites were seen in the *ripply1* morphants **(B")**, and 6-9 posterior somites were observed in the *foxc1a-ripply1* double morphants **(B'")**. The expression of *mesp-ba* in control embryos was detected as 1-2 bands at 12.5 and 22 hpf **(C, D)** (black arrowheads). In *foxc1a* morphants *mesp-ba* expression was missing or markedly reduced at 12.5 and 22 hpf **(C', D')**. In *rippy1* morphants *mesp-ba* expanded anteriorly at both time points **(C", D")**. The *foxc1a-rippl1y1* double morphants had 1-3 bands of *mesp-ba* expression at both 12.5 and 22 hpf **(C'", D'")**. The expression of *tbx6* in control-injected embryos was detected in the entire PSM at 12.5 and 22 hpf **(E, F)**. In *fox1a* morphants *tbx6* expression was reduced and spanned a smaller domain **(E', F')**. In *ripply1* morphants the expression of *tbx6* expanded anteriorly at both 12.5 and 22 hpf **(E", F")**. The expression domain of *tbx6* in the *foxc1a-ripply1* double morphants was comparable to that seen in the control embryos, and spanned the entire PSM at both time points tested **(E'", F'")**. Asterisks indicate morphological somites.

The *foxc1a* single-morphants and *foxc1a-ripply1* double-morphants seemed to be smaller relative to control morphants, suggesting that the absence of Foxc1a led to impaired axial growth in these fish. To assess embryo elongation, the angle formed between the anterior-most (head) and posterior-most (tailbud) points of the embryos was blindly measured at 12.5 hpf. As the embryo elongates, the head and the tail approach each other on either side of the yolk, forming a smaller angle, until the tailbud detaches from the yolk and the embryo begins to elongate in a more linear fashion (beginning at around 16.5 hpf). Due to the observed defects in somite formation, these measurements were done in age-matched embryos instead of staged embryos. Interestingly, the *foxc1a*-morphants were significantly smaller than their age-matched controls, whereas there was no significant difference between the *ripply1*-morphants and the control embryos (Figure 3.5). The size of the double *foxc1a-ripply1*-morphants was similar to the *foxc1a*-morphants, again being significantly smaller than their age-matched controls. These results suggest that embryo elongation was delayed in the absence of *foxc1a*, and that this phenomenon was not rescued when *ripply1* expression was also reduced.

Figure 3.5 *Foxc1a* Morphants Elongate at a Slower Pace than Control-Injected Siblings

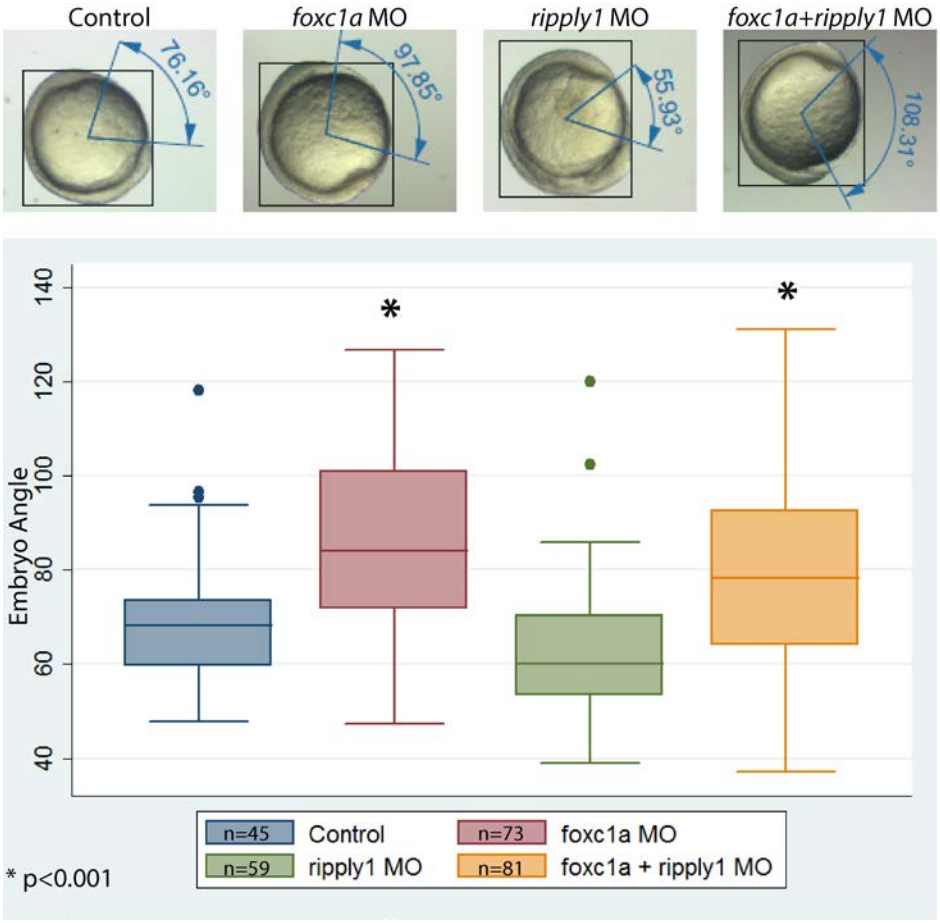

Figure 3.5 *foxc1a* Morphants Elongate at a Slower Pace than Control-injected Siblings. The angles formed between the anterior-most part of the embryo (head) and posterior-most part (tail) measured at 12.5 hpf was significantly larger in *foxc1a* single morphants and *foxc1a-ripply1* double morphants compared to control-injected embryos. The size of *ripply1* morphants was not significantly different than controls.

Normal segmentation of the paraxial mesoderm is highly dependent on the establishment of opposing FGF8 and Retinoic acid (RA) gradients (Dequeant and Pourquie, 2008). When these gradients are disrupted, somite formation and *mesp-ba* expression are affected (Dequeant and Pourquie, 2008). The delays observed in embryo elongation raised the idea that the defects observed in somite formation could result from interference of these gradients. To address this, the expression of *raldh2* (which encodes an enzyme required for the activation of RA) and *fgf8a* were examined in the *foxc1a*- and *ripply1*- single morphants and in the *foxc1a-ripply*1 double morphants (Figure 3.6). In control embryos, *fgf8a* was detected in 2-3 stripes in the midbrain-hindbrain boundary, in the tailbud and in the posterior PSM (purple). The expression of *raldh2* was detected in the anterior PSM (orange, in brackets). These two expression domains did not overlap (Figure 3.6A). In the *foxc1a* single morphants, the positioning of the *raldh2* expression domain relative to that of *fgf8a* was altered; *fgf8a* was detected in the midbrain-hindbrain boundary but was reduced in the tailbud and in the posterior PSM and midbrain-hindbrain boundary. The expression of *raldh2* spanned a smaller domain in the PSM resulting in a larger gap between the expression of *fgf8a* in the tailbud and the expression of *raldh2* in the PSM than the gap seen in control embryos (Figure 3.6B, brackets). In the *ripply1* morphants, the expression of *fgf8a* in the PSM expanded anteriorly and overlapped with that of *raldh2* (Figure 3.5C, brackets). The expression domain of *raldh2* was stronger and expanded compared to controls and covered a larger portion of the PSM, resulting in a smaller distance between the expression domains of these two genes. Finally, in the *foxc1a-ripply1* double morphants the expression

of *fgf8a* was strong in the tailbud but lower in the PSM. The expression of *raldh2* spanned a similar size domain to that seen in the control embryos. The gap between *raldh2* expression and *fgf8a* expression in the posterior PSM also resembled that seen in the controls (Figure 3.6D). This shift in expression manifests in anterior somites more robustly because the requirement for RA signaling decreases in later stage of somitogenesis and therefore posterior somites are less sensitive to these *raldh2* fluctuations (Sirbu and Duester, 2006). These observations demonstrate that *foxc1a* controls somite formation through the regulation of the retinoic acid gradient in the PSM.

Figure 3.6 The Expression of *fgf8a* and *raldh2* in the Double Morphants Resembles that of the Control Embryos

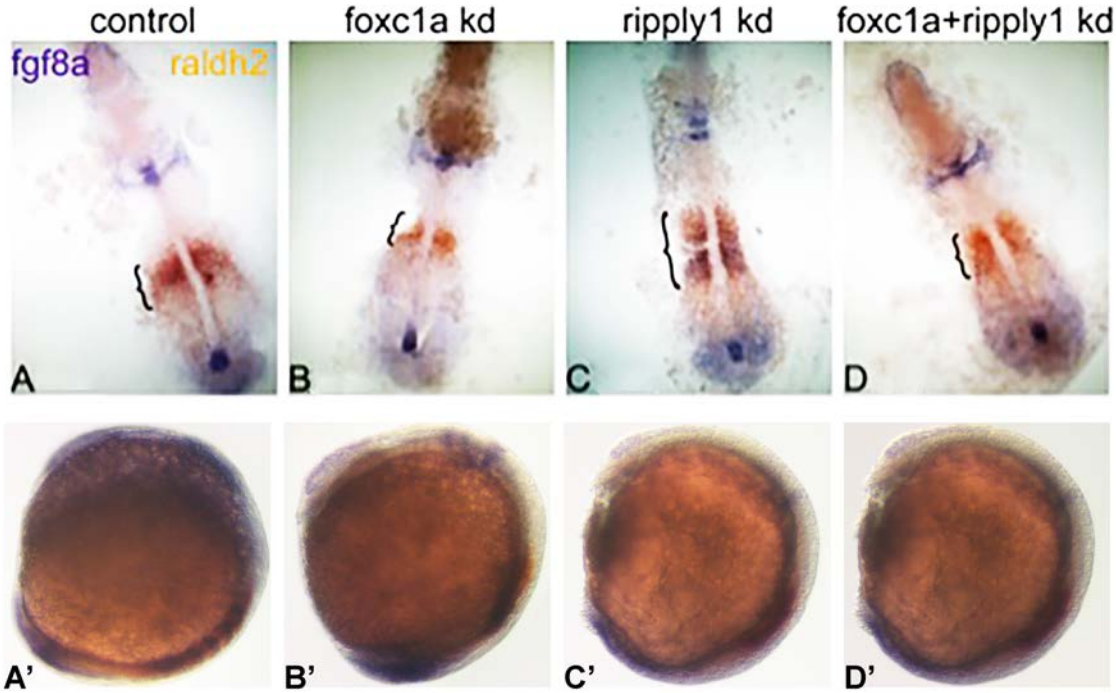

Figure 3.6 The Expression Domain of *raldh2* is Rescued in the Double Morphant Embryos. (A, A') In control-injected embryos, the expression of *raldh2* (orange) was strongly detected in the anterior PSM (black brackets). The expression of *fgf*8a was strongest in the tailbud, and did not overlap with *raldh2* expression in the PSM. **(A')** Sagittal view. **(B, B')** In *foxc1a* morphants the expression domain of *raldh2* (in brackets) was smaller than in the controls, and the expression of *fgf8a* was less intense than in controls and expanded anteriorly. **(B')** Sagittal view. **(C, C')** In the *ripply1* morphants, the expression of *raldh2* spanned a bigger domain and overlapped with the expression of *fgf8a* in the PSM. **(C')** Sagittal view. **(D, D')** In the *foxc1a-ripply1* double morphants the expression domain of *raldh2* resembled that of the control embryos, and did not overlap with *fgf8a* expression in the PSM. **(D')** Sagittal view.

Our lab was recently granted access to *foxc1a* mutant zebrafish. These fish – *foxc1a*^{UA1017} – have a 7 base-pair deletion upstream of the forkhead domain causing a frame-shift mutation and a premature stop codon. The resulting protein is predicted to have 38 amino acids, of which only 12 amino acids match the WT, suggesting the *foxc1a*^{UA1017} is a null allele (Figure 3.7A). To characterize somite formation in these zebrafish mutants, heterozygous parents were crossed and somite formation in the homozygous mutant progeny was observed. Unlike the *foxc1a* morphants, somite formation was observed at 14 hpf in the *foxc1a*^{UA1017} homozygous mutants as well as in the heterozygous and WT siblings (Figure 3.7B). Additionally, all of these embryos appear to grow and elongate at a similar rate regardless of genotype. Interestingly, the expression of *mesp-ba* was reduced in 38.5% of the homozygous *foxc1a*^{UA1017} mutants and undetected in 61.5%, compared to normal *mesp-ba* expression in 89% and 80% of the WT and heterozygous siblings, mimicking what was seen in the *foxc1a* morphants. These observations were statistically significant using Fisher's exact test ($p=1.4x10^{-6}$) (Figure 3.7B, Table 3.1). When the *ripply1* MO was injected into these embryos, somite formation was observed in only 6% of embryos (4/65), while 94% (61/65) lacked morphological somites at 14 hpf. The expression of *mesp-ba* appeared to be normal in 14 embryos (Figure 3.8A), 5 embryos had slightly elevated expression (Figure 3.8B) and 29 embryos had greatly expanded *mesp-ba* expression, similar to what was seen in the *ripply1* single morphants (Figure 3.8C). Analysis of the genotypes of these zebrafish embryos revealed that 78.5% of the WT and 72% of the heterozygous mutants had expanded *mesp-ba* expression compared to zero of the

homozygous mutants. In contrast, only 21.5% and 12% of the WT and heterozygous embryos, respectively, had normal *mesp-ba* expression, whereas 89% of the homozygous mutants had 1-3 stripes of *mesp-ba* detected in the anterior PSM. Statistical analysis using Fisher's exact test indicated that these findings are statistically significant ($p=3.3x10^{-5}$). These observations are summarized in Table 3.2.

Figure 3.7 *foxc1a*^{UA1017} Mutants Develop Somites but *mesp-ba* Expression is Still Reduced

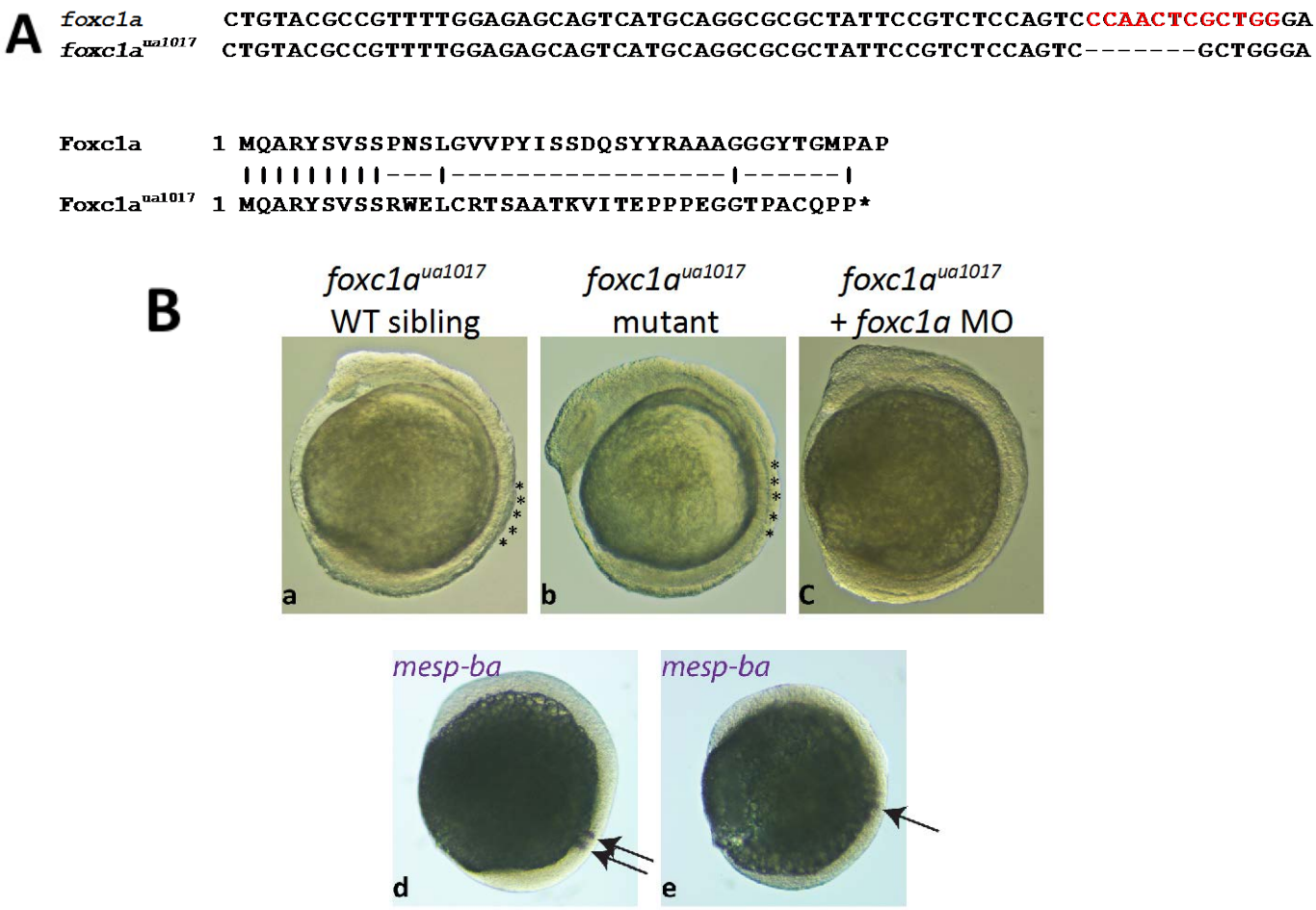

Figure 3.7 Characterization of the *foxc1a*^{UA1017} mutation. (A) The *foxc1*^{UA1017} mutation consists of a seven base-pair deletion upstream of the *foxc1a* forkhead domain and is predicted to result in a truncated protein of 38 amino-acids, of which only 12 correspond to the WT protein. **(B)** *foxc1a*^{UA1017} homozygous mutants (b) and WT siblings (a) develop anterior somites at 14 hpf (asterisks). Injections of *foxc1a* MO into the *foxc1a*^{UA1017} resulted in lack of anterior somite formation (c). The expression of *mesp-ba* in *foxc1a*^{UA1017} homozygous mutants is reduced (d), whereas in heterozygous and WT siblings (e) it was detected as two stripes in the anterior PSM (black arrows).

Table 3.1 The Expression of *mesp-ba* is Reduced in *foxc1a*^{UA1017} Homozygous Mutants

	Normal (%)	Reduced (%)	No signal (%)	Total
WTs	8 (89%)	1 (11%)	-	**9**
Heterozygotes	16 (80%)	2 (10%)	2 (10%)	**20**
Mutants	-	5 (38.5%)	8 (61.5%)	**13**
Total	**24**	**8**	**10**	**42**

Table 3.1 The expression of *mesp-ba* is reduced in *foxc1a*^{UA1017} homozygous mutants. The *foxc1a*^{UA1017} homozygous mutants had either reduced *mesp-ba* expression (38.5%) or no expression (61.5%). The majority of heterozygous mutants (80%) had normal *mesp-ba* expression, with only 20% having reduced or no expression. The expression of *mesp-ba* was detected in all wild-type siblings, whereas 89% had normal and 11% had reduced expression. $p=1.4x10^{-6}$ using Fisher's exact test.

Figure 3.8 *ripply1* Knockdown Leads to Rescue of *mesp-ba* Expression in the Absence of *foxc1a*

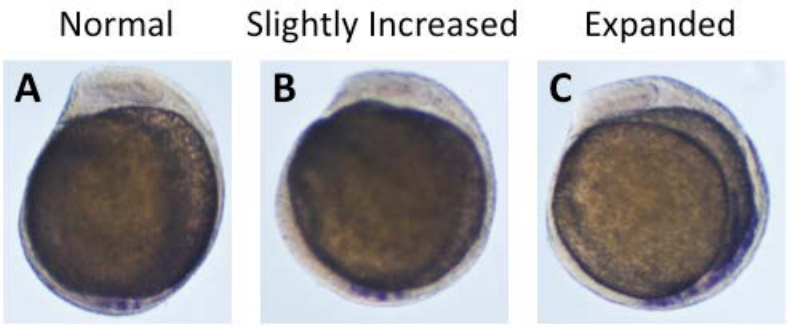

Figure 3.8 *ripply1* Knockdown Leads to Rescue of *mesp-ba* Expression in the Absence of *foxc1a*. **(A)** Normal *mesp-ba* expression appears as 1-3 bands in the anterior PSM. **(B)** Slightly increased *mesp-ba* expression appears as 4-6 stripes and **(C)** Expanded expression has >6 stripes of *mesp-ba*. Representative images.

Table 3.2 Knocking Down *ripply1* in *foxc1a*^{UA1017} Mutants Results in Rescue of *mesp-ba* Expression.

	Normal	Slightly Increased	Expanded	**Total**
WTs	3 (21.5%)	-	11 (78.5%)	**14**
Heterozygotes	3 (12%)	4 (16%)	18 (72%)	**25**
Mutants	8 (89%)	1 (11%)	-	**9**
Total	**14**	**5**	**29**	**48**

Table 3.2 Knocking down *ripply1* in *foxc1a*^{ua1017} mutants results in rescue of *mesp-ba* expression. Eighty-nine percent of homozygous mutants had normal *mesp-ba* expression; none had expanded expression. One homozygous mutant had a slightly increased *mesp-ba* expression (11%). In contrast, 78.5% of WT embryos and 72% of heterozygous mutants had expanded *mesp-ba* expression, and 16% of heterozygous mutants had slightly increased expression. Only 21.5% and 12% of WT and heterozygous mutants, respectively, had normal *mesp-ba* expression. $p=3.3x10^{-5}$ using Fisher's exact test.

In order to evaluate the differences observed between the *foxc1a* morphants and the *foxc1a* homozygous mutants the *foxc1a* MO was injected into the heterozygous *foxc1a*^{UA1017} crossed embryos. The observed phenotypes in these progeny resembled those seen in the *foxc1a* morphants and not of the *foxc1a*^{UA1017} homozygous mutants; the anterior somites failed to develop and the expression of *mesp-ba* was reduced in all the embryos regardless of genotype. A previous study using *foxc1a* mutant line, *foxc1a*^{nju18}, also reported that formation of the anterior somites and *mesp-ba* expression appeared normal in their homozygous mutant embryos (Li et al., 2015). This suggests that the effects seen in the *foxc1a* morphants could either be due to a more efficient knockdown of the Foxc1a protein, or due to a secondary effect of the *foxc1a* morpholino. However, the success of the rescue experiments suggest that the *foxc1a* morphant phenotype is specific to loss of Foxc1a in the injected embryos. I therefore turned to analyze the protein product of the UA1017 and nju18 mutations. Analysis of the *foxc1a* gene sequences of both the nju18 and UA1017 mutations revealed that although both mutations introduce stop codons into the gene sequence, resulting in truncation of the protein upstream of the forkhead domain, there are downstream methionine residues before the Forkhead domain that could reinitiate translation of the mRNA. In the UA1017 allele, alternate translation would be starting at basepair 210 whereas in the nju18 allele a methionine could form starting at position 207. This means that transcription of these genes could result in truncated, active *foxca1* alleles. To assess this possibility, plasmids containing the *foxc1a*^{UA1017} and *foxc1*^{nju18} mutations were designed by Dr. Fred B. Berry (FBB) and acquired from IDT. Western blot

analysis performed by FBB revealed that Foxc1a proteins are detected in both mutations although they seem to be slightly smaller than the WT protein (Figure 3.9). Transactivation assays performed using the three alleles of Foxc1a and a 6X Foxc1 BS reporter resulted in a 40-fold increased activation of the WT Foxc1a compared with empty pGL4.23, indicating that the zebrafish Foxc1a protein is able to bind and activate the FOXC1 reporter. Expression of Foxc1a^{UA1017} resulted in more than 14-fold activation, and Foxc1a^{nju18} resulted in a 3-fold activation of the FOXC1 reporter. These results indicate that both *foxc1a*^{UA1017} and *foxc1a*^{nju18} retain the ability to produce a partially functional form of the Foxc1a protein although with reduced ability to activate the Foxc1 target binding site.

Since the *foxc1a* morpholino is translation-blocking it is not effective against existing mRNA, so the presence of maternal *foxc1a* mRNA in the zygote could still result in translation of Foxc1a. To exclude the possibility that some of the differences observed between the *foxc1a* morphants and the two *foxc1a* mutant lines were the result of maternally-contributed *foxc1a* mRNA, mRNA was collected from wild-type embryos at the 1-2 cell stage as well as embryos at 12.5 hpf, and RT-PCR was used to amplify *foxc1a*. Maternally expressed *ef1α* and non-maternally-expressed *tal1* were used for comparison as positive and negative controls, respectively. While *ef1α* was amplified from the sample collected from the 1-2 cell stage embryos, no *foxc1a* or *tal1* were detected (Figure 3.10). In the 12.5hpf, both *ef1α* and *foxc1a* have been amplified, but not *tal1*, which is not predicted to be expressed until later in development (Fleisch et al., 2013). Taken together, these results demonstrate that the differences observed between the *foxc1a* morphants, in

which anterior somite formation appears to be halted, and the *foxc1a* mutants, in which the somites do form despite decreased expression of *mesp-ba,* are the result of an incomplete reduction of Foxc1a protein function in the mutant fish.

Figure 3.9 Luciferase Transactivation Assays Demonstrate that Foxc1a^{UA1017} and Foxc1a^{nju18} are Both Functional Proteins Capable of Activating the FOXC1 6X Binding Site Reporter

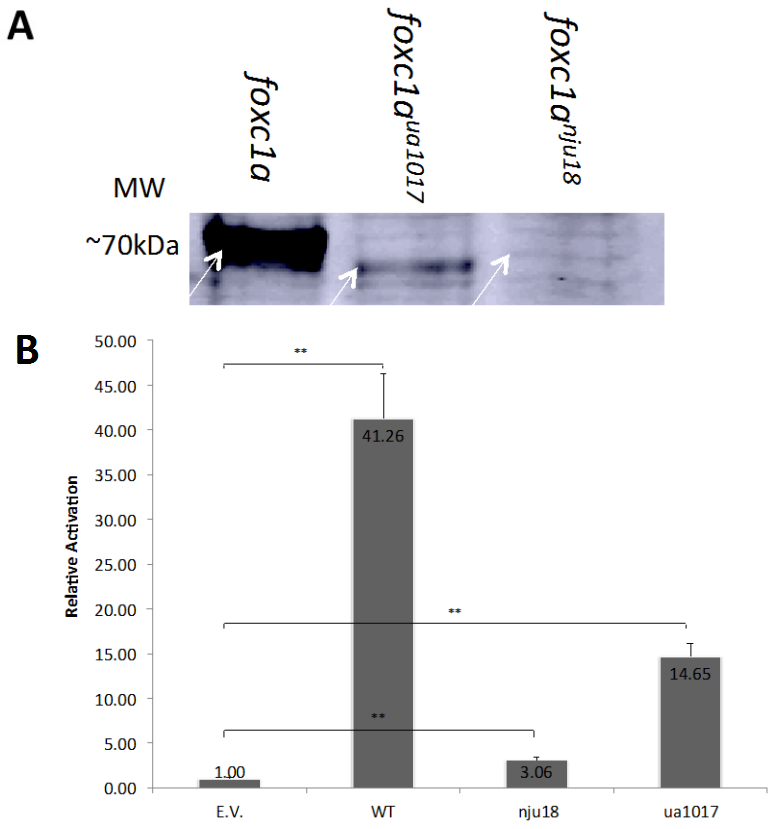

Figure 3.9 Luciferase Transactivation Assays Demonstrate that Foxc1a^{UA1017} and Foxc1a^{nju18} are Both Functional Proteins Capable of Activating the FOXC1 6X Binding Site Reporter. (A) Western blot analysis of *foxc1a*, *foxc1a^{UA1017}* and *foxc1a^{nju18}*. White arrows point to detected proteins. Membrane was blotted with αFoxc1 antibody (Table 2.6). **(B)** Expression of WT Foxc1a protein resulted in 41.26-fold activation of the FOXC1 6X BS reporter, compared to empty pGL4.23 vector. Expression of Foxc1a^{nju18} resulted in 3-fold increase in activation, and Foxc1a^{UA1017} resulted in 14.65-fold activation. Error bars represent standard deviation of three independent biological replicates. Statistical significance was determined using the Mann-Whitney U test. Error bars represent standard deviation from three biological replicates.

Figure 3.10 *foxc1a* is Not Maternally Contributed to Zebrafish Embryos in the 1-2 Cell Stage

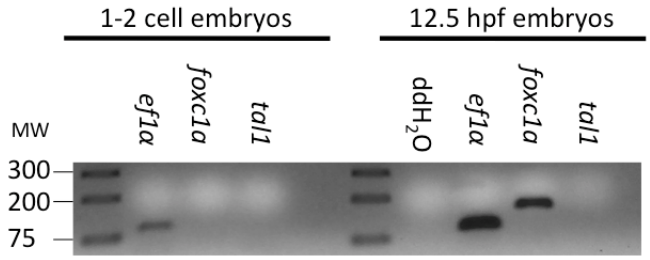

Figure 3.10 *foxc1a* is not maternally contributed to zebrafish embryos in the 1-2 cell stage. PCR amplification demonstrating that *foxc1a* was not detected in 1-2 cell embryos, whereas it was amplified in 12.5 hpf embryos. A positive control, *ef1α*, which is maternally contributed to the developing embryo, is detected in both the 1-2 cell stage and the 12.5 hpf embryos; *tal1,* which is not maternally contributed nor expressed at 12.5 hpf embryos, was not detected in either sample.

DISCUSSION

My results demonstrate that *foxc1a* genetically interacts with *ripply1* to regulate the expression of *mesp-ba* and *tbx6* expression through regulation of the RA pathway in the PSM. In recent years there has been accumulating evidence suggesting the Foxc1 has an important role in somitogenesis and subsequent axial skeletal development (Kume et al., 2001; Li et al., 2015; Skarie and Link, 2009; Topczewska et al., 2001a). Mice with null *Foxc1* mutations have defects in the development somite-derived axial skeletal elements such as incomplete formation of the neural arches and misshapen vertebrae (Kume et al., 2001). In zebrafish, disruption of the Foxc1a protein results in lack of somite formation at the 7-somite stage (Topczewska et al., 2001a). More recently, it has been shown that formation of the anterior somites was altered in a *foxc1a* mutant line (Li et al., 2015). However, how *foxc1a* exerts its function on somitogenesis is still not clearly understood. This report shows that *foxc1a* and *ripply1* genetically interact to regulate the expression of *mesp-ba* and the formation of the somites in the PSM. For this analysis, morpholino-mediated gene knockdowns were utilized to evaluate the function of Foxc1 during somitogenesis and to assess the mechanisms through which Foxc1 acts to regulate *mesp-ba* expression. These *foxc1a*-morpholinos are well characterized, and have been used in the past to study several developmental processes such angiogenesis and cardiac development (Acharya et al., 2011; Skarie and Link, 2009; Veldman and Lin, 2012). When *foxc1a* was knocked down in zebrafish embryos, a lack of anterior somite formation was observed, whereas the

posterior somites continued to form normally. This is not a result of transient efficacy of the morpholino, given that reduced expression of *mesp-ba* in these embryos was observed at later time points as well as the effect seen on the expression domain of *tbx6*, which was smaller and more anteriorly positioned in the morphants compared to the control-injected embryos. These phenotypes have also been successfully rescued by co-injections of the *foxc1a*-MO with *foxc1a* mRNA, suggesting they are specific to the reduced expression of Foxc1a.

Mammals have two *Foxc* paralogues, *Foxc1* and *Foxc2*. Zebrafish, on the other hand, have no *Foxc2* orthologue but two paralogues of *Foxc1*, *Foxc1a* and *Foxc1b* (Topczewska et al., 2001a). Both *Foxc1* and *Foxc2* are expressed in the mouse PSM, however the phenotypes observed in the compound, homozygous $Foxc1^{-/-}$ $Foxc2^{-/-}$ mouse embryos are much more severe than those observed in the single *Foxc1*-null or *Foxc2*-null mice, suggesting that these two genes share some compensatory roles. In zebrafish, on the other hand, the phenotypes observed in the double *foxc1a*/*foxc1b* knockdown embryos closely resemble those of a single *foxc1a* knockdown, and knocking down *foxc1b* alone does not appear to inhibit somite formation (Topczewska et al., 2001b). The focus of this project was therefore to utilize the simplified zebrafish animal model to discern the role of *foxc1a* in somitogenesis.

In addition to the lack of formation of anterior somites following a *foxc1a* knockdown, *mesp-ba* expression was reduced throughout somitogenesis, and the *tbx6* expression domain was shifted anteriorly and seemed smaller than in the

control-injected animals. When *ripply1*, a part of the Mesp-ba–Tbx6 regulatory network, was knocked down, a complete lack of somite formation was seen, and the expression domains of both *mesp-ba* and *tbx6* expanded anteriorly due to lack of repression in the absence of Ripply1. Surprisingly, knocking down *foxc1a* and *ripply1* together resulted in a morphological phenotype resembling that of the *foxc1a* single morphants, with a lack of anterior somite formation and restored formation of the posterior somites. The expression of *mesp-ba* and *tbx6* was rescued and resembled those seen in control embryos. Interestingly, the *foxc1a* morphants displayed a significant delay in embryonic elongation compared to both the *ripply1* morphants and controls. This elongation delay was not rescued in the double *foxc1a-ripply1* morphants, which led to the hypothesis that the anterio-posterior gradients in the PSM are affected in the *foxc1a* morphants. The expression of these gradients was analyzed next, through the expression patterns of *fgf8a* and *raldh2*, components of the Fgf and retinoic acid signaling pathways, respectively. In control-injected embryos, *raldh2* was detected in the anterior PSM, whereas *fgf8a* expression was observed in the posterior PSM and in the tailbud. Their expression domains were detected immediately adjacent to one another, with no overlap. In the *foxc1a* morphants, these expression domains were further away from each other. The expression of *raldh2* spanned a smaller domain in the anterior PSM, creating a gap between the posterior boundary of *raldh2* and the anterior boundary of *fgf8a* expression in the posterior PSM. In contrast, *fgf8a* expression extends anteriorly in the *ripply1* morphants, overlapping with the expression domain of *raldh2*. Strikingly, both of these phenotypes were rescued in the double morphants

and the expression domains of *raldh2* and *fgf8a* were restored; they were detected adjacent to one another but not overlapping. This suggests that the Fgf-RA gradients are altered in the absence of *foxc1* or *ripply1*, but these effects are countered when both of these gene products are missing together.

Furthermore, the findings outlined here demonstrate that *mesp-ba* expression can be detected in the absence of *foxc1a,* when *ripply1* is also reduced. This indicates that Foxc1a does not directly regulate expression of *mesp-ba*. Instead, Foxc1a is required to establish the permissibility of the anterior PSM by regulating the FGF8a-RALDH2 gradient balance. When Foxc1a is absent elongation is delayed, resulting in an altered balance between the FGF and RA opposing gradients in the PSM. Previously it has been shown that RA directly down-regulates the expression of FGF8 in the PSM to define the position of the determination front. MESP2 can be expressed, and the segmental pre-pattern established, only when the level of FGF8 goes below a certain threshold (Dubrulle et al., 2001; Dubrulle and Pourquie, 2004b). It has also been demonstrated that the antagonistic gradients of retinoic acid and FGF signaling are required for determination of intersomitic boundaries and for permitting the expression of *Mesp2* and that a disruption of these opposing gradients affects *Mesp2* expression (Goldbeter et al., 2007). Moreover, in 2006 Sirbu and Duester demonstrated that retinoic acid signaling is only necessary for normal formation of the anterior somites. They have also shown that changes in the retinoic acid gradient affect the position of MESP2 expression along the anterio-posterior axis (Sirbu and Duester, 2006). Therefore, if Foxc1a is affecting these

opposing gradients their imbalance is in turn affecting the expression of *mesp-ba* and formation of the anterior somites.

Taken together, these observations lead to the conclusion that *foxc1a* and *ripply1* genetically interact to control somite formation and the expression of *mesp-ba* in the PSM by regulating the expression levels of Fgf8a and Raldh2. When Foxc1a is reduced, the balance between these gradients is disrupted and the permissibility of the anterior PSM cells and the expression of *mesp-ba* are affected. When *ripply1* is also knocked down, the displacement of the *tbx6* expression domain allows *mesp-ba* to be expressed in the tissue that contains the necessary levels of Fgf8a and Raldh2. This coinciding expression allows Tbx6 to induce *mesp-ba* expression and, consequently, restore the formation of the anterior somites. Importantly, the detection of *mesp-ba* and *tbx6* in the double morphants, in the absence of Ripply1, suggests that these genes could be regulated by a mechanism independent of Ripply1. My findings also demonstrate that segmentation of the somites can occur in the absence of *mesp-ba* expression. It would be interesting to see how somitogenesis would be affected in a zebrafish overexpressing *foxc1a*. If *foxc1a* is directly regulating *raldh2* expression, overexpression of Foxc1a would result in increased RA signaling in the PSM and a subsequent posterior shift in *mesp-ba* expression. Additionally, if the defects seen in the *foxc1a* morphants result from reduced *raldh2* expression, it would be reasonable to hypothesize that rescue of *raldh2* expression in the PSM would restore anterior somite formation, even in the absence of *foxc1a*. Performing these additional experiments would help understand the nature of the *foxc1a* regulation of *raldh2.*

Figure 3.11 Proposed Role of Foxc1 in Somitogenesis

Figure 3.11 Proposed Role of Foxc1 in Somitogenesis.

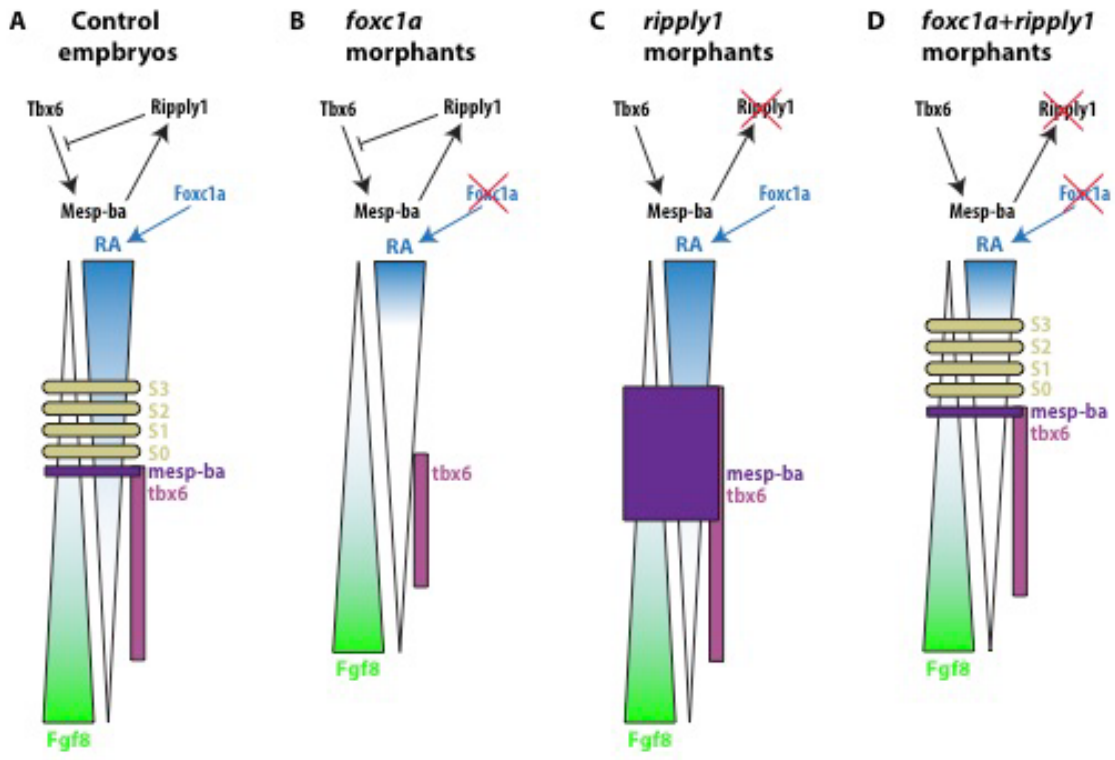

Based on the findings described here, I propose that Foxc1a acts to regulate somite formation by regulating the RA signaling gradient in the PSM through *raldh2*. **(A)** In WT embryos, *tbx6* is expressed throughout the posterior PSM. In the anterior PSM, RA (blue) and FGF8 (green) signaling are both a threshold levels that allow *mesp-ba* (purple) activation by Tbx6 (pink), promoting morphological formation of the somites (brown). **(B)** In the absence of *foxc1a*, embryonic elongation is delayed, the balance between RA and Fgf8 signaling is affected and *tbx6* expression is smaller and shifted anteriorly. The altered expression domains prevent *mesp-ba* expression and somite formation. **(C)** When *ripply1* is knocked down, *tbx6* and *mesp-ba* expression are expanded anteriorly; lack of *mesp-ba* inactivation prevents somite formation. **(D)** When both *foxc1a* and *ripply1* are knocked down together, the balance between

RA and Fgf8 signaling is affected, as seen in the *foxc1a* single morphants, while *tbx6* expression is expanded, as seen in the *ripply1* single morphants. However, the lack of *mesp-ba* repression in the absence of *ripply1* allows the expanded *tbx6* domain to overlap with the required threshold levels of RA and Fgf8. This allows *mesp-ba* to be expressed in the anterior PSM.

Finally, these results indicate that *foxc1a* has a differential role in somite formation in that anterior somites fail to form in the absence of *foxc1a* but posterior somite segmentation can still occur. This finding is consistent with several previous reports underlying differences in the formation of the anterior and the posterior somites. Most notably, the difference between the Foxc1 effect seen in anterior somite formation compared to posterior somite formation is a result of the differential requirement for RA signaling in the posterior PSM, as discussed above (Sirbu and Duester, 2006). Additionally, several other genes have been found to have different regulatory roles in anterior versus posterior somites. The requirement for *Lunatic fringe* and Notch oscillations, for example, is different in anterior and posterior body formation (Shifley and Cole, 2008; Stauber et al., 2009). In mice with complete ablation of *Lfng* formation of the anterior somites was irregular, whereas the posterior somites formed normally. Formation of the corresponding cervical, thoracic and lumbar vertebrae was defective, while the sacral and tail vertebrae were unaffected (Stauber et al., 2009). Similarly, when only the oscillatory expression of *Lfng* in the PSM was abrogated while rostro-caudal expression in the anterior PSM remained intact, formation of the thoracic and lumbar vertebrae was severely defective, but the development of sacral and tail vertebrae was only minimally affected (Shifley et al., 2008). In contrast, in the zebrafish mutants *after eight (aei),* and *deadly seven (des)*, which have mutations in two members of the Notch signaling pathway, *deltaD*, and *notch1a*, respectively, anterior somites develop normally, while the posterior somites are fail to form (Durbin et al., 2000; Gray et al., 2001; Henry et al., 2005; Jiang et al., 1996; Sieger et

al., 2003; Therapontos and Vargesson, 2010; van Eeden et al., 1996). Finally, mutations in *integrin-α5* disrupt only the formation of the anterior somites, while posterior somites are unaffected (Julich et al., 2005). These accumulating observations suggest that the formation of the anterior somites and the posterior somites are regulated through different molecular mechanisms, although the mechanistic foundations of these differences are yet to be understood. Together, these studies support my findings of a differential regulation of somite formation in the anterior vs. posterior somites.

Recently, we have been granted access to a new *foxc1a* mutant line, *foxc1a*^{UA1017}, courtesy of Dr. Ordan Lehman. This CRISPR-generated mutant line has a 7 base-pair deletion upstream of the translation start site and was predicted to generate a truncated, null-Foxc1a. Surprisingly, both the homozygous and heterozygous *foxc1a* mutants, as well as their WT siblings, developed anterior somites. This was in contrast to the *foxc1a* morpholino findings, but consistent with a previous report by Li et al., in which they used a different *foxc1a* mutant line, *foxc1a*^{nju18}, and have reported normal somite formation (Li et al., 2015). However, the expression of *mesp-ba* in the *foxc1a*^{UA1017} mutants was still decreased compared to their heterozygous and WT siblings. When *ripply1* was knocked down in these mutants, the expression of *mesp-ba* was restored, similar to what was seen in the *foxc1a* morphants. These results led us to hypothesize that the mutant line might not be a true null. Western blot analysis performed by FBB revealed that both the *foxc1a*^{UA1017} and *foxc1*^{nju18} protein can be detected using an α-Foxc1 antibody. Correspondingly, luciferase transactivation assays showed that both proteins have

the capacity to activate a 6X *FOXC1* BS reporter, although to a lesser degree than the full size Foxc1a protein. These results indicate that both the *foxc1a*^{UA1017} and *foxc1a*^{nju18} mutant lines are not true knockouts, and that these mutations result not in a loss but in a hypomorph Foxc1a protein with reduced function. Finally, to rule out the presence of functional Foxc1a in the morphant embryos, the existence of maternally-contributed *foxc1a* mRNA in the WT embryos was analyzed. Since the morpholino used is a translation blocking morpholino, it would not be affecting maternal mRNA, which in turn could lead to Foxc1a being expressed in the early stages of embryonic development and skewed observations. However, no *foxc1a* was detected in the 1-2 cell stages WT embryos, in contrast to *ef1α,* which is maternally contributed (Fleisch et al., 2013). This suggests that *foxc1a* mRNA is not maternally contributed, and that the *foxc1a* morpholino should result in a complete knockdown of Foxc1a in early embryonic development. The differences seen between the mutant lines and the morphants are therefore likely to be derived from a more complete ablation of Foxc1a in the morphant fish than in these mutant lines. Alternatively, the differences in somitogenesis between the mutants and morphants could also be a result of *foxc1b* compensation. Morpholino knockdowns of *foxc1b* suggest that despite its overlapping expression with *foxc1a* in the PSM, it does not have an important role in somitogenesis (Topczewska et al., 2001a; Topczewska et al., 2001b). However, it is possible that when *foxc1a* expression is absent *foxc1b* assumes a compensatory function. Due to the immediate effect of the morpholino, this would not occur in the *foxc1a* morphants. It would therefore be valuable to

inject the *foxc1b* morpholino into the *foxc1a* mutants and observe somite formation as well as the expression patterns of *mesp-ba*, *raldh2* and *fgf8a.*

My results demonstrate that *foxc1a* serves an important role in regulating the retinoic acid gradient in the PSM, and has a direct effect on somitogenesis and axial skeletal patterning. I have shown that this effect is more critical during anterior somite formation than in posterior somites. I have also demonstrated that *mesp-ba* is not required for somite formation, and that the genetic interaction between *foxc1a* and *ripply1* helps regulate intersomitic boundary determination and somite segmentation.

CHAPTER 4. FOXC1 DRIVES HYPERTROPHIC MATURATION OF CHONDROCYTES

Once the somites have formed, the various cell populations within each somite give rise to the elements of the axial skeleton. In mouse and humans, the sclerotome gives rise to the cartilage and bones, the dermamyotome gives rise to the skin and muscle of the back, the syndetome gives rise to the tendons and the myotome gives rise to the skeletal muscles (Brand-Saberi et al., 1996; Brent et al., 2003; Dubrulle and Pourquie, 2003; Kato and Aoyama, 1998; Ordahl and Le Douarin, 1992). The mesenchymal precursors in the sclerotome give rise to three major tissues: immature cartilage, mature cartilage and bone (Gomez-Picos and Eames, 2015). Bone formation can occur through intramembranous or endochondral ossification. In intramembranous ossification, mesenchymal cells differentiate directly into osteoblasts that secrete and mineralize bone matrix. These bones include the flat bones (including calvaria, mandible and maxilla) as well as the clavicle (Long, 2012, Ornitz, 2005). In endochondral ossification on the other hand, mesenchymal cells give rise to a cartilage template of the bone that will then mineralize and ossify. The long bones and some craniofacial bones (including the mandibular condyle and sphenoid bone) as well as the bony element of the vertebral column are formed by endochondral ossification (Yoshida et al., 2015). While some of the cartilage gets transforms into bone, some cartilages remain in an early, immature differentiation state or undergo hypertrophy and cartilage maturation.

During endochondral ossification of the axial skeleton, sclerotome-derived mesenchymal cells condense and differentiate into chondrocytes. Proliferating chondrocytes mature and undergo hypertrophy and ultimately die by apoptosis, after which blood vessels invade the cartilage template of the bone, carrying in the osteoblasts which will give rise to the bone.

SOX9 is considered to be a master regulator of chondrogenesis, initiating the specification and differentiation of chondrocytes (Lefebvre et al., 1998). The expression patterns of SOX9 and Runx2 during mesenchymal condensation are predictive of differentiation into immature cartilage (where only SOX9 is expressed), mature cartilage (where Runx2 is expressed and SOX9 is expressed at low levels), or bone (where only Runx2 is expressed) (Eames and Helms, 2004, Eames et al., 2004). *Foxc1* also plays an important role during cartilage formation. *Foxc1* is expressed in mesenchymal condensations that give rise to cartilage and bone, as well as in resting, proliferating and hypertrophic chondrocytes (Yoshida et al., 2015). In E12.5 mice, *Foxc1* expression was high in the developing limb buds, and at E15.5 it was high in tibia chondrocytes (Yoshida et al., 2015). Additionally, at E13.5 *Foxc1* expression was high in proliferating chondrocytes and perichondrial cells of the developing limb bud (Yoshida et al., 2015). In newborn mice, *Foxc1* expression was detected in resting, proliferating and hypertrophic chondrocytes in the tibial growth plate, where FOXC1 has been shown to promote the expression of target genes such as *PTHrP* and *Col10a1* by partnering with IHH and GLI2 (Yoshida et al., 2015).

Recently, Ohba et al. used a ChIP-Seq study to characterize SOX9 binding and chromatin organization within mouse rib-derived chondrocytes. Among other findings, they demonstrated the existence of four SOX9 peaks in distal elements of *Foxc1* suggesting that *Foxc1* might be a target of SOX9 (Ohba et al., 2015). Furthermore, a different study suggested that there is increased SOX9 binding in the vicinity of FOXC1 binding motifs, raising the idea that FOXC1 and SOX9 have similar downstream targets (Liu and Lefebvre, 2015). However, its role in early chondrogenic differentiation is not yet understood. In addition, little is known about the factors that regulate *Foxc1* expression. Understanding the factors regulating cartilage and bone formation is vital to developing orthopedic therapies and evolving new and current tissue-engineering techniques. Here, I aim to characterize the role of *Foxc1* in chondrogenesis through analysis of its interactions with SOX9.

RESULTS

In zebrafish, lineage tracing studies analyzing somite differentiation into skeletal tissues have yet to be completed. In the mouse model, on the other hand, several studies have indicated that mesenchymal cells originating in the somite-derived sclerotome undergo endochondral ossification and contribute to the formation of the cartilage and bony elements of the axial skeleton (Brand-Saberi and Christ, 2000; Brent and Tabin, 2002). For this reason, mouse embryonic stem cells (ESCs) (TT2) were utilized to discern how FOXC1 acts in chondrogenic differentiation, and directed towards a chondrogenic lineage by the addition of growth factors at different time points during the differentiation assay (Figure 2.2) (Kawaguchi et al., 2005; Yu et al., 2015). In short, ESCs were cultured as hanging drop for 2 days, after which the cell condensations were transferred to suspension cultures containing 0.1 M retinoic acid (RA) and allowed to differentiate and proliferate for an additional 3 days. The RA growth factor was removed on day 5 and the cell condensations were kept in suspension cultures. On day 7, the condensations were plated on gelatin-coated tissue culture plate with or without 10 μg/ml TGFβ3. Cells were harvested on days 0, 5, 7 and 13 and RT-qPCR was performed to compare and quantify changes in gene expression. These time points were selected as they represent various stages during chondrogenesis; on day 0, the cells should still retain their pluripotency potential. By day 5, following a 3-day incubation of the mesenchymal condensations with or without RA, chondrogenic differentiation should be initiated, and the expression of early chondrogenic markers was expected to be detected. On day 13 chondrocytes were expected to

start their maturation and progress towards a hypertrophic state (Kawaguchi et al., 2005; Yu et al., 2015). To validate the efficiency of the assay in promoting differentiation, the expression of the pluripotent markers *Oct4* and *Sox2* were assessed using RT-qPCR to confirm that the ES cells have undergone differentiation and lost their pluripotency. The expression of both genes was high on day 0 while neither gene was expressed on days 5 and 13 (Figure 4.1).

Figure 4.1 TT2 ESCs Lost their Pluripotent Potential During the Differentiation Assay

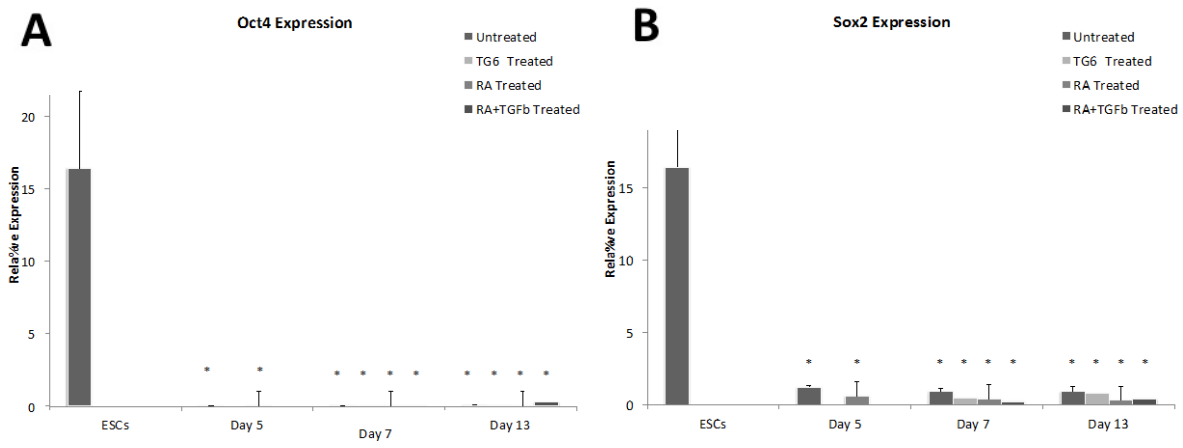

Figure 4.1 TT2 ESCs lost their pluripotent potential during the differentiation assay. RT-qPCR of **(A)** *Oct4* and **(B)** *Sox2* expression in untreated and RA- TGFβ3 treated TT2 cells on days 5, 7 and 13 of the differentiation assay. Asterisks represent $p<0.001$. Error bars represent standard deviation from three separate biological replicates. Data was analyzed using one-way ANOVA.

Next, to confirm that the differentiation pathway the cells were progressing along was indeed chondrogenic, the mRNA expression of various chondrogenic and osteogenic markers was assessed. When mesenchymal cells start forming condensed aggregates they express *Runx2* and *Col2*, both of which decline once the cells undergo chondrogenic commitment rather than an osteogenic one (Bruderer et al., 2014; Gomez-Picos and Eames, 2015). Here, the expression of *Runx2* was increased in the first phases of the differentiation assay, as the cells formed embryoid bodies and began to differentiate. *Runx2* expression peaked by day 7, following the RA treatment. On day 7, the cells were treated with TGFβ3 to promote their chondrogenic commitment and the expression of *Runx2* thus declined by day 13 (Figure 4.2A). Similarly, the expression of *Col2* was low in the embryonic stems cells and increased by day 5, when the cells have formed condensations and were treated with the osteogenic growth factor retinoic acid. It then declined 3-fold over the next 2 days and decreased even more by day 13 (Figure 4.2B). In contrast, the expression of the late chondrogenic marker *Col10*, which is expressed once the cells have started their switch from prehypertrophic to hypertrophic chondrocytes (Gomez-Picos and Eames, 2015), was low on days 0, 5 and 7, and then increased on day 13, following the differentiation treatment (Figure 4.2C). The expression of the early chondrogenic marker *Sox5* in the treated cells gradually increased throughout the differentiation assay, and remains elevated for up to 21 days of differentiation (Figure 4.2D). *Sox6* expression, on the other hand, was elevated by day 5, when chondrogenic differentiation is initiated, and greatly increases by day 13, when the cells were actively undergoing chondrogenesis. By day 21, when chondrocyte

maturation presumably began, the expression of *Sox6* decreased (Figure 4.2E). Likewise, the expression of *Sox9* in the RA-TGFβ3 treated cells increased on day 5, when the cells have formed condense aggregates and were treated with retinoic acid. The expression of *Sox9*, the master regulator of chondrogenesis, was then markedly increased by day 13 when the cells were actively undergoing chondrogenesis. By day 21, when maturation takes place, the expression of *Sox9* is decreased and is not significantly different from the expression in the undifferentiated stem cells (Figure 4.2F). Interestingly, the expression of *Sox9* in the untreated cells on day 21 is elevated to the same level seen on day 13 in the treated cells (Figure 4.2F). This could suggest that under the differentiation conditions and in the absence of leukemia inhibitory factor, ES cells can spontaneously undergo chondrogenic differentiation even without the addition of growth factors, although at a much slower rate. Taken together, these results suggest that the chondrogenic differentiation assay used here can successfully induce chondrogenesis in ESCs.

Figure 4.2 Differentiation Assay Led to Up-regulation of Chondrogenic Gene Expression

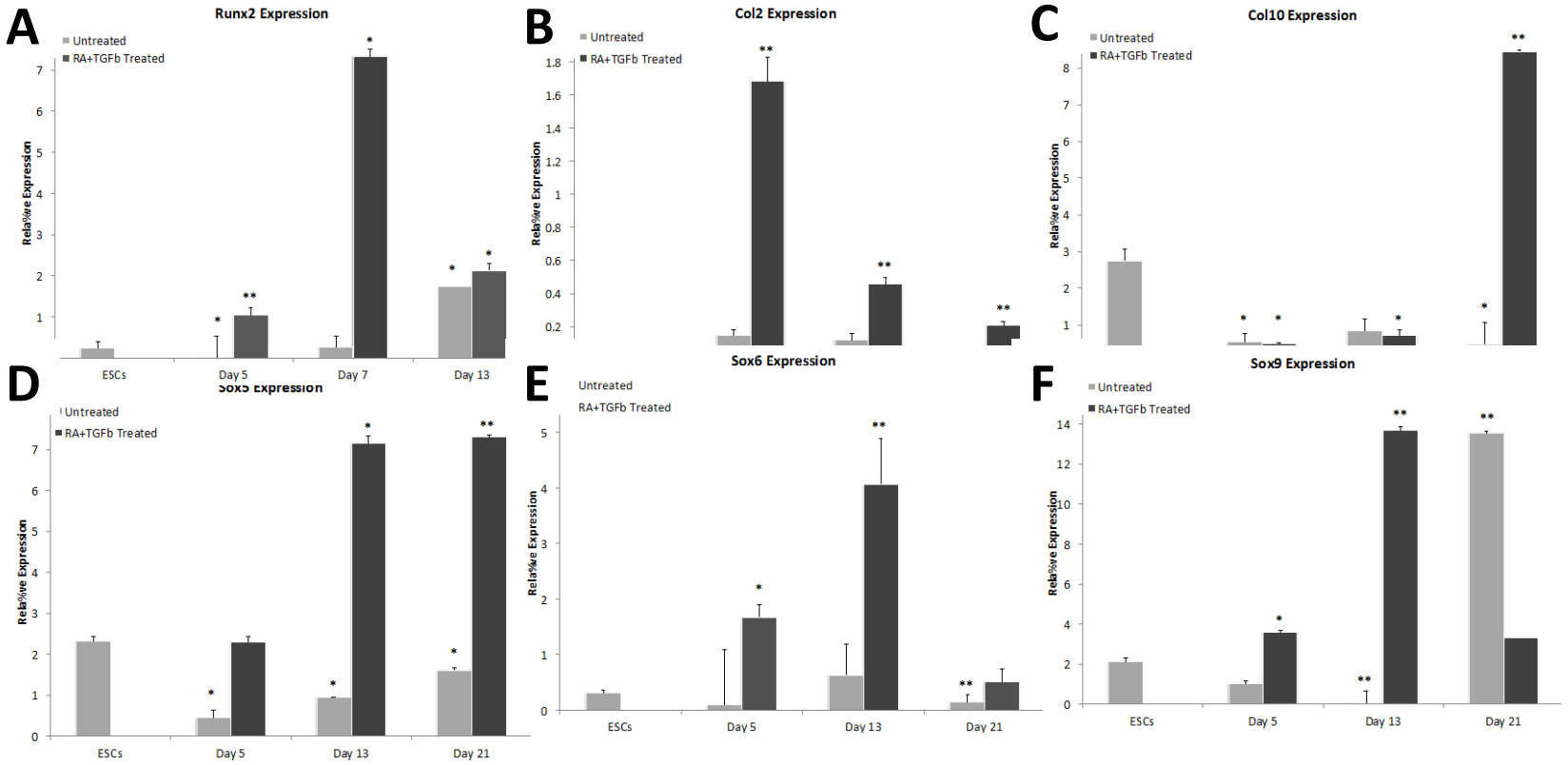

Figure 4.2 The differentiation assay led to up-regulation of chondrogenic gene expression. RT-qPCR measurement of **(A)** *Runx2* **(B)** *Col2* **(C)** *Col10* **(D)** *Sox5* **(E)** *Sox6* and **(F)** *Sox9* expression in untreated and RA- TGFβ3 treated TT2 cells on days 5, 7 and 13 and/or 21 of the differentiation assay. * = $p<0.05$; ** = $p<0.01$. Error bars represent standard deviation from three separate biological replicates. Data was analyzed using one-way ANOVA.

The expression of *Foxc1* mRNA during chondrogenic differentiation was assessed next. By day 5, following RA supplementation to the treated TT2 cells, the expression of *Foxc1* was significantly elevated compared to the untreated cells (Figure 4.3). The level of *Foxc1* expression relatively increased in both groups by day 7 (after 48 hours with no growth factor supplementation to the ES media), but remained higher in the treated cells compared to the untreated cells. Interestingly, *Foxc1* expression decreased by day 13 in the treated cells, and resembled that of the untreated cells. By day 21 of differentiation, the expression of *Foxc1* in both the treated and untreated groups continued to decline and did not differ between the groups. These data suggest that Foxc1 is important in the initial stages of chondrogenic differentiation, when the chondrogenic differentiation cascade is initiated, and is required less for the switch from pre-hypertrophic to hypertrophic chondrocytes which occurs later in the differentiation process.

Figure 4.3 *Foxc1* mRNA Expression Increases Following RA-TGFβ3 Treatment

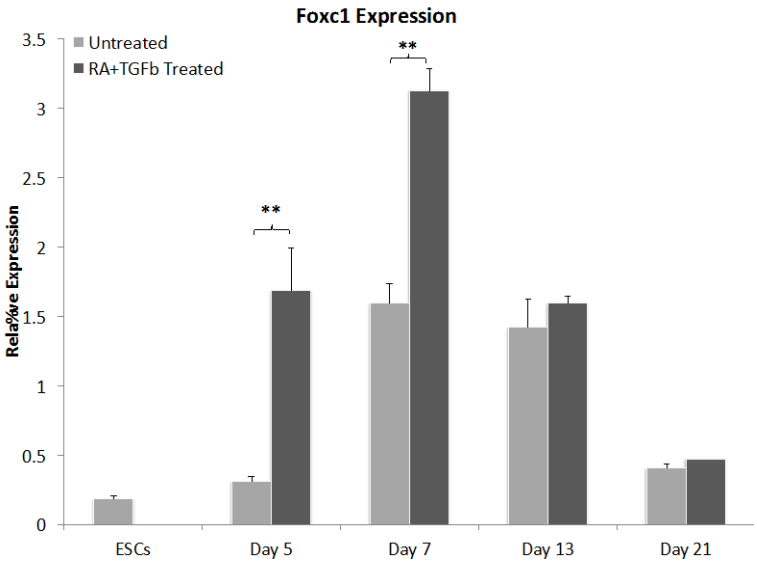

Figure 4.3 *Foxc1* mRNA Expression Increases Following RA-TGFβ3 Treatment. RT-qPCR measurement of *Foxc1* expression in untreated and RA- TGFβ3 treated TT2 cells on days 5, 7 and 13 of the differentiation assay. **=p<0.001. Error bars represent standard deviation from three separate biological replicates. Data was analyzed using one-way ANOVA.

Foxc1 expression analyses point to an important role of *Foxc1* in chondrogenic differentiation, yet little is known about how *Foxc1* is regulated in early chondrogenesis. A review of a recent study that used ChIP-Seq to examine SOX9 binding domains in rib-derived chondrocytes (Ohba et al., 2015) identified four SOX9 peaks in proximity to *Foxc1* (Figure 4.4A). Three of these peaks lie upstream to *Foxc1* at -42kb, -41kb and -27kb (distal element A, B, and C, respectively) and one lies downstream at +10kb (distal element D) (Figure 4.4A). To functionally evaluate these regions for *Foxc1* regulation, their evolutionary conservation in mammals and other vertebrates was analyzed using the UCSC genome browser (Kent et al., 2002). This analysis revealed that distal element A is highly conserved in vertebrate species (Figure 4.4B). Similarly, distal element B, while having less overall conservation, has several regions within it that are highly conserved (Figure 4.4C). In contrast, distal elements C and D show little evolutionary conservation in the vertebrate species analyzed (Figure 4.4D, E). This suggests that distal elements A and B have important functions in vertebrate development, whereas conservation of distal elements C and D is likely to be less crucial for survival and development. Distal B was blasted against the Human genome using Blastz and Multiz to identify the analogous sequence to the mouse *Foxc1* distal element B (Blanchette et al., 2004; Chiaromonte et al., 2002). An evolutionary conserved region lying 31kb upstream of the human *FOXC1* was identified. Due to the abundance of available histone and chromatin data for numerous cell types, this human region was then used to study chromatin annotations. Histone modification markers in the vicinity of this element were

annotated in osteoblasts and compared to those found in skeletal muscle using data collected by the Encode Project (Meyer et al., 2016) (Figure 4.5). The distal B region bears several annotations of an active enhancer (Meyer et al., 2016). Dnase-seq indicates that the distal B region is transcriptionally active. Additionally, the peaks seen for H3K4me1 and H3K4me2 suggest that this region is functioning as an active enhancer. Finally, the signals obtained for H3K4me3 and H3K27me3 are could be part of bivalent chromatin regulation, which have been shown to regulate promoters and enhancers of key developmental genes (Bernstein et al., 2006; Vastenhouw and Schier, 2012). This analysis suggests that the chromatin region containing the *Foxc1* distal element B is more transcriptionally active in osteoblasts than it is in skeletal muscle myotubes.

Figure 4.4 Foxc1 Distal Elements A and B Are Conserved in Mammals

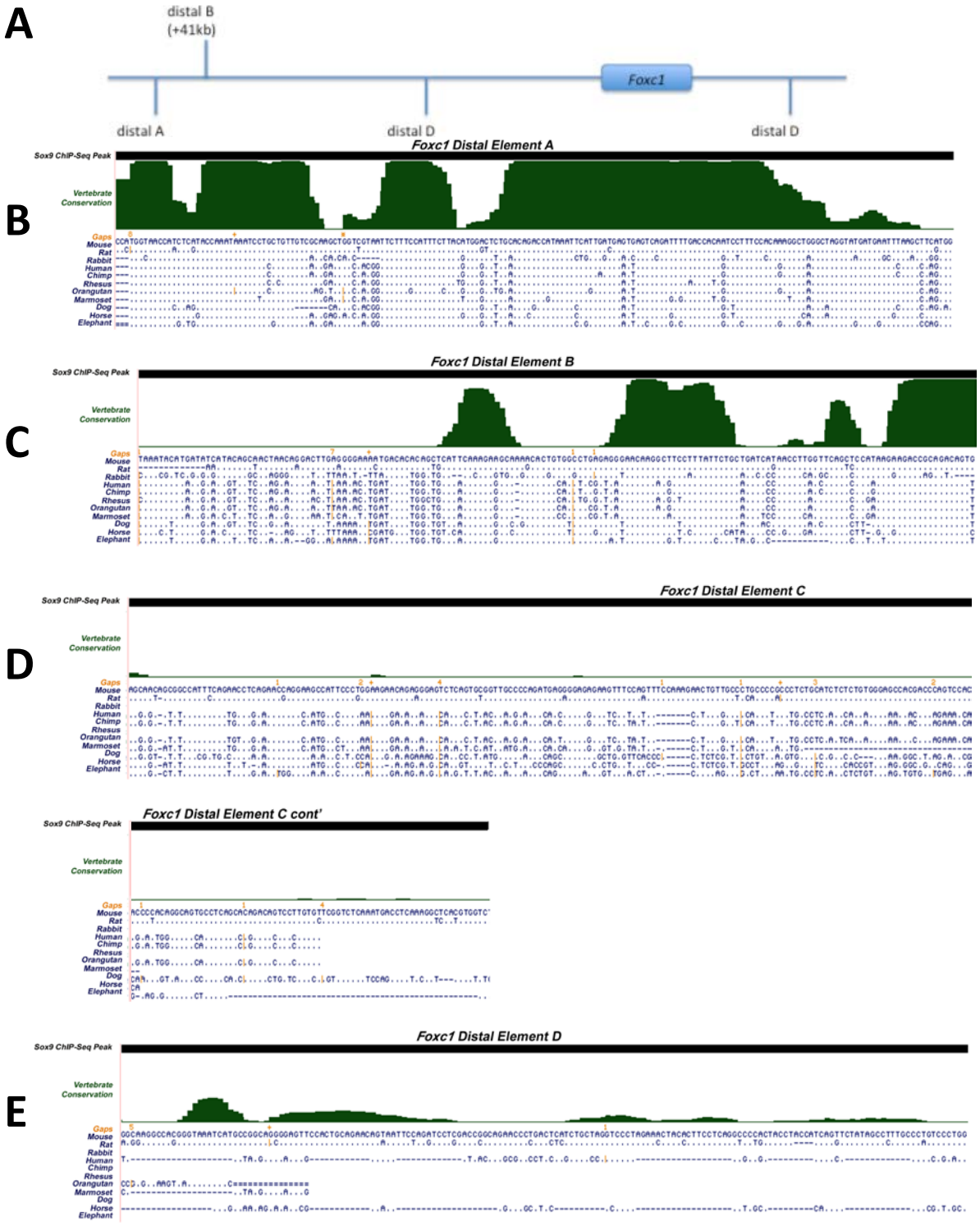

Figure 4.4 Foxc1 Distal Elements A and B Are Conserved in Mammals. (A) Ohba et al. found four SOX9 enriched regions in close proximity to *Foxc1* (Ohba et al., 2015). Distal element A, B, and C are upstream of the transcription start site and distal element D is downstream of *Foxc1*. **(B)** Distal element A is evolutionary conserved in other mammals. **(C)** Distal element B has three regions of high evolutionary conservation in mammals. **(D)** There seems to be no evolutionary conservation of distal element C. **(E)** Distal element D has little evolutionary conservation. Generated using UCSC Genome Browser (Kent et al., 2002).

Figure 4.5 Mapping of Histone Modifications Around the Foxc1 Distal Element

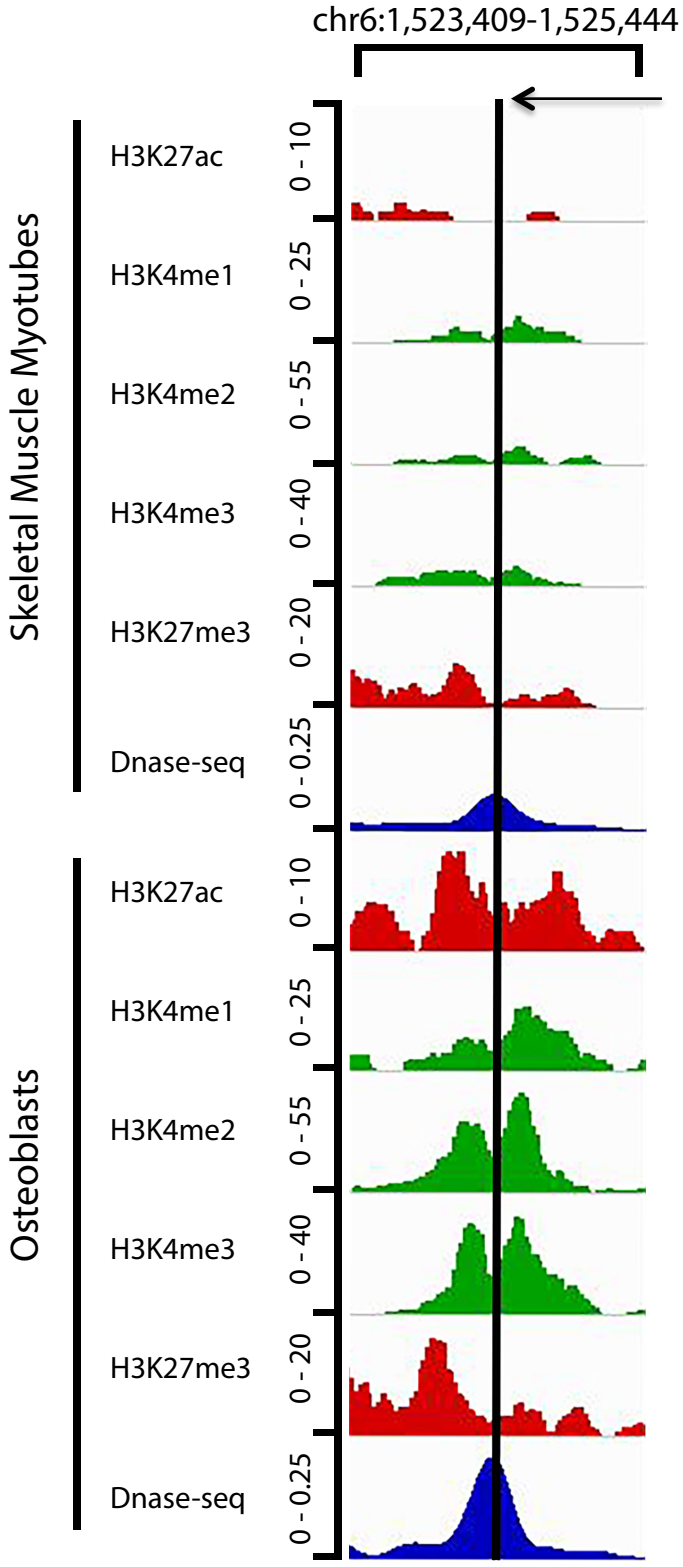

Figure 4.5 Mapping of Histone Modifications Around the *Foxc1* Distal Elements. Analysis of ChIP-Seq data from the Encode Project reveals there is an increased signal for data collected using H3K27ac, H3K4me1, H3K4me2, H3K4me3, and Dnase-seq in osteoblasts compared to skeletal muscle myotubules. H3K27me3, a repressive marker, has a peak upstream of the distal element, with a decreased signal overlapping the distal element itself (Meyer et al., 2016). Plots represent number of DNA fragments obtained at each position across the genome.

Chromatin immunoprecipitation was used next to determine if SOX9 physically binds to each of the four *Foxc1* distal elements. Here, endogenous SOX9 expression was induced in TT2 ESCs, and an α-SOX9 antibody was used to precipitate bound chromatin. TT2 ESCs were cultured as monolayers in the presence of Activin A for 4 days (Wang et al., 2003). Under these conditions, endogenous SOX9 expression was detected in the treated cells compared to untreated TT2 cells (Figure 4.6A). An α-SOX9 antibody was used to precipitate chromatin from the Activin A-treated cells, along with rabbit IgG and αH3ac which served as negative and positive controls for the ChIP reaction, respectively. Primers specific to each of the 4 distal elements were then used to try and recover the DNA that was bound to the SOX9 protein and primers specific for *Col2 intron 1* were used as positive control for the SOX9 interaction, as described in (Oh et al., 2010). As expected, all four distal elements as well as *Col2 intron 1* have been amplified in the input sample as well as in the αH3ac precipitated samples, while none of the regions tested were detected in the sample containing the rabbit IgG (Figure 4.6B-E). Both Distal B and *Col2 intron 1* have been recovered from the sample precipitated with αSOX9 (Figure 4.6B), whereas distal elements A, C and D were not (Figure 4.6C-E). Taken together, these results suggest that SOX9 physically binds to distal element B.

Figure 4.6 Endogenously Expressed SOX9 Binds to Distal Element B in a Chromatin Immunoprecipitation Assay

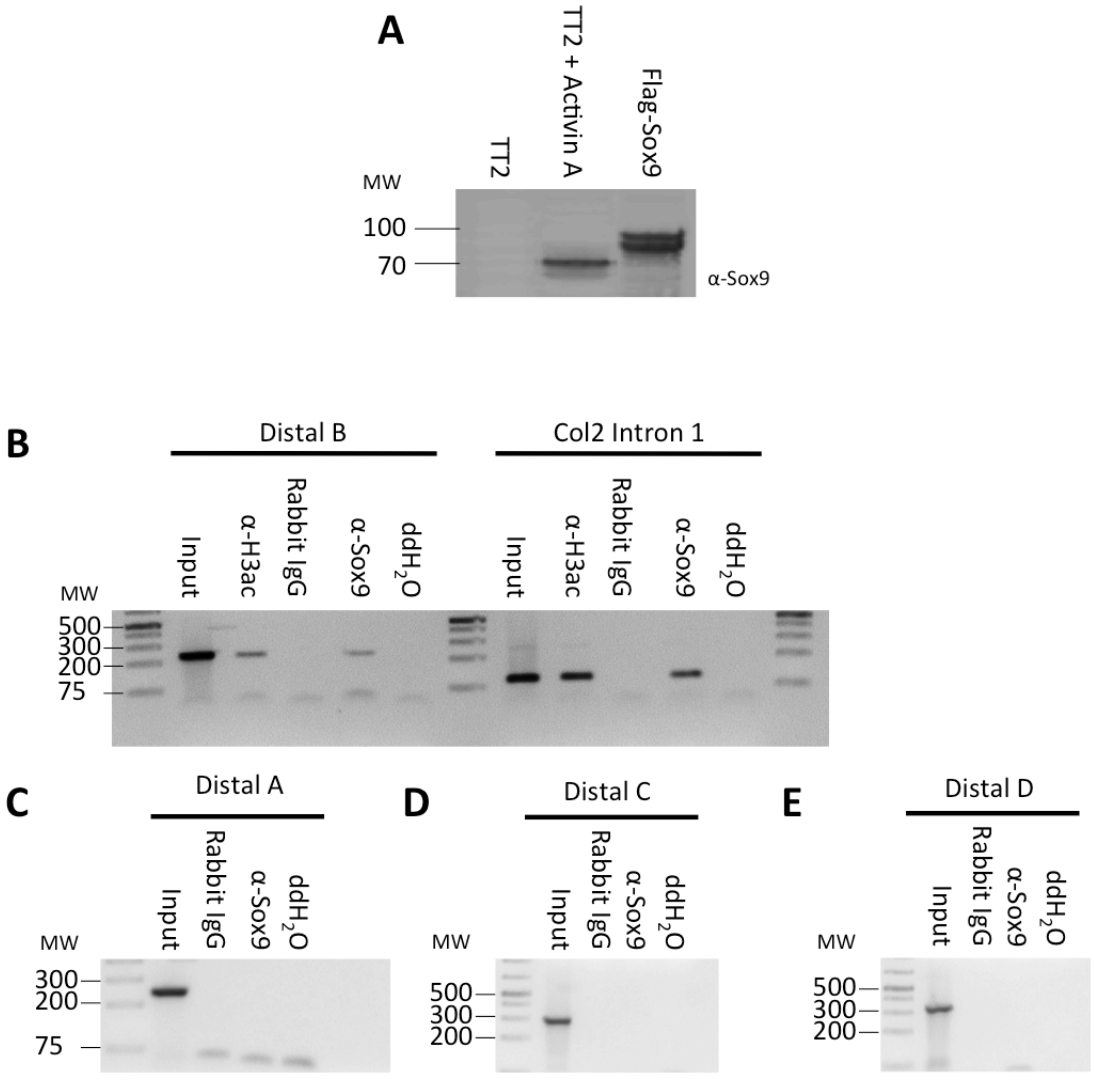

Figure 4.6 Endogenous SOX9 Binds to Distal Element B in a Chromatin Immunoprecipitation Assay. (A) SOX9 was detected in protein lysate prepared from TT2 cells treated with Activin A but not in untreated TT2 cells when blotted with α-SOX9 antibody. Flag-SOX9 was used as positive control. **(B)** Distal B and *Col2 Intron 1* were amplified from input samples treated with Activin A and in chromatin eluted with either α-SOX9 or αH3ac (positive control) but not in chromatin eluted with rabbit IgG (negative control) **(C, D, E)** Distal A, C and D were amplified from input samples, but were not recovered from chromatin eluted with αSOX9. Rabbit IgG was used as negative control.

To assess whether the interaction between SOX9 and the *Foxc1* distal element B is a functional one, a luciferase transactivation assay was utilized (Figure 4.7A). The four distal element regions were cloned into a pGL4.23 reporter vector containing a minimal promoter. Co-transfection of U2OS cell with SOX9 along with the distal B reporter construct led to an over 20-fold activation compared to co-transfection with an empty pFlag vector alone. In contrast, co-transfection of SOX9 with distal elements A, C or D, or an empty pGL4.23 reporter, resulted in no significant activation of those reporters. An analysis of the *Foxc1* distal element B using the Find Individual Motif Occurrences (FIMO) computer software revealed the existence of a sequence matching the PWM of the SOX9 DNA binding motif within the element (Figure 4.7B) (Grant et al., 2011). Manual search for the SOX9 binding motif WWCAAWG (Oh et al., 2010) helped identify 3 potential SOX9 binding sites within the element (designated BS1, BS2, and BS3, Figure 4.8A). To assess the requirement of these potential binding sites for Foxc1 activation, luciferase reporter constructs containing serial deletions of these sites were generated and used in transactivation assay (Figure 4.8A). The relative activation of the empty pGL4.23 in the presence of SOX9 was 5-fold that of the empty reporter, however this difference was not statistically significant (Figure 4.8B). When each potential binding site was deleted alone, the relative activation was significantly different in the presence of SOX9 compared to empty pFlag. The full-length distal B construct generated a 32-fold increase in relative activation compared to the empty reporter. When only BS1 was deleted (del 1), 15% of wild-type activation was retained; when BS2 was deleted (del 2) 36% of the wild type activation was retained, and when BS3 was

deleted (del 3) activation was 26% compared to the wild-type construct. Additionally, when only one potential BS was present, there still appeared to be activation of the reporter. Reporter construct with BS1 alone (BS2 and BS3 deleted, del 4) resulted 19% retained activation. BS3 alone (BS1 and BS2 deleted, del 5) led to retention of 51% activation. When all three potential sites were deleted (del 6), there was no significant activation. These data suggest that all three potential binding sites might be able to facilitate the activation of the *Foxc1 distal element B* by SOX9. Previous DNA motif analysis demonstrated that SOX9 often binds cartilage targets as a homodimer to facilitate activation of enhancer elements (Bridgewater et al., 2003; Han and Lefebvre, 2008; Sock et al., 2003), and therefore it would be reasonable to expect a higher activation level of the enhancer element when more than one BS is present in the construct.

Figure 4.7 SOX9 Induces Activation of the Reporter Vector Through Distal Element B

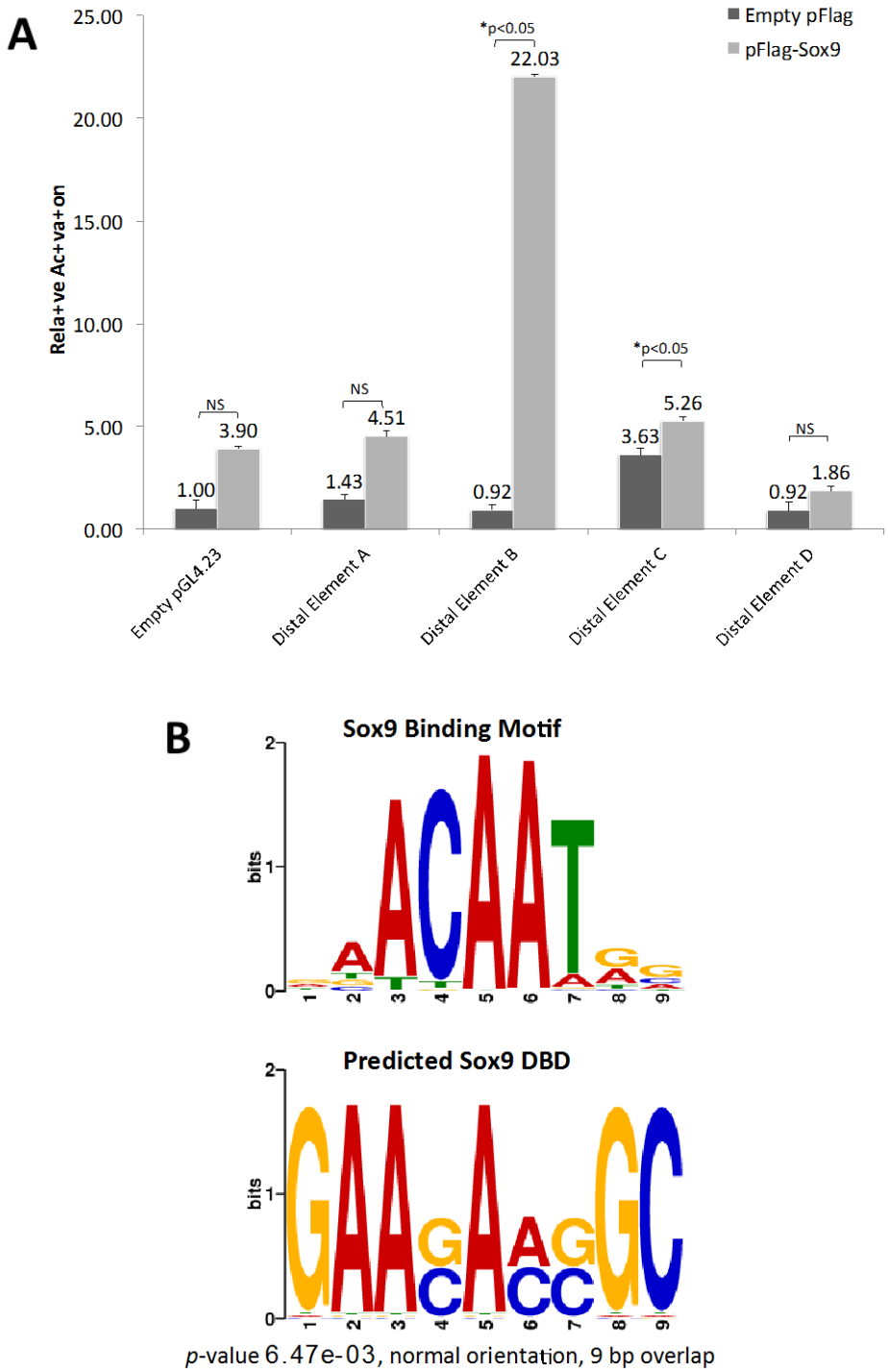

Figure 4.7 SOX9 Induces Activation of the Reporter Vector through Distal Element B. (A) U2OS cells were transfected with empty pGL4.23 or with reporter constructs containing distal elements A-D along with Flag-SOX9 or empty Flag vector. $p<0.05$. Data was analyzed using student's t-test. Error bars indicate standard deviation. **(B)** Analysis of Foxc1 distal B DNA sequence using FIMO revealed the existence of a sequence matching the PWM of the SOX9 DNA binding motif within the distal B element (Grant et al., 2011).

Figure 4.8 Distal Element B Contains Three Potential SOX9 Binding Sites Sufficient to Induce Activation

A

Full length: (BS1, BS2, BS3)
TAAATACATGATATCATACAGCAACTAACAGGA**CTTGAG**GGGAAAATGACACACAGCTCAT**TCAAA**GAAGCAAAACACTGTGGCCTGAGAGGGA**ACAAGG**CTTCCTTTATTCTGCTGATCATAACC

Del 1: (156 bp)
TAAATACATGATATCATACAGCAACTAACAGGA----------GGGAAAATGACACACAGCTCAT**TCAAA**GAAGCAAAACACTGTGGCCTGAGAGGGA**ACAAGG**CTTCCTTTATTCTGCTGATCATAACC

Del 2: (157 bp)
TAAATACATGATATCATACAGCAACTAACAGGA**CTTGAG**GGGAAAATGACACACAGCTCAT----------GAAGCAAAACACTGTGGCCTGAGAGGGA**ACAAGG**CTTCCTTTATTCTGCTGATCATAACC

Del 3: (155 bp)
TAAATACATGATATCATACAGCAACTAACAGGA**CTTGAG**GGGAAAATGACACACAGCTCAT**TCAAA**GAAGCAAAACACTGTGGCCTGAGAGGGA----------CTTCCTTTATTCTGCTGATCATAACC

Del 4: (122 bp)
TAAATACATGATATCATACAGCAACTAACAGGA**CTTGAG**GGGAAAATGACACACAGCTCAT----------TTCCTTTATTCTGCTGATCATAACC

Del 5: (129 bp)
TAAATACATGATATCATACAGCAACTAACAGGA----------AGCAAAACACTGTGGCCTGAGAGGGA**ACAAGG**CTTCCTTTATTCTGCTGATCATAACC

Del 6: (94 bp)
TAAATACATGATATCATACAGCAACTAACAGGA----------CTTCCTTTATTCTGCTGATCATAACC

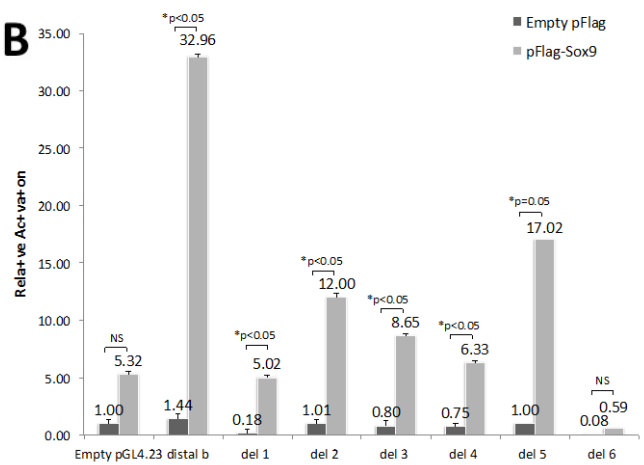

Figure 4.8 Distal Element B Contains Three Potential SOX9 Binding Sites Sufficient to Induce Activation. **(A)** Three potential SOX9 binding sites were identified in Distal Element B (BS1-3). Luciferase reporter constructs containing serial deletions of these regions were generated. **(B)** U2OS cells were transfected with empty pGL4.23 or with reporter constructs along with Flag-SOX9 or empty Flag vector. $p<0.05$. Data was analyzed using student's t-test. Error bars indicate standard deviation.

To better understand the role of Foxc1 during the formation of mesenchymal condensation and early chondrogenic differentiation, FOXC1 was overexpressed in the TT2 cells and the chondrogenic differentiation assay was repeated. The TT2 cells were transfected with HA-Hs. *FOXC1* on day -1 of the ES differentiation assay to allow for FOXC1 overexpression at the onset of the study, during formation of the embryoid bodies. The progression of chondrogenesis was then evaluated using RT-qPCR. HA-Hs. FOXC1 protein was identified in the transfected TT2 cells 48 hours post-transfection using WB (Figure 4.9A). Similarly, in transfected TT2 cells, *FOXC1* mRNA was detected at high levels on day 0 of the differentiation assay (24 hours post-transfection) compared to the untransfected cells. The level of *FOXC1* mRNA was lower on day 2 of the differentiation assay, when the embryoid bodies were formed and transferred to suspension cultures. On day 5 the level of *FOXC1* was slightly lower, and was detected at levels comparable to untransfected cells by day 13 (Figure 4.9B). These results demonstrate that the TT2 *FOXC1* transfections were effective in promoting overexpression of FOXC1 during the chondrogenic differentiation assay. The expression of endogenous mouse *Foxc1* was low on days 0 and 2 in all test groups (Figure 4.10A). On day 5 of differentiation, the expression of *Foxc1* was significantly higher in the transfected, RA+TGFβ3 group, compared to the untransfected RA+TGFβ3 treated group. This effect was also seen on day 13 of differentiation (Figure 4.10A). The expression of the chondrogenic and osteogenic markers in the FOXC1-overexpression system was assessed next.

The expression of *Sox9* (Figure 4.11A) on days 0 and 2 was not different between the test groups, but on day 5 of differentiation it was significantly higher in the transfected, RA+TGFβ3 treated group compared to the untransfected control group. By day 13 of differentiation, the expression of *Sox9* was not different between the transfected and untransfected cells. The expression of *Runx2* was significantly higher in the transfected, treated cells on day 5 of differentiation and did not appear to be decreased following the addition of TGFβ3 to the media by day 13 (Figure 4.11B). *Sox6* expression resembled that of endogenous *Foxc1*, in that there was no difference in expression between the transfected and untransfected cells on days 0 and 2, but following retinoic acid treatment, on day 5 of differentiation, the *FOXC1*-transfected cells had a significantly higher expression of *Sox6* compared to the treated, untransfected controls (Figure 4.11C). Following TGFβ3 treatment, on day 13 of differentiation, the expression of *Sox6* in the transfected, treated cells was lower compared to day 5, but still significantly higher than in the treated, untransfected cells (Figure 4.11C).

Figure 4.9 HA-Hs. FOXC1 was Overexpressed in Transfected TT2 ES Cells

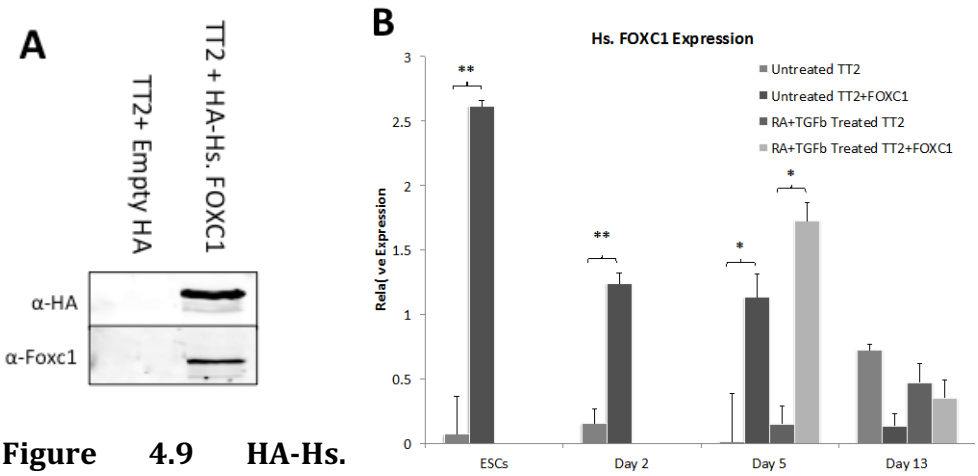

Figure 4.9 HA-Hs. FOXC1 was Overexpressed in Transfected TT2 Cells. (A) HA-Hs. FOXC1 expression was detected on a western blot using both α-HA and α-Foxc1 antibodies. **(B)** *FOXC1* mRNA levels were measured using RT-qPCR in samples collected from untransfected or transfected TT2 cells on days 0, 2, 5, and 13 of the differentiation assay. **=p<0.001; *= p<0.05. Error bars represent standard deviation from three separate biological replicates. Data was analyzed using one way ANOVA.

Figure 4.10 Endogenous *Foxc1* Expression in the Hs. *FOXC1*-Overexpressing Cells Increased Following a Decline in *Hs. FOXC1* Levels

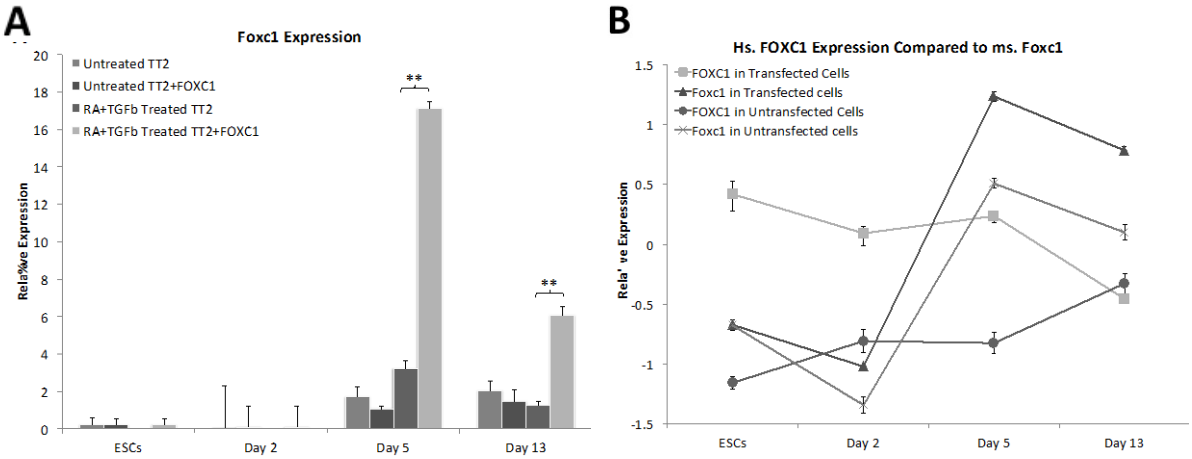

Figure 4.10 Endogenous *Foxc1* expression in the Hs. *FOXC1*-overexpressiong cells increased following a decline in *Hs. FOXC1* levels. **(A)** The expression of endogenous, mouse *Foxc1* levels in the FOXC1-transfected TT2 cells was measured using RT-qPCR on days 0, 2, 5 and 13 in the treated, transfected cells and compared to levels in untreated transfected cells or treated untransfected cells. **(B)** Comparing the levels of Hs. FOXC1 and endogenous Foxc1 in the RA+TGFβ3 treated groups using RT-qPCR. ** = $p<0.001$. Data was analyzed using one-way ANOVA . Error bars represent standard deviation from three separate biological replicates.

Figure 4.11 Expression of the Chondrogenic Markers *Sox9*, *Sox6* and *Runx2* was Elevated in the Treatment Group Overexpressing *FOXC1*

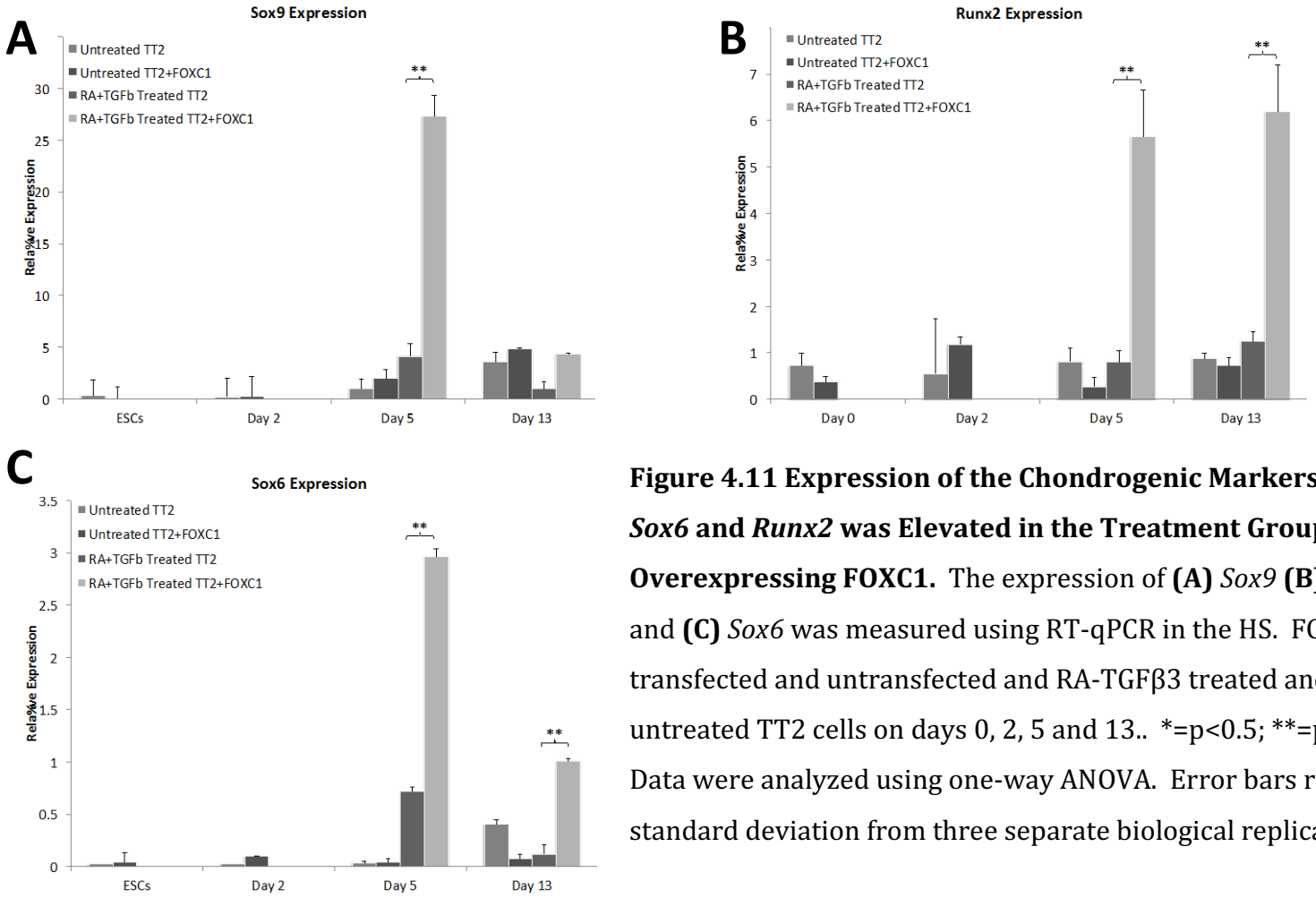

Figure 4.11 Expression of the Chondrogenic Markers *Sox9*, *Sox6* and *Runx2* was Elevated in the Treatment Group Overexpressing FOXC1. The expression of **(A)** *Sox9* **(B)** *Runx2* and **(C)** *Sox6* was measured using RT-qPCR in the HS. FOXC1 transfected and untransfected and RA-TGFβ3 treated and untreated TT2 cells on days 0, 2, 5 and 13.. *=p<0.5; **=p<0.01. Data were analyzed using one-way ANOVA. Error bars represent standard deviation from three separate biological replicates.

When mesenchymal cells undergo chondrogenesis and osteogenesis, they secrete various extra-cellular matrix (ECM) proteins. The relative amount of sulfated glycosaminoglycan (sGAG) was measured on day 13 of differentiation as a measure of relative ECM production in the different treatment groups (Figure 4.12). In the untreated groups the relative amount of sGAG did not differ regardless of transfected construct. In the RA-TGFβ3 treated groups, there was a significant increase in the relative amount of sGAG measured in the FOXC1-overexpressing culture compared to the cells transfected with empty HA vector (Figure 4.12), indicating increased production of proteoglycans in these samples. Moreover, histological staining demonstrated that the RA-TGFβ3 treatment resulted in more condensed ECM production on day 13 of differentiation in both the TT2 cells and in the FOXC1 overexpressing cells compared to untreated condensations (Figure 4.13A). In the untreated TT2 cells, Alkaline phosphatase (AP) staining was undetected on day 13 of differentiation whereas in the RA-TGFβ3 treated TT2 cells there was strong AP staining in the center of the culture, weakly radiating outwards (Figure 4.13B). In the untreated TT2 cells overexpressing FOXC1, there was weak AP staining throughout the culture and in the RA-TGFβ3 treated ones there was very strong AP staining in the center of the condensation as well as radiating around it. The histological and sGAG analyses indicate that FOXC1 overexpression in the differentiating cells leads to increased production of cartilage-specific ECM. Taken together, these results indicate that Foxc1 has an important role in driving chondrogenesis and in regulating the expression of the chondrogenic genes *Sox9* and *Sox6*. The increase in *Runx2* expression on day 5 of the differentiation assay,

and the fact that this expression level did not significantly change by day 13, suggests that the cells have gone through hypertrophic maturation. Taken together, these results demonstrate that Foxc1 is effective in promoting an increase in the pace of chondrogenic differentiation and maturation.

Figure 4.12 Sulfated-GAG Production was Increased in Cells Overexpressing *Foxc1*

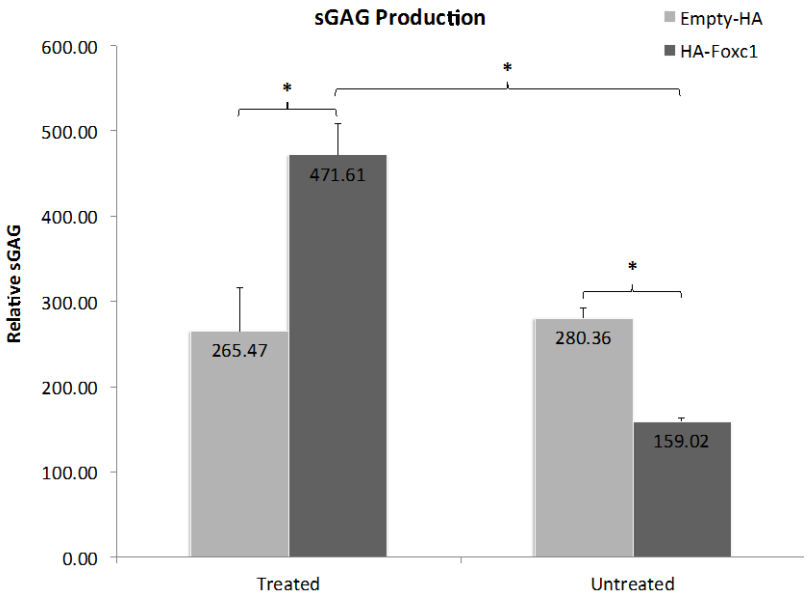

Figure 4.12 sGAG Production was Increased in Cells Overexpressing FOXC1. Production of glycosaminoglycan was measured on day 13 in the *FOXC1* and empty-HA transfected cultures with or without RA-TGFβ3 treatment. *=$p<0.05$ using the Mann-Whitney U test. Error bars indicate standard deviation in two biological replicates containing three technical replicates each.

Figure 4.13 *FOXC1* Overexpression Resulted in Increased Production of ECM and Alkaline Phosphatase

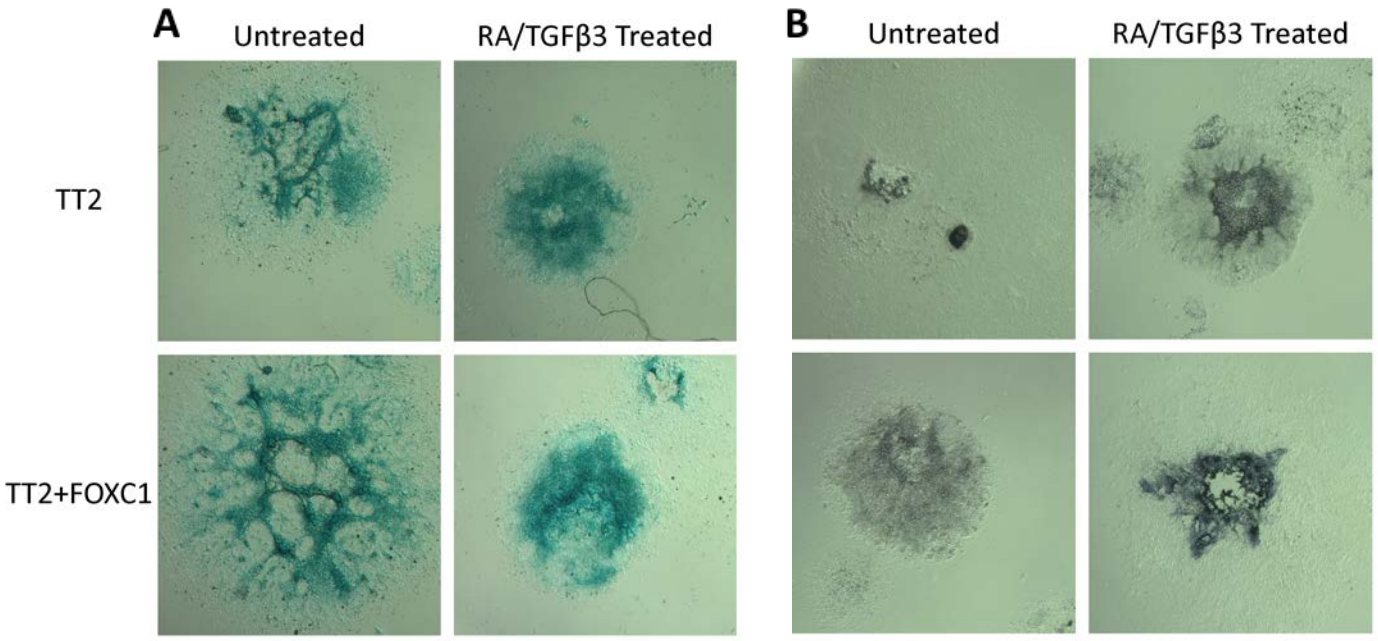

Figure 4.13 FOXC1 Overexpression Resulted in Increased Production of ECM and Alkaline Phosphatase. (A) Alcian blue staining in the untreated TT2 cells and TT2_Hs. FOXC1 cells was spread over a larger surface area compared to the RA-TGFβ3 groups. In the TT2+ RA-TGFβ3 and in the treated cells overexpressing FOXC1 Alcian blue staining was more concentrated in the center of the aggregate. **(B)** Untreated TT2 cells had little alkaline phosphatase (AP) staining on day 13 of differentiation. TT2 cells treated with RA-TGFβ3 had stronger AP staining in the center of the aggregate, and weak AP staining radiating outwards. TT2 cells overexpressing FOXC1 had weak AP staining throughout the condensation. TT2 cells overexpressing FOXC1 and treated with RA-TGFβ3 had very strong AP staining in the center of the condensation as well as in the periphery of the condensation. Images are representative of 3 biological replicates.

To further evaluate the role of *Foxc1* in chondrogenic differentiation, knocking *Foxc1* out of the TT2 embryonic stem cells was attempted using the CRISPR genome editing system. The aim was to demonstrate that *Foxc1* is necessary for chondrogenic differentiation. Following single colony isolation, high resolution melt (HRM) analysis was used to validate that the knockout was successful. All five cell lines appeared to have a shift in peak melting temperature, indicating mutations have been generated (Figure 4.14). DNA samples were sent for sequencing to map out the exact mutation in each cell line. Returned sequences revealed that while most of the *Foxc1* gene has been amplified correctly, the regions of the gene targeted by the PAM sequences were not sequenced properly and individual basepairs could not be identified. These sequencing results suggest that the samples sent for sequencing analysis contained mixed allelic populations and that single clones would have to be generated in order to identify the exact mutation in each cell line. However, cloning *Foxc1* into a Gateway-system entry vector proved challenging and was not successfully verified. Using *Foxc1* primers available in the lab containing attB sites, which would allow insertion into the pDonr vector, resulted in cloning of *Foxl2* instead of *Foxc1*. Similarly, using primers specifically designed for the CRISPR cell lines resulted in cloning of *Foxl2*. Several different primer sets were used with little success. Unfortunately, this made identifying and characterizing the CRISPR-generated mutation difficult and therefore prevented further analysis of these cell lines.

Figure 4.14 HRM Analysis of CRIPR-generated mutations in Foxc1

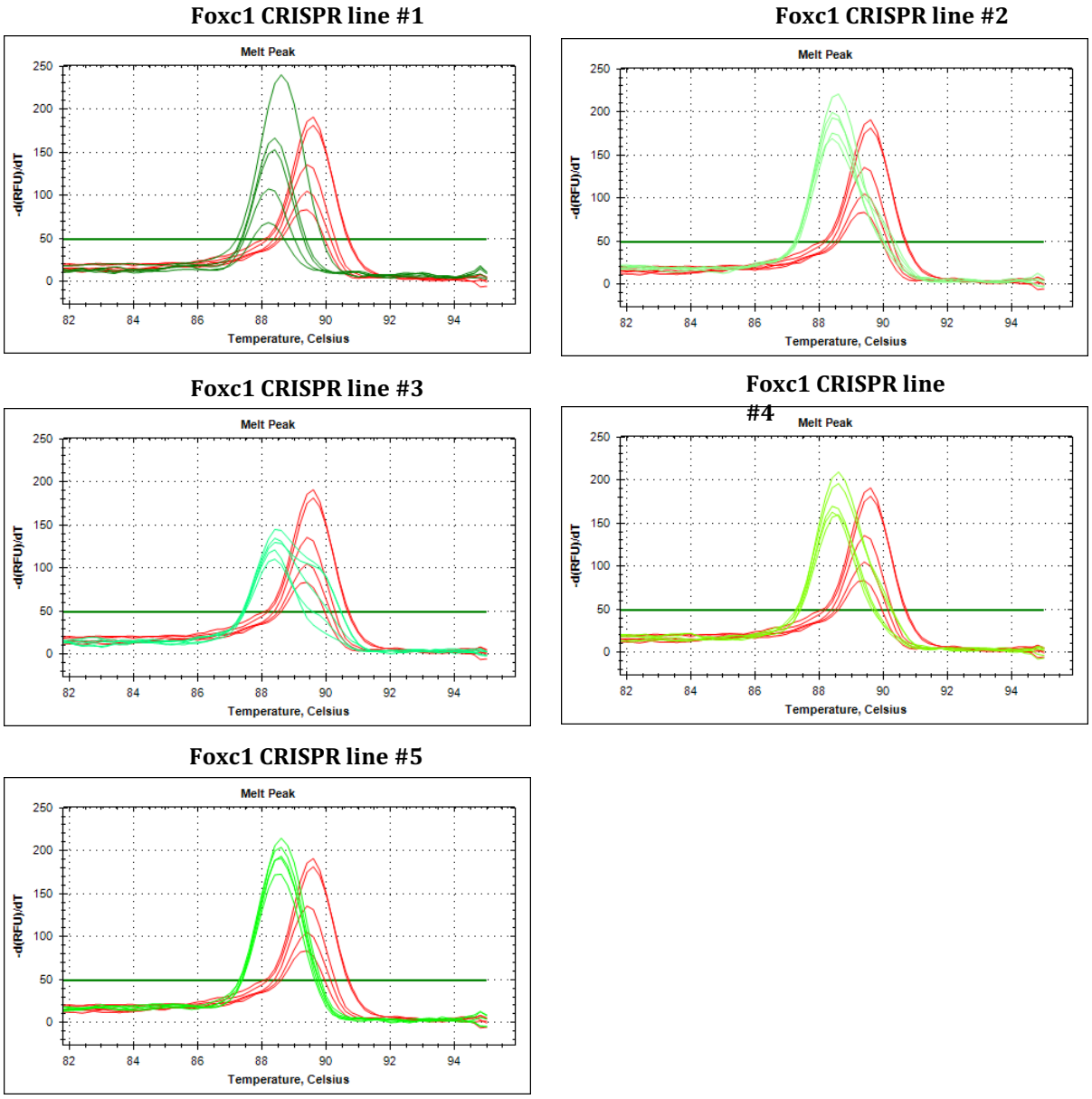

Figure 4.14 HRM analysis of five cell lines with CRISPR-derived mutations in *Foxc1*. High resolution melt analysis of the five individual cell lines treated with the *Foxc1*-CRISPR revealed a shift in the melting temperature peaks of all five lines.

To expand on the role of Foxc1 in endochondral differentiation, physical interactions between Foxc1 and SOX9 were assessed next. A previous study found SOX9 binding sites in close proximity to Foxc1 binding motifs (Liu and Lefebvre, 2015). This raised the idea that Foxc1 and SOX9 could have similar downstream targets and are acting in cooperation to regulate gene expression. The BioID system, in which a biotin ligase is fused to the bait protein and biotinylates proteins that come into close proximity (Roux et al., 2012), was utilized to test whether Foxc1 and SOX9 physically associate with one another. U2OS cells were transfected with either BioID-Foxc1 or an empty BioID vector along with Flag-SOX9 or empty Flag, in the presence of biotin. When co-transfected with BioID-Foxc1, Flag-SOX9 was recovered from the precipitated sample. In the sample containing the empty BioID vector no Flag-SOX9 has been detected (Figure 4.15). This suggests that SOX9 comes in close proximity to Foxc1 and has been biotinylated by the BioID-Foxc1. However, while the BioID assay suggests that Foxc1 have a SOX9 physical association, it does not point to direct physical interaction between the two proteins. The HaloTag pull-down system was used next to assess the existence of a direct physical interaction. In this assay, a bait protein is recombined into a vector containing a Halo tag. The Halo tag forms a covalent bond with the Halo resin and any proteins that directly bind to the bait protein can be precipitated and recovered. The Halo-FOXC1 protein (~120kDa), Flag-SOX9 (~80kDa) and empty Halo vector (~35kDa) were all detected in the input samples (Figure 4.16). However, following the elution of the precipitated proteins, no Flag-SOX9 was detected. These results

suggest that SOX9 and Foxc1 do not physically interact with each other, although they do come in close proximity to one another.

Figure 4.15 Foxc1 Comes in Close Proximity to SOX9 In a Cell Culture System

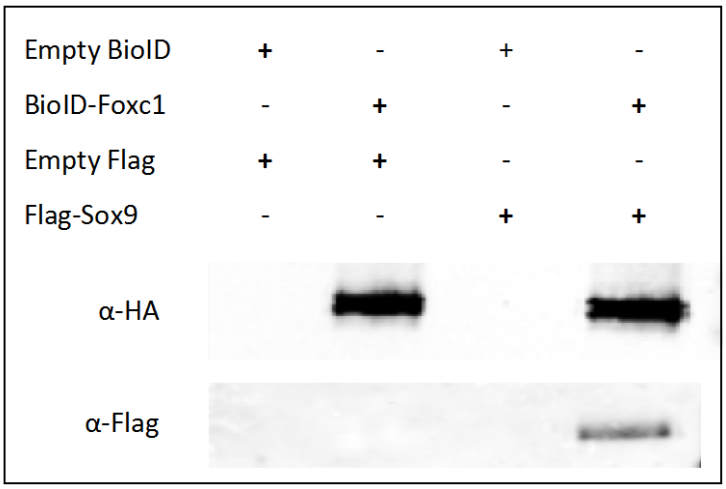

Figure 4.15 Foxc1 Comes in Close Proximity to SOX9 in a Cell Culture System. Biotinylated Flag-SOX9 was precipitated from the sample containing BioID-Foxc1 but was not detected in the sample containing the empty BioID vector. Empty flag was not detected when transfected with either the empty BioID vector or with the BioID-Foxc1. Membrane was blotted with αHA and αFlag antibodies.

Figure 4.16 No Evidence was Found for a Foxc1 and SOX9 Physical Interaction

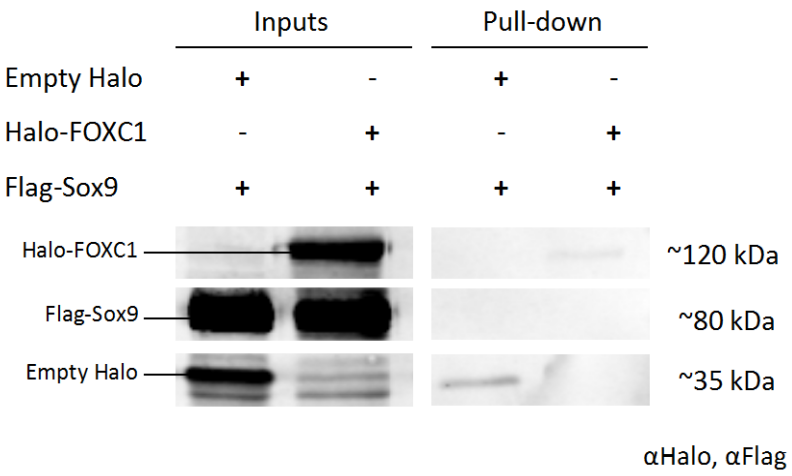

Figure 4.16 No evidence was found for a Foxc1 and SOX9 physical interaction. Flag-SOX9 was detected in both the input sample containing Halo-FOXC1 and the sample containing the empty Halo vector, however it was not detected in either of the pull down samples when blotted with αHalo and αFlag antibodies.

The idea that FOXC1 and SOX9 could be coming in close proximity to one another but do not form a direct physical interaction led to the hypothesis that they might be both binding to a similar DNA region to co-regulate downstream target genes. Inspection of the ChIP-Seq data generated by Ohba et al. exposed two full Foxc1 binding sites within the SOX9 peaks in *Sox6*, *Sox6-1* and *Sox6-2* (Ohba et al., 2015) (Figure 4.17A). Chromatin immunoprecipitation was used next to investigate whether both Foxc1 and SOX9 can bind to these DNA regions. TT2 cells were stimulated with Activin A to induce chondrogenic differentiation, and the expression of SOX9 and Foxc1 were validated using western blots (Figures 4.6A and 4.18A, respectively). In lysates precipitated with α-SOX9, *Sox6-1* was successfully recovered whereas *Sox6-2* was not (Figure 4.17B). Rabbit IgG and αH327ac were used as internal controls and *Col2 intron 1* was used as a technical control (Figure 4.17C). Analysis of *Sox6-1* using FIMO revealed the existence of a sequence matching the PWM the SOX9 DNA binding motif (Figure 4.1D). Similarly, in lysates precipitated with α-Foxc1, *Sox6-1* was recovered but *Sox6*-2 was not (Figure 4.18B). *Msx2* was used here as a technical control (Mirzayans et al., 2012) (Figure 4.18C). Analysis of the *Sox6-1* sequence showed enrichment of the Foxc1 DNA binding motif (Figure 4.18D). Lastly, analysis of the *Sox6-1* sequence using the UCSC genome browser revealed evolutionary conservation of several Foxc1 and SOX9 DNA binding domains, suggesting these domains have an important and conserved regulatory function in mammals (Figure 4.19).

Figure 4.17 *Sox6-1* was Successfully Recovered Following Chromatin Immunoprecipitation with α-SOX9

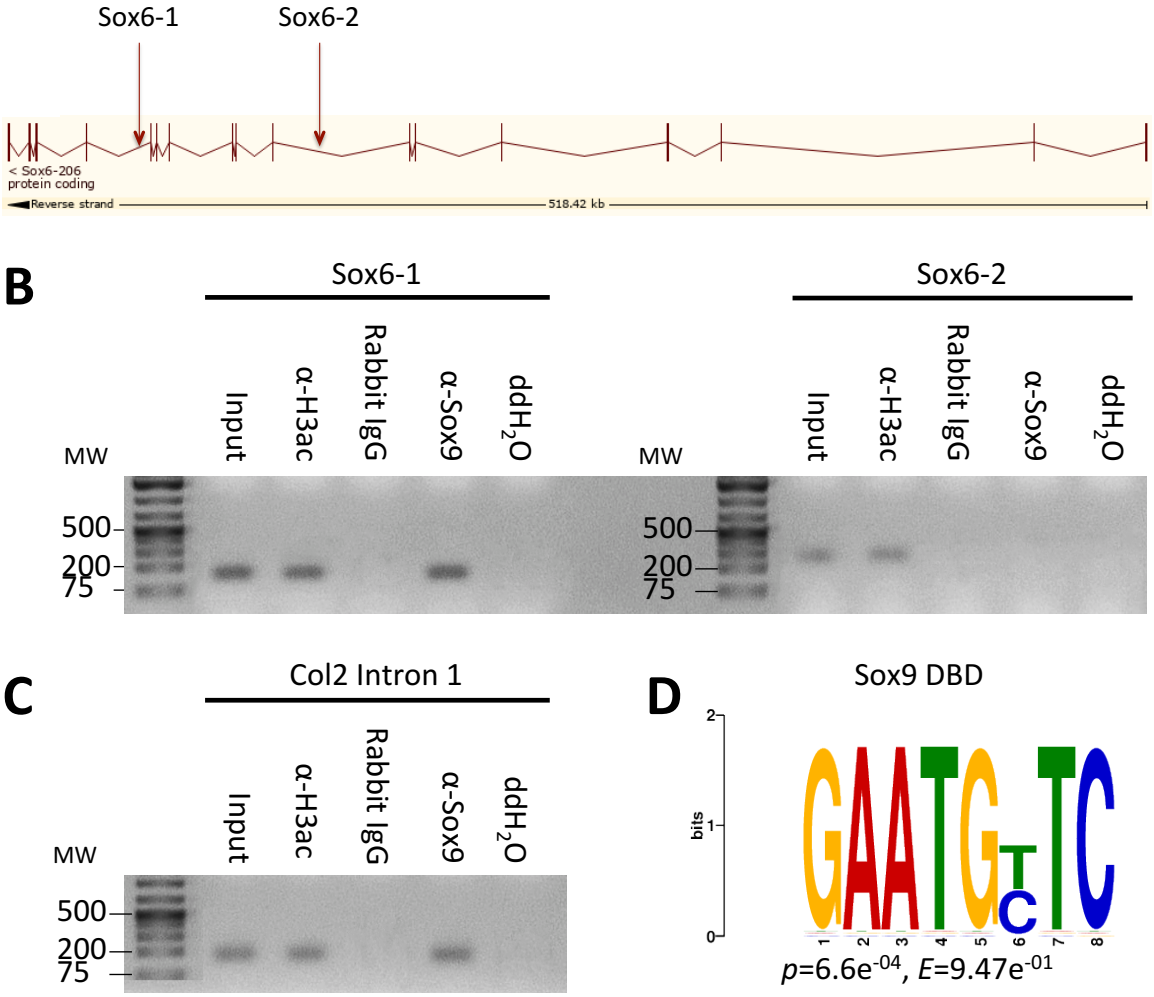

Figure 4.17 *Sox6-1* was successfully recovered following chromaton immunoprecipitation with α-SOX9. **(A)** SOX9 and Foxc1 DNA binding domains were found in close proximity to each other within introns 7 and 13 of *Sox6*. **(B)** *Sox6-1* and *Sox6-2* were detected in the input sample and in the α-H3ac lysate (positive control) but only *Sox6-1* was recovered from the α-SOX9 lysate. Rabbit IgG was used as a negative control. **(C)** *Col2 intron 1* was used as a technical positive control for SOX9 ChIP (Oh et al., 2010). **(D)** Sequence analysis of *Sox6-1* revealed enrichment of the SOX9 DNA binding domain (Grant et al., 2011).

Figure 4.18 Chromatin Immunoprecipitation with α-Foxc1 Led to Recovery of *Sox6-1*

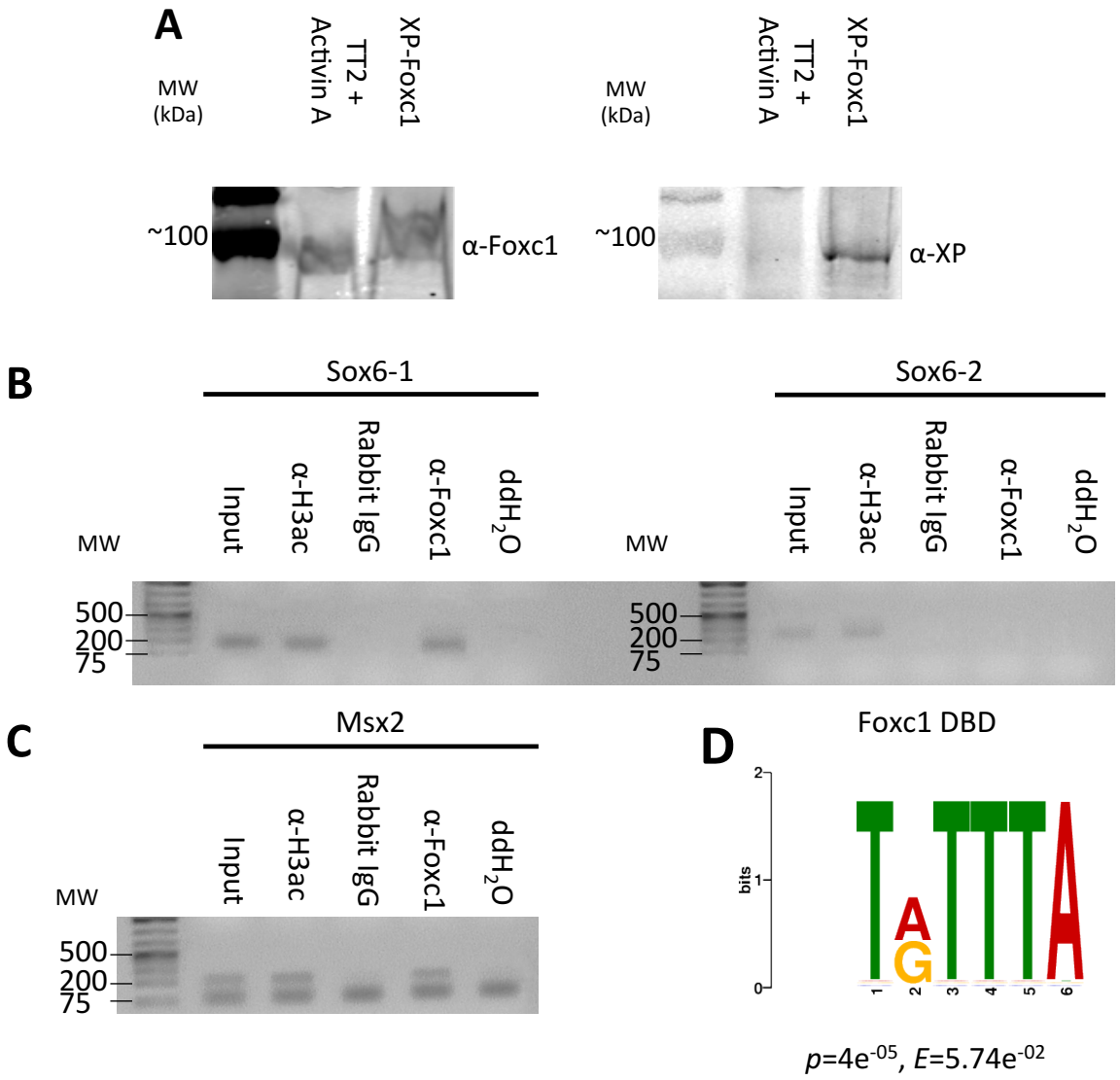

Figure 4.18 Chromatin immunoprecipitation with α-Foxc1 led to recovery of *Sox6*-1. **(A)** Endogenous Foxc1 protein was detected in TT2 cells stimulated with Activin A. **(B)** Both *Sox6-1* and *Sox6-2* were detected in the input sample and were recovered successfully using the α-H3ac (positive control), but chromatin immunoprecipitation with α-Foxc1 resulted in recovery of the *Sox6-1* region only and not the *Sox6-2* region. **(C)** *Msx2* was used as a technical positive control

(Mirzayans et al., 2012). It was successfully recovered using the α-Foxc1 and αH3ac antibodies but not using the rabbit IgG (negative control). **(D)** Sequence analysis of *Sox6-1* revealed enrichment of the Foxc1 DNA binding domain (Grant et al., 2011).

Figure 4.19 *Sox6*-1 is Evolutionary Conserved in Vertebrates

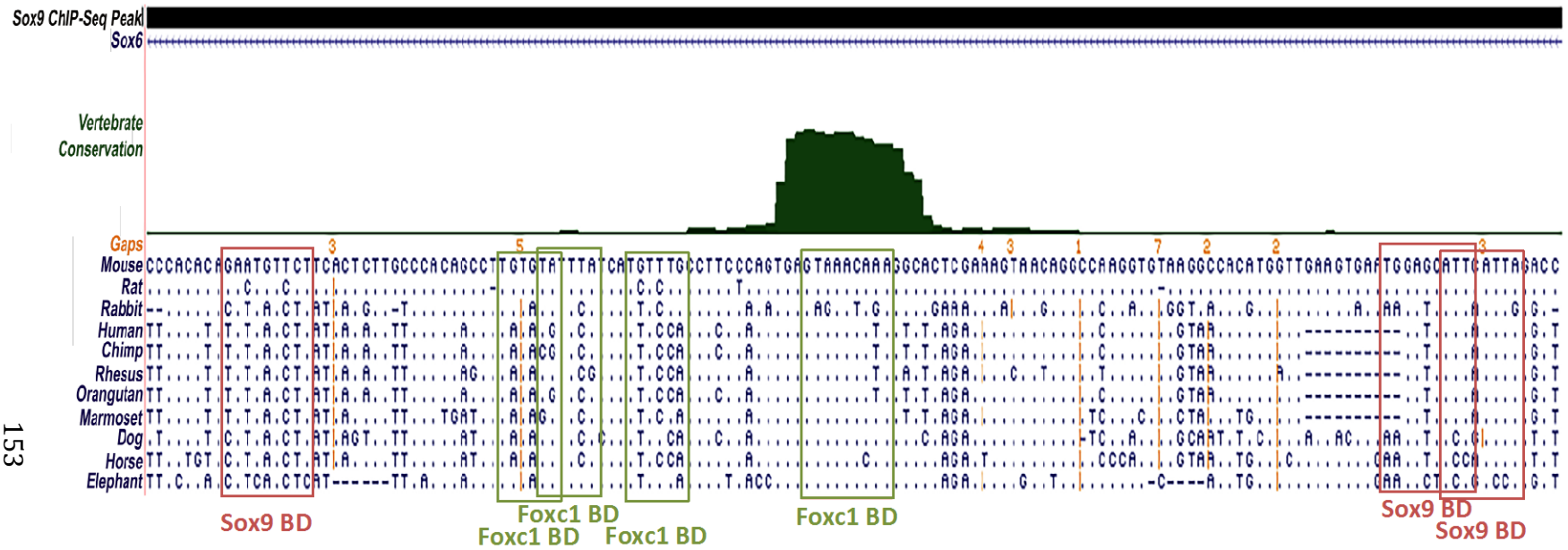

Figure 4.19 *Sox6*-1 is evolutionary conserved in vertebrates. The *Sox6*-1 domain has several regions that are well conserved in other vertebrate species. One of the putative Foxc1 DBD (green) and one of the putative SOX9 DBD (red) show high conservation of the binding domain sequence.

DISCUSSION

Accumulating evidence in recent years points to the important regulatory role of Foxc1 in chondrogenic differentiation. Foxc1 expression has been detected in mesenchymal condensations prior to their chondrogenic differentiation, as well as in resting, proliferating and hypertrophic chondrocytes (Hiemisch et al., 1998a; Hiemisch et al., 1998b; Kume et al., 1998; Yoshida et al., 2015). Foxc1 has also been detected in the differentiated cartilage of the ribs and sternum and limb buds (Yoshida et al., 2015), suggesting it is involved in all stages of chondrogenesis. Mice with *Foxc1* mutations have defects in ossification of the lateral neural arches, rib cage and sternum. In these mice the vertebral bodies are smaller and the skull vault and hyoid bone fail to form; the ossification centers in the sternum and vertebrae are missing or are reduced in size and the limbs are significantly shorter (Kume et al., 1998). Furthermore, hypertrophic chondrocytes were missing in the sternum of *Foxc1* mutants and the hypertrophic zone in the tibial growth plate was longer than in wild-type mice (Yoshida et al., 2015). It has been shown that in the late stages of chondrogenesis, Foxc1 directly interacts with GLI2 and IHH to regulate the expression of type 10 collagen and PTHrP, markers of hypertrophic chondrocytes (Yoshida et al., 2015). This interaction helps to elucidate some of the roles of Foxc1 during late-stage chondrogenesis; it suggests that Foxc1 is involved in the progression from pre-hypertrophic to hypertrophic chondrocytes. However, the role that Foxc1 plays in early chondrogenesis, during the differentiation of mesenchymal stem cells into proliferating and prehypertrophic chondrocytes, is still

unclear. It is also unknown how Foxc1 is regulated during these developmental processes. Here I sought to investigate the genetic interactions between *Foxc1* and SOX9. Specifically, I analyzed *Foxc1* expression during the formation of the mesenchymal condensation and early chondrogenesis, I evaluated the regulation of *Foxc1* by SOX9, and I explored a potential interaction between SOX9 and Foxc1 in *Sox6* regulation.

Overexpression of FOXC1 in embryonic stem cells that give rise to mesenchymal condensations leads to an initial increase in the expression of chondrogenic markers such as *Sox9*, *Sox6* and *Sox5*, followed by a stable increase of *Runx2* expression. These three *Sox* genes are known to act in concert to regulate chondrogenic differentiation, and SOX9 in particular is considered to be an initiator of chondrogenic differentiation. Increased *Sox9* expression in cells overexpressing FOXC1 suggests that downstream chondrogenic targets would also be upregulated leading to increased chondrogenic differentiation. The increase in *Runx2* expression at the later stages of the differentiation assay indicates that the cells have begun to hypertrophy. Together with the increase in sGAG and ECM production following FOXC1 overexpression, this suggests that Foxc1 functions to drive chondrogenesis at an increased pace compared to cells with normal Foxc1 expression.

My results show that SOX9 directly regulates the expression of *Foxc1* through the *Foxc1* enhancer element B. The *Foxc1* distal element B was successfully recovered using chromatin immunoprecipitation performed on both overexpressed Flag-SOX9 and endogenously expressed SOX9, demonstrating that SOX9 directly

binds distal element B. Sox proteins in general have a preferential binding activation of enhancer elements rather than promoters of their down-stream targets (Kamachi and Kondoh, 2013). The *Foxc1* enhancer element B lies 41kb upstream of the *Foxc1* start site, and contains three possible SOX9 binding sites. Transactivation luciferase assays demonstrate that SOX9 binding leads to markedly increased activation of the *Foxc1* distal B reporter and that the identified binding domains within distal element B are individually sufficient for SOX9 activation of the reporter. This observation falls in line with the idea that SOX9 usually binds as a dimer to promote activation of downstream targets (Oh et al., 2010). While SOX9 has been shown to activate transcription through monomeric binding of DNA, it appears that this function is more common in sex determination, whereas in chondrogenesis SOX9 functions mainly in a dimeric fashion (Bernard et al., 2003). However, whether SOX9 dimerization is required for the activation of *Foxc1* distal element B requires further analysis.

My findings also demonstrate that SOX9 and Foxc1 come in close proximity to one another in a mammalian cell system, indicating that these two proteins might be working together to regulate the downstream targets. No evidence was found for a direct SOX9-Foxc1 physical interaction; however, they may come in close contact during regulation of common target genes. Liu and Lefebvre found enrichment of SOX9 binding domain in close proximity to Fox binding motifs (Liu and Lefebvre, 2015). It is therefore possible that Foxc1 and SOX9 both bind to the same downstream targets, a proximity that would fall in line with the BioID-Foxc1 observations presented here. Review of the ChIP-Seq data generated by Ohba et al.

revealed two regions within the *Sox6* gene, one in intron 7 and the other in intron 13, that have been recovered using an α-SOX9 antibody and are enriched with Foxc1 DNA binding motif (Ohba et al., 2015). Analysis of these regions, *Sox6-1* and *Sox6-2*, determined that *Sox6-1* was recovered in ChIP of either Foxc1 or SOX9 while *Sox6-2* was not. Motif analysis of the sequence has shown that there are three potential SOX9 binding motifs and four potential Foxc1 binding motifs within the *Sox6-1* region. While the overall basepair conservation of *Sox6-1* is lacking, there is increased conservation in the areas where those DNA binding domains were discovered, suggesting a conserved evolutionary function. Together, these results indicate that Foxc1 and SOX9 might be co-regulating *Sox6* expression during chondrogenic differentiation by binding the *Sox6-1* region.

Understanding how *Foxc1* acts to regulate the formation of endochondral bones would provide new research avenues for therapeutic strategies for defects in cartilage and bone, including tissue-engineering reserch. Current findings have demonstrated that lack of *Foxc1* expression or mutations in *Foxc1* can lead to severe defects in the formation of the axial skeleton and other long bones, in additon to anomalies in intramembraneous bone formation. It is therefore important to understand where Foxc1 fits in the pathway leading from mesenchymal condensations to ossifyed bone. Previous studies have demonstrated that Foxc1 has an important role in regulating EMT (Hopkins et al., 2017) as well as in promoting hypertrophic differentiation of mature chondrocytes (Yoshida et al., 2015). Little is known, however, about how *Foxc1* is regulated during these processes, or what downstream targets it acts on. My results demonstrate that SOX9 directly regulates

Foxc1 expression through the *Foxc1* distal element B and that SOX9 and Foxc1 could potentially be co-regulating *Sox6* expression through *Sox6-1*. Additionally, I have shown that *Foxc1* overexpression results in increased expression of chondrogenic markers and amplified differentiation. These findings provide insight into the function and regulation of Foxc1 during endochondral differentiation and expand on existing models of chondrogenesis.

Figure 4.20 Proposed Foxc1 Role in Chondrogenic Differentiation

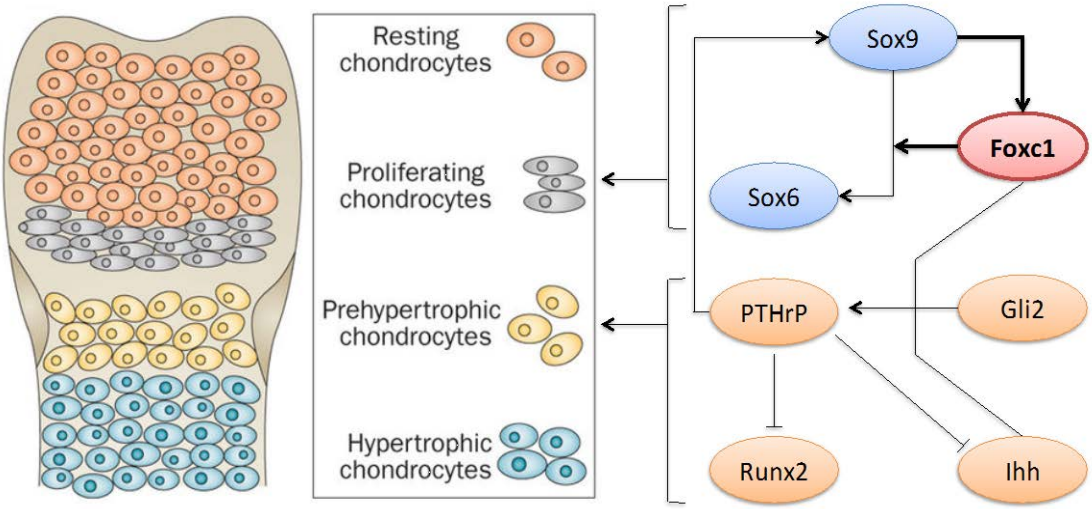

Figure 4.20 Proposed Foxc1 Role in Chondrogenic Differentiation. Based on my findings, I propose that in proliferating chondrocytes, Foxc1 interacts with SOX9 to induce activation of downstream chondrogenic targets, particularly *Sox6*. This helps to promote proliferation of chondrocytes and cartilage growth. Later, in prehypertrophic chondrocytes, Foxc1 interacts with GLI2 and IHH to suppress hypertrophy through PTHrP (Yoshida et al., 2015). Figure adapted with permission from (Alman, 2015).

CHAPTER 5. CONCLUSIONS AND FUTURE DIRECTIONS

Anomalies of the skeleton often cause pain and disability and are associated with poor quality of life. Unfortunately, the primary causes of many skeletal deformities are still not clearly understood. Many such anomalies are a result of defects in early embryonic development – early differentiation and patterning events that underlie the formation of primordial structures and development of precursors. FOXC1 is a forkhead box transcription factor that plays an important role in skeletal formation early in embryonic development. While mutations in *FOXC1* have mostly been associated with defects in the development of the eye, many patients with *FOXC1* mutation also suffer from skeletal abnormalities (Berry et al., 2006; Berry et al., 2008; Gripp et al., 2013; Hong et al., 1999; Kim et al., 2013; Kume, 2009; Kume et al., 1998; Kume et al., 2001). Additionally, Foxc1 animal models have been shown to have severe skeletal defects when Foxc1 is missing or nonfunctional (Kume et al., 1998; Kume et al., 2001). The expression of Foxc1 has been detected in various stages of skeletal development, from mesenchymal progenitors to mesodermal ones, from differentiating osteoblasts and chondroblasts to mature ossification centers and hypertrophic zones (Hayashi and Kume, 2008; Hiemisch et al., 1998a; Hiemisch et al., 1998b; Hopkins et al., 2016; Kume et al., 2001; Mirzayans et al., 2012; Siegenthaler et al., 2013). While there have been many advances in understanding what role Foxc1 plays in these processes, many questions still remain unanswered. Here, I characterize some of the roles of Foxc1

in early skeletal patterning and differentiation events. Specifically, I analyze some of the genetic interaction involving Foxc1 in somitogenesis and early cartilage formation.

FOXC1 CONTROLS ANTERIOR SOMITE FORMATION THROUGH THE RETINOIC ACID GRADIENT

Characterization of the role of Foxc1a in somitogenesis was partially achieved using the morpholino technology. The main concerns with using morpholinos are incomplete knockdown of the gene or gene product and the possibility of secondary effects of the morpholino. In addition, the morpholino effect is transient, and is diluted as the embryo grows. To address these issues, a few precautionary measures have been taken. First, the *foxc1a* morphants were compared to embryos injected with a similar concentration of an industry-standard control. Therefore, any changes observed are not a result of the physical piercing of the chorion and/or yolk but can be attributed to the morpholino used. Also, the rescue experiments performed confirmed that the phenotypes observed in the *foxc1a*-MO injected embryos can be rescued with *foxc1a* mRNA. This suggests that these observations are a result of the specific affect of the morpholino on *foxc1a* and not on secondary, non-specific targets. In addition, the phenotypes presented here mimic what was seen previously in the mice models (Kume et al., 2001) as well as in the *mib*^{nn2002} mutant fish model, which has a complete deletion of *foxc1a* (Hsu et al., 2015). Finally, injections of the *foxc1a* morpholino into the *foxc1a*^{UA1017} mutants, which replicated what was seen in the morphants rather than the native mutants, provide additional evidence of the more complete knockdown of *foxc1a* achieved here using the morpholino technology.

Foxc1 expression is important for anterior somite formation

The work detailed here demonstrates that *foxc1a* controls somite formation through regulation of the *raldh2-fgf8a* gradients in the presomitic mesoderm of the zebrafish embryo. Down-regulation of *foxc1a* leads to reduced expression of the boundary determination factor *mesp-ba* and an anterior shift of the *tbx6* expression domain, resulting in defects in somite formation. My results indicate that the role of Foxc1a in somitogenesis is critical for the formation of the anterior somites, whereas the posterior somites still form, and that Foxc1 controls somite formation by altering the expression domain of *raldh2* in the PSM. There have been several reports showing that the spatial expression of retinoic acid is crucial for the formation of the anterior somites but less critical during the development of the posterior ones. For example, mice deficient in the RA repressor Cyp26a1 exhibited elevated RA expression in the tailbud, and anterior agenesis (Abu-Abed et al., 2001; Abu-Abed et al., 2003; Sakai et al., 2001). Therefore, it would stand to reason that an altered expression domain of *raldh2* caused by lack of *foxc1a* would manifest in anterior somite abnormalities, with a lesser effect on the posterior somites. Expanding on the mechanisms through which Foxc1 regulates *raldh2*, whether directly or through mediator-targets, would give further insight into the regulation of retinoic acid, an important growth factor, in the PSM. One way in which this could be achieved would be by placing beads soaked in RA or Cyp26a at the anterior or posterior PSM at the onset of somitogenesis (~12 hpf). If Foxc1a expression is regulating somite formation through regulation of RA signaling, increasing RA signaling in Foxc1a morphants would restore anterior somite formation. In

addition, since both Foxc1 and retinoic acid are important regulators of various other tissues such as eye development and osteochondrogenic differentiation, learning how they interact with one another could help elucidate how defects in other organs arise.

Somite boundary formation can proceed in the absence of *mesp-ba*

This report provides evidence that somitic boundary formation can proceed when *mesp-ba* is reduced or missing for the first time. *Mesp2*, the mouse orthologue of *mesp-ba*, has been considered to be the boundary determination gene and several papers have reported that somitic boundaries do not form in the absence of MESP2 (Morimoto et al., 2005; Saga, 2007). However, the results detailed herein clearly demonstrate that even when *mesp-ba* expression is reduced in the posterior somites, intersomitic boundaries do form. This suggests that boundary formation can be regulated via an alternate mechanism when *mesp-ba* is missing. What this mechanism might be remains to be investigated. Zebrafish embryos have two copies of *Mesp2, mesp-ba* and *mesp-bb* (Cutty et al., 2012; Yabe et al., 2016). It is therefore possible that when *mesp-ba* is reduced *mesp-bb* can compensate and drive boundary formation. Methods such as RNA-Seq could also be utilized to detect the expression of which genes are altered in the posterior PSM of mutant fish compared to wild-type siblings and to identify possible alternate candidate boundary formation genes.

Somitogenesis – Future directions

Given that the *foxc1a* mutants in which somite formation was characterized thus far do not appear to be true null mutants, it would be interesting to see how somite formation would proceed in true *foxc1a* mutants. Currently, the only zebrafish model available with a complete *foxc1a* deletion is the *mib*^{nn2002} mutant (Hsu et al., 2015). These mutants have an arm deletion on chromosome 2, covering both *mib* and *foxc1a.* Somite formation in these zebrafish mutants closely resembles what was seen in the *foxc1a* morphants discussed herein, notably lack of formation of the anterior 7-9 somites, with restored formation of the posterior somites (Hsu et al., 2015). The expression domain of *tbx6* in these fish is smaller, mimicking the observations in the *foxc1a* morphants. Importantly, injections of *foxc1a* mRNA have partially rescued the *mib*^{nn2002} anterior somite phenotype, indicating that *foxc1a* is crucial for this developmental process (Hsu et al., 2015). Additionally, the *mib* allele does not result in a somite phenotype, further indicating that the defect in somitogenesis observed in the *mib*^{nn2002} mutants is a result of the loss of *foxc1a* (Itoh et al., 2003; Lawson et al., 2001; Schier et al., 1996). Unfortunately, the *mib*^{nn2002} mutants also exhibit increased cell death that was not alleviated with *foxc1a* mRNA injection, suggesting it could be an outcome of the *mib* deletion. It would therefore be rational to expect that complete *foxc1a* deletion would phenocopy the somitogenesis defects seen in the *mib*^{nn2002} mutants without mimicking the cell death seen in those mutants, enabling further analysis. Until such a model is available, using the *mib*^{nn2002} mutant zebrafish for ongoing somitogenesis studies

would provide a more comprehensive and accurate model than other *foxc1a* knockout models currently available.

It is also important to address the possibility that *foxc1b* is compensating for the absence of *foxc1a* in both the mutants and the morphants. Expression of *foxc1b* in the PSM has been documented before, although knocking it down did not lead to a somitogenesis phenotype (Topczewska et al., 2001a). However it is possible that when Foxc1a is missing, Foxc1b is able to bind and regulate downstream targets. In *foxc1a* mutants it is also possible that spontaneous *foxc1b* mutations evolve to offset the lack of *foxc1a* expression. These possibilities could be assessed using whole-mount *in-situ* hybridization of *foxc1b* mRNA or immunofluorescence of Foxc1b in *foxc1a* mutants and morphants. Additionally, inactivating *foxc1b* in these fish, either through a mutation or transient knockdown, could further demonstrate its role in somitogenesis.

It would be valuable to see how the precursors contained within the somites are affected in *foxc1a* mutants and morphants. The somites contain sclerotome, myotome, dermamyotome, and syndetome precursors. However, vertebral bones in zebrafish grow through mineralization of the notochord and not from sclerotomal precursors (Bensimon-Brito et al., 2012). It would be curious to see what downstream defects arise from the anomalies observed in the zebrafish somites and what organs and tissues are derived from these precursor populations. A more suitable model to study the downstream effects of *Foxc1* misregulation on the formation of the vertebral column would be a null-*Foxc1* mouse model. In-vivo

lineage tracing in these animals can provide additional information into how loss of intersomitic boundaries and positional identity manifest in derived tissues. Cells that will give rise to sclerotomal tissues can be identified by the expression of *Pax1* and *Pax9* (Mise et al., 2008; Rodrigo et al., 2003), whereas myotome precursors express *Myod, Myf5* and *Pax3* (Hammond et al., 2007). Methods such as immunohistochemistry and *in-situ* hybridization could be used to trace the expression of these markers in the anterior, unsegmented paraxial mesoderm in *Foxc1*-null embryos. If *Foxc1* is indeed critical mostly for the development of sclerotome-derived tissues, the expression of *Pax1a* and *Pax9* would be affected whereas *Myod, Myf5* and *Pax3* would be expressed normally. It is possible however that reduced expression of *Foxc1* would also impact the formation of myotome-derived tissues. To better place Foxc1 in the developmental pathway leading from somite formation to formation of vertebral elements, it would be prudent to know whether other tissues are affected, and to what extent. Further, this information could help elucidate the differential effect Foxc1 has on anterior somite versus posterior ones by examining the expression of downstream regulators of sclerotomal differentiation.

FOXC1 HAS AN IMPORTANT REGULATORY ROLE DURING CARTILAGE FORMATION

The role of *Foxc1* in skeletal development has also been shown to be crucial for proper formation of the bony elements of the skeleton. However, how Foxc1 functions to exert these functions is still not completely understood. Recent studies have shown that Foxc1 has an important role in regulating the switch between FGFR1 and FGFR2 during epithelial to mesenchymal transition (EMT) (Hopkins et al., 2017), which is necessary for the formation of mesenchymal condensations. FOXC1 expression is also important for the commitment of progenitor cells to osteoblast differentiation (Hopkins et al., 2016). These results provide some insight into the phenotypes observed in *Foxc1* mutants, although mainly into defects in the formation of intramembranous bones such as the bones of the skull vault and clavicle. Anomalies in the formation of endochondral bones have also been frequently observed, yet the role of Foxc1 during endochondral bone formation is still mostly unknown. This report points to an interesting and important regulatory role of Foxc1 during the initial stages of chondrogenic differentiation.

Foxc1 overexpression leads to early hypertrophy of chondrocytes

While Foxc1 seems to be important for chondrogenic formation, it is unknown how the regulation of chondrogenic markers is impacted in the absence of Foxc1. Previous studies have shown that Foxc1 is critical for the progression of hypertrophy in maturing chondrocytes. The study outlined here also demonstrates

that hypertrophy occurs earlier in cells overexpressing FOXC1. This study, however, is limited by the transiency of the FOXC1 overexpression. As demonstrated above, Hs. FOXC1 mRNA levels decline during the differentiation assay. The effects seen here are a result of increased Foxc1 function in the early stages of chondrogenic differentiation – before and during chondrocyte proliferation. While qPCR measurements were corrected for the amount of mRNA in the samples, it is possible that increased proliferation leads to an increase in density of the chondrogenic aggregates, thus driving early hypertrophy. Two ways of testing for this would be to (a) use a cell line stably expressing FOXC1 and (b) to knock Foxc1 out. Stable, increased expression of FOXC1 would allow one to observe differentiation for a longer time period without having the cells revert to normal expression. Additionally, it would provide a more consistent model of Foxc1 misexpression in humans and animal models. Knocking out Foxc1 in the TT2 ESCs used here, and putting these cells through the chondrogenic differentiation assay, would provide insight into how the expression of chondrogenic genes is affected. If Foxc1 overexpression does indeed work to accelerate the pace of chondrogenic differentiation in these cells, it would stand to reason that its absence would lead to attenuation in chondrogenesis but not to its early termination. Since accumulating evidence suggests that Foxc1 is important in hypertrophic chondrocytes, one could speculate that its absence could lead to increased proliferation of pre-hypertrophic chondrocytes and delayed maturation. One of the hurdles in learning the role of Foxc1 in skeletal development is the unviability of mouse embryos with homozygous *Foxc1* mutations. Conditional, tissue-specific knockouts of *Foxc1* could

potentially help overcome this obstacle and allow examination of both intramembranous and endochondral bone formation in *Foxc1*-null tissues. This could possibly be achieved using conditional knockdown mice under Col2a regulation. Since *Col2a* is expressed in the early stages of chondrogenesis and intramembranous ossification (Bruderer et al., 2014; Gomez-Picos and Eames, 2015; Oh et al., 2010), this would result in tissue-specific knockdown of *Foxc1* in osteogenic and chondrogenic progenitor cells. Additionally, conditional *Foxc1* knockout in committed endochondral progenitors would help elucidate how Foxc1 regulates cartilage development and identify potential Foxc1 downstream targets. For this, a different conditional knockout model could be used, under control of SOX9, SOX5 or SOX6.

SOX9 regulated Foxc1 expression through the Foxc1 distal element B

Several reports have indicated that a genetic interaction exists between the chondrogenic master regulator SOX9 and Foxc1 (Liu and Lefebvre, 2015; Ohba et al., 2015). Four SOX9 binding regions have been identified in close proximity to the *Foxc1* start site, three upstream of the gene and one down stream (Ohba et al., 2015). ChIP analysis performed on overexpressed Flag-SOX9, as well as on endogenously expressed SOX9, demonstrated that SOX9 directly binds to the *Foxc1* distal element B. Further analysis of this element has shown that there are three putative SOX9 binding domains within this region and that each one is sufficient on its own for SOX9 activation of the reporter gene. These results fall in line with other

reports demonstrating that SOX9 often binds to target genes as a homodimer and that several SOX9 binding sites are often found in close proximity to one another (Bridgewater et al., 2003; Han and Lefebvre, 2008; Sock et al., 2003). It is still unclear, however, whether SOX9 activates the *Foxc1* distal element B through dimeric binding. To validate the direct binding of SOX9 binding to distal element B, one could use electrophoretic mobility shift assay (EMSA) to rule out any intermediates in the reaction. It is also worth noting that there are likely to be other factors regulating *Foxc1* expression in chondrogenesis. Preventing SOX9 binding of this element, either by competing it out or by creating specific mutations in it, would demonstrate the requirement of SOX9 for *Foxc1* expression. Identifying how *Foxc1* expression is regulated during the various stages of chondrogenesis would help place it within the cascade of events leading to proper cartilage formation.

Foxc1 and SOX9 potentially co-regulate *Sox6* expression during chondrogenesis

My results demonstrate that SOX9 and Foxc1 come in close association to one another but do not directly physically interact. It is possible, though, that they could both be binding to the same downstream targets, leading to biotinylation of SOX9 by the BioID-Foxc1. A recent report found an increased enrichment of FOX binding motifs in close vicinity to SOX9 binding sites (Liu and Lefebvre, 2015). Inspection of the ChIP-Seq data produced Ohba et al., 2015 helped identify two regions within *Sox6*, a known SOX9 target, containing possible Foxc1 binding elements lying close to SOX9 binding motifs. It is likely that SOX9 and Foxc1 are both necessary for the

regulation of *Sox6* during chondrogenesis. ChIP analysis demonstrated that both protein bind to the *Sox6*-1 element. Neither protein was successful at recovering *Sox6*-2 in this assay. This suggests that Foxc1 and SOX9 are co-regulating *Sox6* expression through *Sox6*-1. Analysis of *Sox6*-1 for the presence of DNA binding motif revealed that there is an enrichment of both SOX9 and Foxc1 DBDs. Specifically, four putative Foxc1 DBDs and three putative SOX9 DBDs have been identified. While the evolutionary conservation of this region is not uniform, there are areas within it that seem to be better conserved than others suggesting these regions have an important regulatory function. Transactivation assays would be useful to assess the regulatory function of this potential co-regulation. Foxc1 can function as both an activator and a repressor. The cooperative function between SOX9-Foxc1 in the regulation of *Sox6* could therefore have an additive, positive activation of *Sox6* or a negative feedback for its repression. In addition, EMSA could be utilized to demonstrate whether Foxc1, SOX9 or both proteins can bind this DNA fragment. Co-regulation could require simultaneous binding of both proteins, which would result in a greater shift of the complex. Competitive binding of these proteins would result in a lesser shift in the presence of each protein alone. Conducting a Foxc1 ChIP-Seq study using rib-derived chondrocyte, similar to the one conducted by Ohba et al., will allow identification of other mutual downstream targets of Foxc1 and SOX9 co-regulation. This study would also provide insight into other potential targets of Foxc1 in chondrogenesis, either independently or together with other transcription factors. Assessing the co-regulatory functions of Foxc1 and SOX9 could provide important insights into the roles they play in chondrogenic

differentiation. Identifying mutual downstream targets would lead to expansion of current knowledge and allow for the development of new and updated differentiation assays.

My results demonstrate that Foxc1 has an important role in various stages of skeletal regulation. However, how Foxc1 is regulated in these tissues, and the molecular mechanisms through which it acts, are still unknown. Further identification of FOXC1 targets is essential to understanding how these tissues are formed in normal development and how irregularities in Foxc1 expression lead to the development of skeletal defects.

Skeletal deformities can have life-long debilitating effects on the quality of life of the individual. Current therapies include surgical intervention, transplantation, and external support, such as casts or the back brace used for scoliosis. Cartilage-specific defects are often treated by complete or partial removal of the defective tissue or by transplantation. These therapeutic techniques are complicated and only offer partial restoration of movement in most patients. In the last decade research into alternative methods of cartilage regeneration has been extensive. Many studies are examining the use of stem cells either during surgical intervention at the site of injury or ex-situ, to grow tissue-engineered cartilage that could replace the dependency on cadaver cartilage. However, in order to fully utilize these new technologies, we must first gain complete understanding of how these processes occur in natural development and only then will we be able to mimic them in laboratory settings. In order to stimulate stem cells to regenerate

cartilaginous tissue, we must first understand the molecular mechanisms that drive this differentiation process. The work presented here provides some insights into the genetic interactions that drive embryonic stem cells to undergo chondrogenic differentiation. It outlines some of the genetic interactions that regulate chondrogenic maturation and hypertrophy and provides a foundation for additional research into endochondral ossification.

REFERENCES

Abu-Abed, S., Dolle, P., Metzger, D., Beckett, B., Chambon, P., Petkovich, M., 2001. The retinoic acid-metabolizing enzyme, CYP26A1, is essential for normal hindbrain patterning, vertebral identity, and development of posterior structures. Genes Dev 15, 226-240.

Abu-Abed, S., Dolle, P., Metzger, D., Wood, C., MacLean, G., Chambon, P., Petkovich, M., 2003. Developing with lethal RA levels: genetic ablation of Rarg can restore the viability of mice lacking Cyp26a1. Development 130, 1449-1459.

Acharya, M., Huang, L., Fleisch, V.C., Allison, W.T., Walter, M.A., 2011. A complex regulatory network of transcription factors critical for ocular development and disease. Hum Mol Genet 20, 1610-1624.

Akiyama, H., Chaboissier, M.C., Martin, J.F., Schedl, A., de Crombrugghe, B., 2002. The transcription factor Sox9 has essential roles in successive steps of the chondrocyte differentiation pathway and is required for expression of Sox5 and Sox6. Genes Dev 16, 2813-2828.

Alman, B.A., 2015. The role of hedgehog signalling in skeletal health and disease. Nat Rev Rheumatol 11, 552-560.

Aoyama, H., Asamoto, K., 1988. Determination of somite cells: independence of cell differentiation and morphogenesis. Development 104, 15-28.

Aoyama, H., Asamoto, K., 2000. The developmental fate of the rostral/caudal half of a somite for vertebra and rib formation: experimental confirmation of the resegmentation theory using chick-quail chimeras. Mech Dev 99, 71-82.

Aulehla, A., Johnson, R.L., 1999. Dynamic expression of lunatic fringe suggests a link between notch signaling and an autonomous cellular oscillator driving somite segmentation. Dev Biol 207, 49-61.

Aulehla, A., Wehrle, C., Brand-Saberi, B., Kemler, R., Gossler, A., Kanzler, B., Herrmann, B.G., 2003. Wnt3a plays a major role in the segmentation clock controlling somitogenesis. Dev Cell 4, 395-406.

Bakayoko, S., Guirou, N., 2015. [Distichiasis: an anomaly of eyelashes]. Pan Afr Med J 20, 55.

Barna, M., Niswander, L., 2007. Visualization of cartilage formation: insight into cellular properties of skeletal progenitors and chondrodysplasia syndromes. Dev Cell 12, 931-941.

Barrantes, I.B., Elia, A.J., Wunsch, K., Hrabe de Angelis, M.H., Mak, T.W., Rossant, J., Conlon, R.A., Gossler, A., de la Pompa, J.L., 1999. Interaction between Notch signalling and Lunatic fringe during somite boundary formation in the mouse. Curr Biol 9, 470-480.

Bell, R., Brice, G., Child, A.H., Murday, V.A., Mansour, S., Sandy, C.J., Collin, J.R., Brady, A.F., Callen, D.F., Burnand, K., Mortimer, P., Jeffery, S., 2001. Analysis of lymphoedema-distichiasis families for FOXC2 mutations reveals small insertions and deletions throughout the gene. Hum Genet 108, 546-551.

Benayoun, B.A., Caburet, S., Veitia, R.A., 2011. Forkhead transcription factors: key players in health and disease. Trends Genet 27, 224-232.

Bensimon-Brito, A., Cardeira, J., Cancela, M.L., Huysseune, A., Witten, P.E., 2012. Distinct patterns of notochord mineralization in zebrafish coincide with the localization of Osteocalcin isoform 1 during early vertebral centra formation. BMC Dev Biol 12, 28.

Bernard, P., Tang, P., Liu, S., Dewing, P., Harley, V.R., Vilain, E., 2003. Dimerization of SOX9 is required for chondrogenesis, but not for sex determination. Human molecular genetics 12, 1755-1765.

Bernstein, B.E., Mikkelsen, T.S., Xie, X., Kamal, M., Huebert, D.J., Cuff, J., Fry, B., Meissner, A., Wernig, M., Plath, K., Jaenisch, R., Wagschal, A., Feil, R., Schreiber, S.L., Lander, E.S., 2006. A bivalent chromatin structure marks key developmental genes in embryonic stem cells. Cell 125, 315-326.

Berry, F.B., Lines, M.A., Oas, J.M., Footz, T., Underhill, D.A., Gage, P.J., Walter, M.A., 2006. Functional interactions between FOXC1 and PITX2 underlie the sensitivity to FOXC1 gene dose in Axenfeld-Rieger syndrome and anterior segment dysgenesis. Hum Mol Genet 15, 905-919.

Berry, F.B., O'Neill, M.A., Coca-Prados, M., Walter, M.A., 2005a. FOXC1 transcriptional regulatory activity is impaired by PBX1 in a filamin A-mediated manner. Mol Cell Biol 25, 1415-1424.

Berry, F.B., Saleem, R.A., Walter, M.A., 2002. FOXC1 transcriptional regulation is mediated by N- and C-terminal activation domains and contains a phosphorylated transcriptional inhibitory domain. J Biol Chem 277, 10292-10297.

Berry, F.B., Skarie, J.M., Mirzayans, F., Fortin, Y., Hudson, T.J., Raymond, V., Link, B.A., Walter, M.A., 2008. FOXC1 is required for cell viability and resistance to oxidative stress in the eye through the transcriptional regulation of FOXO1A. Hum Mol Genet 17, 490-505.

Berry, F.B., Tamimi, Y., Carle, M.V., Lehmann, O.J., Walter, M.A., 2005b. The establishment of a predictive mutational model of the forkhead domain through the analyses of FOXC2 missense mutations identified in patients with hereditary lymphedema with distichiasis. Hum Mol Genet 14, 2619-2627.

Bessho, Y., Hirata, H., Masamizu, Y., Kageyama, R., 2003. Periodic repression by the bHLH factor Hes7 is an essential mechanism for the somite segmentation clock. Genes Dev 17, 1451-1456.

Bessho, Y., Miyoshi, G., Sakata, R., Kageyama, R., 2001. Hes7: a bHLH-type repressor gene regulated by Notch and expressed in the presomitic mesoderm. Genes Cells 6, 175-185.

Bi, W., Deng, J.M., Zhang, Z., Behringer, R.R., de Crombrugghe, B., 1999. Sox9 is required for cartilage formation. Nat Genet 22, 85-89.

Biris, K.K., Dunty, W.C., Jr., Yamaguchi, T.P., 2007. Mouse Ripply2 is downstream of Wnt3a and is dynamically expressed during somitogenesis. Dev Dyn 236, 3167-3172.

Blanchette, M., Kent, W.J., Riemer, C., Elnitski, L., Smit, A.F., Roskin, K.M., Baertsch, R., Rosenbloom, K., Clawson, H., Green, E.D., Haussler, D., Miller, W., 2004. Aligning multiple genomic sequences with the threaded blockset aligner. Genome Res 14, 708-715.

Brand-Saberi, B., Christ, B., 2000. Evolution and development of distinct cell lineages derived from somites. Curr Top Dev Biol 48, 1-42.

Brand-Saberi, B., Wilting, J., Ebensperger, C., Christ, B., 1996. The formation of somite compartments in the avian embryo. Int J Dev Biol 40, 411-420.

Brent, A.E., Schweitzer, R., Tabin, C.J., 2003. A somitic compartment of tendon progenitors. Cell 113, 235-248.

Brent, A.E., Tabin, C.J., 2002. Developmental regulation of somite derivatives: muscle, cartilage and tendon. Curr Opin Genet Dev 12, 548-557.

Brice, G., Mansour, S., Bell, R., Collin, J.R., Child, A.H., Brady, A.F., Sarfarazi, M., Burnand, K.G., Jeffery, S., Mortimer, P., Murday, V.A., 2002. Analysis of the phenotypic abnormalities in lymphoedema-distichiasis syndrome in 74 patients with FOXC2 mutations or linkage to 16q24. J Med Genet 39, 478-483.

Bridgewater, L.C., Walker, M.D., Miller, G.C., Ellison, T.A., Holsinger, L.D., Potter, J.L., Jackson, T.L., Chen, R.K., Winkel, V.L., Zhang, Z., McKinney, S., de Crombrugghe, B., 2003. Adjacent DNA sequences modulate Sox9 transcriptional activation at paired Sox sites in three chondrocyte-specific enhancer elements. Nucleic Acids Res 31, 1541-1553.

Bronner-Fraser, M., 1994. Neural crest cell formation and migration in the developing embryo. FASEB J 8, 699-706.

Brooks, J.K., Coccaro, P.J., Jr., Zarbin, M.A., 1989. The Rieger anomaly concomitant with multiple dental, craniofacial, and somatic midline anomalies and short stature. Oral Surg Oral Med Oral Pathol 68, 717-724.

Bruderer, M., Richards, R.G., Alini, M., Stoddart, M.J., 2014. Role and regulation of RUNX2 in osteogenesis. Eur Cell Mater 28, 269-286.

Burgess, R., Rawls, A., Brown, D., Bradley, A., Olson, E.N., 1996. Requirement of the paraxis gene for somite formation and musculoskeletal patterning. Nature 384, 570-573.

Campanelli, M., Gedeon, T., 2010. Somitogenesis clock-wave initiation requires differential decay and multiple binding sites for clock protein. PLoS Comput Biol 6, e1000728.

Caplan, A.I., Pechak, D., 1987. The cellular and molecular embryology of bone formation. Bone and mineral research 5, 117-183.

Carlsson, P., Mahlapuu, M., 2002. Forkhead transcription factors: key players in development and metabolism. Dev Biol 250, 1-23.

Chen, L., Li, C., Qiao, W., Xu, X., Deng, C., 2001. A Ser(365)-->Cys mutation of fibroblast growth factor receptor 3 in mouse downregulates Ihh/PTHrP signals and causes severe achondroplasia. Hum Mol Genet 10, 457-465.

Chiaromonte, F., Yap, V.B., Miller, W., 2002. Scoring pairwise genomic sequence alignments. Pac Symp Biocomput, 115-126.

Childers, N.K., Wright, J.T., 1986. Dental and craniofacial anomalies of Axenfeld-Rieger syndrome. J Oral Pathol 15, 534-539.

Christ, B., Ordahl, C.P., 1995. Early stages of chick somite development. Anat Embryol (Berl) 191, 381-396.

Cinquin, O., 2007. Understanding the somitogenesis clock: what's missing? Mech Dev 124, 501-517.

Clark, K.L., Halay, E.D., Lai, E., Burley, S.K., 1993. Co-crystal structure of the HNF-3/fork head DNA-recognition motif resembles histone H5. Nature 364, 412-420.

Cohn, M.J., Tickle, C., 1996. Limbs: a model for pattern formation within the vertebrate body plan. Trends Genet 12, 253-257.

Colvin, J.S., Bohne, B.A., Harding, G.W., McEwen, D.G., Ornitz, D.M., 1996. Skeletal overgrowth and deafness in mice lacking fibroblast growth factor receptor 3. Nat Genet 12, 390-397.

Conlon, R.A., Reaume, A.G., Rossant, J., 1995. Notch1 is required for the coordinate segmentation of somites. Development 121, 1533-1545.

Cooke, J., Zeeman, E.C., 1976. A clock and wavefront model for control of the number of repeated structures during animal morphogenesis. Journal of theoretical biology 58, 455-476.

Cordes, R., Schuster-Gossler, K., Serth, K., Gossler, A., 2004. Specification of vertebral identity is coupled to Notch signalling and the segmentation clock. Development 131, 1221-1233.

Cotterell, J., Robert-Moreno, A., Sharpe, J., 2015. A Local, Self-Organizing Reaction-Diffusion Model Can Explain Somite Patterning in Embryos. Cell Syst 1, 257-269.

Cremer, H., Lange, R., Christoph, A., Plomann, M., Vopper, G., Roes, J., Brown, R., Baldwin, S., Kraemer, P., Scheff, S., et al., 1994. Inactivation of the N-CAM gene in

mice results in size reduction of the olfactory bulb and deficits in spatial learning. Nature 367, 455-459.

Cutty, S.J., Fior, R., Henriques, P.M., Saude, L., Wardle, F.C., 2012. Identification and expression analysis of two novel members of the Mesp family in zebrafish. Int J Dev Biol 56, 285-294.

Dale, J.K., Malapert, P., Chal, J., Vilhais-Neto, G., Maroto, M., Johnson, T., Jayasinghe, S., Trainor, P., Herrmann, B., Pourquie, O., 2006. Oscillations of the snail genes in the presomitic mesoderm coordinate segmental patterning and morphogenesis in vertebrate somitogenesis. Dev Cell 10, 355-366.

Dale, R.F., 1987. Primary lymphoedema when found with distichiasis is of the type defined as bilateral hyperplasia by lymphography. J Med Genet 24, 170-171.

de Crombrugghe, B., Schmidt, A., 1987. Structure and expression of collagen genes. Methods Enzymol 144, 61-74.

de la Pompa, J.L., Wakeham, A., Correia, K.M., Samper, E., Brown, S., Aguilera, R.J., Nakano, T., Honjo, T., Mak, T.W., Rossant, J., Conlon, R.A., 1997. Conservation of the Notch signalling pathway in mammalian neurogenesis. Development 124, 1139-1148.

Delfini, M.C., Dubrulle, J., Malapert, P., Chal, J., Pourquie, O., 2005. Control of the segmentation process by graded MAPK/ERK activation in the chick embryo. Proc Natl Acad Sci U S A 102, 11343-11348.

Deng, C., Wynshaw-Boris, A., Zhou, F., Kuo, A., Leder, P., 1996. Fibroblast growth factor receptor 3 is a negative regulator of bone growth. Cell 84, 911-921.

Dequeant, M.L., Pourquie, O., 2008. Segmental patterning of the vertebrate embryonic axis. Nature reviews. Genetics 9, 370-382.

Diez del Corral, R., Olivera-Martinez, I., Goriely, A., Gale, E., Maden, M., Storey, K., 2003. Opposing FGF and retinoid pathways control ventral neural pattern, neuronal differentiation, and segmentation during body axis extension. Neuron 40, 65-79.

Dressler, P., Gramer, E., 2006. [Morphology, family history, and age at diagnosis of 26 patients with Axenfeld-Rieger syndrome and glaucoma or ocular hypertension]. Ophthalmologe 103, 393-400.

Duband, J.L., Dufour, S., Hatta, K., Takeichi, M., Edelman, G.M., Thiery, J.P., 1987. Adhesion molecules during somitogenesis in the avian embryo. J Cell Biol 104, 1361-1374.

Dubrulle, J., McGrew, M.J., Pourquie, O., 2001. FGF signaling controls somite boundary position and regulates segmentation clock control of spatiotemporal Hox gene activation. Cell 106, 219-232.

Dubrulle, J., Pourquie, O., 2003. Welcome to syndetome: a new somitic compartment. Dev Cell 4, 611-612.

Dubrulle, J., Pourquie, O., 2004a. Coupling segmentation to axis formation. Development 131, 5783-5793.

Dubrulle, J., Pourquie, O., 2004b. fgf8 mRNA decay establishes a gradient that couples axial elongation to patterning in the vertebrate embryo. Nature 427, 419-422.

Dunwoodie, S.L., Clements, M., Sparrow, D.B., Sa, X., Conlon, R.A., Beddington, R.S., 2002. Axial skeletal defects caused by mutation in the spondylocostal dysplasia/pudgy gene Dll3 are associated with disruption of the segmentation clock within the presomitic mesoderm. Development 129, 1795-1806.

Durbin, L., Sordino, P., Barrios, A., Gering, M., Thisse, C., Thisse, B., Brennan, C., Green, A., Wilson, S., Holder, N., 2000. Anteroposterior patterning is required within segments for somite boundary formation in developing zebrafish. Development 127, 1703-1713.

Erickson, R.P., Dagenais, S.L., Caulder, M.S., Downs, C.A., Herman, G., Jones, M.C., Kerstjens-Frederikse, W.S., Lidral, A.C., McDonald, M., Nelson, C.C., Witte, M., Glover, T.W., 2001. Clinical heterogeneity in lymphoedema-distichiasis with FOXC2 truncating mutations. J Med Genet 38, 761-766.

Eswarakumar, V.P., Schlessinger, J., 2007. Skeletal overgrowth is mediated by deficiency in a specific isoform of fibroblast growth factor receptor 3. Proc Natl Acad Sci U S A 104, 3937-3942.

Fatima, A., Wang, Y., Uchida, Y., Norden, P., Liu, T., Culver, A., Dietz, W.H., Culver, F., Millay, M., Mukouyama, Y.S., Kume, T., 2016. Foxc1 and Foxc2 deletion causes abnormal lymphangiogenesis and correlates with ERK hyperactivation. J Clin Invest 126, 2437-2451.

Fetterman, C.D., Mirzayans, F., Walter, M.A., 2009. Characterization of a novel FOXC1 mutation, P297S, identified in two individuals with anterior segment dysgenesis. Clin Genet 76, 296-299.

Finegold, D.N., Kimak, M.A., Lawrence, E.C., Levinson, K.L., Cherniske, E.M., Pober, B.R., Dunlap, J.W., Ferrell, R.E., 2001. Truncating mutations in FOXC2 cause multiple lymphedema syndromes. Hum Mol Genet 10, 1185-1189.

Fleisch, V.C., Leighton, P.L., Wang, H., Pillay, L.M., Ritzel, R.G., Bhinder, G., Roy, B., Tierney, K.B., Ali, D.W., Waskiewicz, A.J., Allison, W.T., 2013. Targeted mutation of the gene encoding prion protein in zebrafish reveals a conserved role in neuron excitability. Neurobiology of disease 55, 11-25.

Forsberg, H., Crozet, F., Brown, N.A., 1998. Waves of mouse Lunatic fringe expression, in four-hour cycles at two-hour intervals, precede somite boundary formation. Curr Biol 8, 1027-1030.

Foster, J.W., Dominguez-Steglich, M.A., Guioli, S., Kwok, C., Weller, P.A., Stevanovic, M., Weissenbach, J., Mansour, S., Young, I.D., Goodfellow, P.N., et al., 1994. Campomelic dysplasia and autosomal sex reversal caused by mutations in an SRY-related gene. Nature 372, 525-530.

Fromental-Ramain, C., Warot, X., Messadecq, N., LeMeur, M., Dolle, P., Chambon, P., 1996. Hoxa-13 and Hoxd-13 play a crucial role in the patterning of the limb autopod. Development 122, 2997-3011.

Giampietro, P.F., Dunwoodie, S.L., Kusumi, K., Pourquie, O., Tassy, O., Offiah, A.C., Cornier, A.S., Alman, B.A., Blank, R.D., Raggio, C.L., Glurich, I., Turnpenny, P.D., 2009. Progress in the understanding of the genetic etiology of vertebral segmentation disorders in humans. Ann N Y Acad Sci 1151, 38-67.

Gibson, G.J., Bearman, C.H., Flint, M.H., 1986. The immunoperoxidase localization of type X collagen in chick cartilage and lung. Coll Relat Res 6, 163-184.

Gilbert, S.F., 2000. Developmental biology, 6th ed. Sinauer Associates, Sunderland, Mass.

Goldbeter, A., Gonze, D., Pourquie, O., 2007. Sharp developmental thresholds defined through bistability by antagonistic gradients of retinoic acid and FGF signaling. Dev Dyn 236, 1495-1508.

Goldman, D.C., Martin, G.R., Tam, P.P., 2000. Fate and function of the ventral ectodermal ridge during mouse tail development. Development 127, 2113-2123.

Goldstein, R.S., Kalcheim, C., 1992. Determination of epithelial half-somites in skeletal morphogenesis. Development 116, 441-445.

Gomez, C., Pourquie, O., 2009. Developmental control of segment numbers in vertebrates. J Exp Zool B Mol Dev Evol 312, 533-544.

Gomez-Picos, P., Eames, B.F., 2015. On the evolutionary relationship between chondrocytes and osteoblasts. Front Genet 6, 297.

Gongal, P.A., Waskiewicz, A.J., 2008. Zebrafish model of holoprosencephaly demonstrates a key role for TGIF in regulating retinoic acid metabolism. Hum Mol Genet 17, 525-538.

Gozo, M.C., Aspuria, P.J., Cheon, D.J., Walts, A.E., Berel, D., Miura, N., Karlan, B.Y., Orsulic, S., 2013. Foxc2 induces Wnt4 and Bmp4 expression during muscle regeneration and osteogenesis. Cell Death Differ 20, 1031-1042.

Grant, C.E., Bailey, T.L., Noble, W.S., 2011. FIMO: scanning for occurrences of a given motif. Bioinformatics 27, 1017-1018.

Gray, M., Moens, C.B., Amacher, S.L., Eisen, J.S., Beattie, C.E., 2001. Zebrafish deadly seven functions in neurogenesis. Dev Biol 237, 306-323.

Green, M.C., 1970. The developmental effects of congenital hydrocephalus (ch) in the mouse. Dev Biol 23, 585-608.

Gripp, K.W., Hopkins, E., Jenny, K., Thacker, D., Salvin, J., 2013. Cardiac anomalies in Axenfeld-Rieger syndrome due to a novel FOXC1 mutation. Am J Med Genet A 161A, 114-119.

Grüneberg, H., 1943. Congenital hydrocephalus in the mouse, a case of spurious pleiotropism. Journal of Genetics 45, 1.

Guo, J., Chung, U.I., Kondo, H., Bringhurst, F.R., Kronenberg, H.M., 2002. The PTH/PTHrP receptor can delay chondrocyte hypertrophy in vivo without activating phospholipase C. Dev Cell 3, 183-194.

Hall, B.K., Miyake, T., 1992. The membranous skeleton: the role of cell condensations in vertebrate skeletogenesis. Anat Embryol (Berl) 186, 107-124.

Hammond, C.L., Hinits, Y., Osborn, D.P., Minchin, J.E., Tettamanti, G., Hughes, S.M., 2007. Signals and myogenic regulatory factors restrict pax3 and pax7 expression to dermomyotome-like tissue in zebrafish. Dev Biol 302, 504-521.

Han, Y., Lefebvre, V., 2008. L-Sox5 and Sox6 drive expression of the aggrecan gene in cartilage by securing binding of Sox9 to a far-upstream enhancer. Mol Cell Biol 28, 4999-5013.

Hayashi, H., Kume, T., 2008. Foxc transcription factors directly regulate Dll4 and Hey2 expression by interacting with the VEGF-Notch signaling pathways in endothelial cells. PLoS One 3, e2401.

Hayashi, H., Sano, H., Seo, S., Kume, T., 2008. The Foxc2 transcription factor regulates angiogenesis via induction of integrin beta3 expression. J Biol Chem 283, 23791-23800.

Henry, C.A., Hall, L.A., Burr Hille, M., Solnica-Krezel, L., Cooper, M.S., 2000. Somites in zebrafish doubly mutant for knypek and trilobite form without internal mesenchymal cells or compaction. Curr Biol 10, 1063-1066.

Henry, C.A., McNulty, I.M., Durst, W.A., Munchel, S.E., Amacher, S.L., 2005. Interactions between muscle fibers and segment boundaries in zebrafish. Dev Biol 287, 346-360.

Hiemisch, H., Monaghan, A.P., Schutz, G., Kaestner, K.H., 1998a. Expression of the mouse Fkh1/Mf1 and Mfh1 genes in late gestation embryos is restricted to mesoderm derivatives. Mech Dev 73, 129-132.

Hiemisch, H., Schutz, G., Kaestner, K.H., 1998b. The mouse Fkh1/Mf1 gene: cDNA sequence, chromosomal localization and expression in adult tissues. Gene 220, 77-82.

Hollier, B.G., Tinnirello, A.A., Werden, S.J., Evans, K.W., Taube, J.H., Sarkar, T.R., Sphyris, N., Shariati, M., Kumar, S.V., Battula, V.L., Herschkowitz, J.I., Guerra, R., Chang, J.T., Miura, N., Rosen, J.M., Mani, S.A., 2013. FOXC2 expression links epithelial-mesenchymal transition and stem cell properties in breast cancer. Cancer Res 73, 1981-1992.

Hong, H.K., Lass, J.H., Chakravarti, A., 1999. Pleiotropic skeletal and ocular phenotypes of the mouse mutation congenital hydrocephalus (ch/Mf1) arise from a winged helix/forkhead transcriptionfactor gene. Hum Mol Genet 8, 625-637.

Hopkins, A., Coatham, M.L., Berry, F.B., 2017. FOXC1 Regulates FGFR1 Isoform Switching to Promote Invasion Following TGFbeta-Induced EMT. Mol Cancer Res.

Hopkins, A., Mirzayans, F., Berry, F., 2016. Foxc1 Expression in Early Osteogenic Differentiation Is Regulated by BMP4-SMAD Activity. J Cell Biochem 117, 1707-1717.

Horikawa, K., Radice, G., Takeichi, M., Chisaka, O., 1999. Adhesive subdivisions intrinsic to the epithelial somites. Dev Biol 215, 182-189.

Hrabe de Angelis, M., McIntyre, J., 2nd, Gossler, A., 1997. Maintenance of somite borders in mice requires the Delta homologue DII1. Nature 386, 717-721.

Hsu, C.H., Lin, J.S., Po Lai, K., Li, J.W., Chan, T.F., You, M.S., Tse, W.K., Jiang, Y.J., 2015. A new mib allele with a chromosomal deletion covering foxc1a exhibits anterior somite specification defect. Sci Rep 5, 10673.

Huang, R., Zhi, Q., Wilting, J., Christ, B., 1994. The fate of somitocoele cells in avian embryos. Anat Embryol (Berl) 190, 243-250.

Huang, W., Chung, U.I., Kronenberg, H.M., de Crombrugghe, B., 2001. The chondrogenic transcription factor Sox9 is a target of signaling by the parathyroid hormone-related peptide in the growth plate of endochondral bones. Proc Natl Acad Sci U S A 98, 160-165.

Iida, K., Koseki, H., Kakinuma, H., Kato, N., Mizutani-Koseki, Y., Ohuchi, H., Yoshioka, H., Noji, S., Kawamura, K., Kataoka, Y., Ueno, F., Taniguchi, M., Yoshida, N., Sugiyama, T., Miura, N., 1997. Essential roles of the winged helix transcription factor MFH-1 in aortic arch patterning and skeletogenesis. Development 124, 4627-4638.

Inada, M., Wang, Y., Byrne, M.H., Rahman, M.U., Miyaura, C., Lopez-Otin, C., Krane, S.M., 2004. Critical roles for collagenase-3 (Mmp13) in development of growth plate cartilage and in endochondral ossification. Proc Natl Acad Sci U S A 101, 17192-17197.

Ingalls, T.H., Curley, F.J., 1957. Principles governing the genesis of congenital malformations induced in mice by hypoxia. N Engl J Med 257, 1121-1127.

Inman, K.E., Purcell, P., Kume, T., Trainor, P.A., 2013. Interaction between Foxc1 and Fgf8 during mammalian jaw patterning and in the pathogenesis of syngnathia. PLoS Genet 9, e1003949.

Ito, Y.A., Footz, T.K., Berry, F.B., Mirzayans, F., Yu, M., Khan, A.O., Walter, M.A., 2009. Severe molecular defects of a novel FOXC1 W152G mutation result in aniridia. Invest Ophthalmol Vis Sci 50, 3573-3579.

Ito, Y.A., Footz, T.K., Murphy, T.C., Courtens, W., Walter, M.A., 2007. Analyses of a novel L130F missense mutation in FOXC1. Arch Ophthalmol 125, 128-135.

Itoh, M., Kawagoe, S., Okano, H.J., Nakagawa, H., 2016. Integration-free T cell-derived human induced pluripotent stem cells (iPSCs) from a patient with lymphedema-distichiasis syndrome (LDS) carrying an insertion-deletion complex mutation in the FOXC2 gene. Stem Cell Res 16, 611-613.

Itoh, M., Kim, C.H., Palardy, G., Oda, T., Jiang, Y.J., Maust, D., Yeo, S.Y., Lorick, K., Wright, G.J., Ariza-McNaughton, L., Weissman, A.M., Lewis, J., Chandrasekharappa, S.C., Chitnis, A.B., 2003. Mind bomb is a ubiquitin ligase that is essential for efficient activation of Notch signaling by Delta. Dev Cell 4, 67-82.

Ivanov, K.I., Agalarov, Y., Valmu, L., Samuilova, O., Liebl, J., Houhou, N., Maby-El Hajjami, H., Norrmen, C., Jaquet, M., Miura, N., Zangger, N., Yla-Herttuala, S., Delorenzi, M., Petrova, T.V., 2013. Phosphorylation regulates FOXC2-mediated transcription in lymphatic endothelial cells. Mol Cell Biol 33, 3749-3761.

Iwata, T., Li, C.L., Deng, C.X., Francomano, C.A., 2001. Highly activated Fgfr3 with the K644M mutation causes prolonged survival in severe dwarf mice. Hum Mol Genet 10, 1255-1264.

Jacob, A.L., Smith, C., Partanen, J., Ornitz, D.M., 2006. Fibroblast growth factor receptor 1 signaling in the osteo-chondrogenic cell lineage regulates sequential steps of osteoblast maturation. Dev Biol 296, 315-328.

Jiang, Y.J., Brand, M., Heisenberg, C.P., Beuchle, D., Furutani-Seiki, M., Kelsh, R.N., Warga, R.M., Granato, M., Haffter, P., Hammerschmidt, M., Kane, D.A., Mullins, M.C., Odenthal, J., van Eeden, F.J., Nusslein-Volhard, C., 1996. Mutations affecting neurogenesis and brain morphology in the zebrafish, Danio rerio. Development 123, 205-216.

Jobert, A.S., Zhang, P., Couvineau, A., Bonaventure, J., Roume, J., Le Merrer, M., Silve, C., 1998. Absence of functional receptors for parathyroid hormone and parathyroid hormone-related peptide in Blomstrand chondrodysplasia. J Clin Invest 102, 34-40.

Julich, D., Geisler, R., Holley, S.A., 2005. Integrinalpha5 and delta/notch signaling have complementary spatiotemporal requirements during zebrafish somitogenesis. Dev Cell 8, 575-586.

Kaestner, K.H., Knochel, W., Martinez, D.E., 2000. Unified nomenclature for the winged helix/forkhead transcription factors. Genes Dev 14, 142-146.

Kamachi, Y., Kondoh, H., 2013. Sox proteins: regulators of cell fate specification and differentiation. Development 140, 4129-4144.

Karaplis, A.C., 2008. Embryonic Development of Bone and Regulation of Intramembranous and Endochondral Bone Formation, 3rd ed. Academic Press/Elsevier, San Diego, Calif.

Karaplis, A.C., He, B., Nguyen, M.T., Young, I.D., Semeraro, D., Ozawa, H., Amizuka, N., 1998. Inactivating mutation in the human parathyroid hormone receptor type 1 gene in Blomstrand chondrodysplasia. Endocrinology 139, 5255-5258.

Karaplis, A.C., Luz, A., Glowacki, J., Bronson, R.T., Tybulewicz, V.L., Kronenberg, H.M., Mulligan, R.C., 1994. Lethal skeletal dysplasia from targeted disruption of the parathyroid hormone-related peptide gene. Genes Dev 8, 277-289.

Karp, S.J., Schipani, E., St-Jacques, B., Hunzelman, J., Kronenberg, H., McMahon, A.P., 2000. Indian hedgehog coordinates endochondral bone growth and morphogenesis via parathyroid hormone related-protein-dependent and -independent pathways. Development 127, 543-548.

Karperien, M., van der Harten, H.J., van Schooten, R., Farih-Sips, H., den Hollander, N.S., Kneppers, S.L., Nijweide, P., Papapoulos, S.E., Lowik, C.W., 1999. A frame-shift mutation in the type I parathyroid hormone (PTH)/PTH-related peptide receptor

causing Blomstrand lethal osteochondrodysplasia. J Clin Endocrinol Metab 84, 3713-3720.

Kato, N., Aoyama, H., 1998. Dermomyotomal origin of the ribs as revealed by extirpation and transplantation experiments in chick and quail embryos. Development 125, 3437-3443.

Kawaguchi, J., Mee, P.J., Smith, A.G., 2005. Osteogenic and chondrogenic differentiation of embryonic stem cells in response to specific growth factors. Bone 36, 758-769.

Kawamura, A., Koshida, S., Hijikata, H., Ohbayashi, A., Kondoh, H., Takada, S., 2005. Groucho-associated transcriptional repressor ripply1 is required for proper transition from the presomitic mesoderm to somites. Dev Cell 9, 735-744.

Kent, W.J., Sugnet, C.W., Furey, T.S., Roskin, K.M., Pringle, T.H., Zahler, A.M., Haussler, D., 2002. The human genome browser at UCSC. Genome Res 12, 996-1006.

Kim, G.N., Ki, C.S., Seo, S.W., Yoo, J.M., Han, Y.S., Chung, I.Y., Park, J.M., Kim, S.J., 2013. A novel forkhead box C1 gene mutation in a Korean family with Axenfeld-Rieger syndrome. Mol Vis 19, 935-943.

Kist, R., Schrewe, H., Balling, R., Scherer, G., 2002. Conditional inactivation of Sox9: a mouse model for campomelic dysplasia. Genesis 32, 121-123.

Kobayashi, A., Fujiki, K., Murakami, A., Kato, T., Chen, L.Z., Onoe, H., Nakayasu, K., Sakurai, M., Takahashi, M., Sugiyama, K., Kanai, A., 2004. Analysis of COL8A2 gene mutation in Japanese patients with Fuchs' endothelial dystrophy and posterior polymorphous dystrophy. Jpn J Ophthalmol 48, 195-198.

Koizumi, K., Nakajima, M., Yuasa, S., Saga, Y., Sakai, T., Kuriyama, T., Shirasawa, T., Koseki, H., 2001. The role of presenilin 1 during somite segmentation. Development 128, 1391-1402.

Komaki, F., Miyazaki, Y., Niimura, F., Matsusaka, T., Ichikawa, I., Motojima, M., 2013. Foxc1 gene null mutation causes ectopic budding and kidney hypoplasia but not dysplasia. Cells Tissues Organs 198, 22-27.

Koster, M., Dillinger, K., Knochel, W., 1998. Expression pattern of the winged helix factor XFD-11 during Xenopus embryogenesis. Mech Dev 76, 169-173.

Kovacs, P., Lehn-Stefan, A., Stumvoll, M., Bogardus, C., Baier, L.J., 2003. Genetic variation in the human winged helix/forkhead transcription factor gene FOXC2 in Pima Indians. Diabetes 52, 1292-1295.

Kozhemyakina, E., Cohen, T., Yao, T.P., Lassar, A.B., 2009. Parathyroid hormone-related peptide represses chondrocyte hypertrophy through a protein phosphatase 2A/histone deacetylase 4/MEF2 pathway. Mol Cell Biol 29, 5751-5762.

Kronenberg, H.M., 2003. Developmental regulation of the growth plate. Nature 423, 332-336.

Kronenberg, H.M., Karaplis, A.C., Lanske, B., 1996. Role of parathyroid hormone-related protein in skeletal development. Ann N Y Acad Sci 785, 119-123.

Kulesa, P.M., Fraser, S.E., 2002. Cell dynamics during somite boundary formation revealed by time-lapse analysis. Science 298, 991-995.

Kulesa, P.M., Schnell, S., Rudloff, S., Baker, R.E., Maini, P.K., 2007. From segment to somite: segmentation to epithelialization analyzed within quantitative frameworks. Dev Dyn 236, 1392-1402.

Kume, T., 2009. The cooperative roles of Foxc1 and Foxc2 in cardiovascular development. Adv Exp Med Biol 665, 63-77.

Kume, T., Deng, K., Hogan, B.L., 2000. Murine forkhead/winged helix genes Foxc1 (Mf1) and Foxc2 (Mfh1) are required for the early organogenesis of the kidney and urinary tract. Development 127, 1387-1395.

Kume, T., Deng, K.Y., Winfrey, V., Gould, D.B., Walter, M.A., Hogan, B.L., 1998. The forkhead/winged helix gene Mf1 is disrupted in the pleiotropic mouse mutation congenital hydrocephalus. Cell 93, 985-996.

Kume, T., Jiang, H., Topczewska, J.M., Hogan, B.L., 2001. The murine winged helix transcription factors, Foxc1 and Foxc2, are both required for cardiovascular development and somitogenesis. Genes Dev 15, 2470-2482.

Kusumi, K., Sun, E.S., Kerrebrock, A.W., Bronson, R.T., Chi, D.C., Bulotsky, M.S., Spencer, J.B., Birren, B.W., Frankel, W.N., Lander, E.S., 1998. The mouse pudgy mutation disrupts Delta homologue Dll3 and initiation of early somite boundaries. Nat Genet 19, 274-278.

Lanske, B., Karaplis, A.C., Lee, K., Luz, A., Vortkamp, A., Pirro, A., Karperien, M., Defize, L.H., Ho, C., Mulligan, R.C., Abou-Samra, A.B., Juppner, H., Segre, G.V., Kronenberg, H.M., 1996. PTH/PTHrP receptor in early development and Indian hedgehog-regulated bone growth. Science 273, 663-666.

Lawson, N.D., Scheer, N., Pham, V.N., Kim, C.H., Chitnis, A.B., Campos-Ortega, J.A., Weinstein, B.M., 2001. Notch signaling is required for arterial-venous differentiation during embryonic vascular development. Development 128, 3675-3683.

Leboy, P.S., Shapiro, I.M., Uschmann, B.D., Oshima, O., Lin, D., 1988. Gene expression in mineralizing chick epiphyseal cartilage. J Biol Chem 263, 8515-8520.

Lee, K., Deeds, J.D., Segre, G.V., 1995. Expression of parathyroid hormone-related peptide and its receptor messenger ribonucleic acids during fetal development of rats. Endocrinology 136, 453-463.

Lefebvre, V., Li, P., de Crombrugghe, B., 1998. A new long form of Sox5 (L-Sox5), Sox6 and Sox9 are coexpressed in chondrogenesis and cooperatively activate the type II collagen gene. EMBO J 17, 5718-5733.

Lehmann, O.J., Ebenezer, N.D., Ekong, R., Ocaka, L., Mungall, A.J., Fraser, S., McGill, J.I., Hitchings, R.A., Khaw, P.T., Sowden, J.C., Povey, S., Walter, M.A., Bhattacharya, S.S., Jordan, T., 2002. Ocular developmental abnormalities and glaucoma associated with interstitial 6p25 duplications and deletions. Invest Ophthalmol Vis Sci 43, 1843-1849.

Leimeister, C., Dale, K., Fischer, A., Klamt, B., Hrabe de Angelis, M., Radtke, F., McGrew, M.J., Pourquie, O., Gessler, M., 2000. Oscillating expression of c-Hey2 in the presomitic mesoderm suggests that the segmentation clock may use combinatorial signaling through multiple interacting bHLH factors. Dev Biol 227, 91-103.

Li, J., Yue, Y., Dong, X., Jia, W., Li, K., Liang, D., Dong, Z., Wang, X., Nan, X., Zhang, Q., Zhao, Q., 2015. Zebrafish foxc1a plays a crucial role in early somitogenesis by restricting the expression of aldh1a2 directly. The Journal of biological chemistry 290, 10216-10228.

Linask, K.K., Ludwig, C., Han, M.D., Liu, X., Radice, G.L., Knudsen, K.A., 1998. N-cadherin/catenin-mediated morphoregulation of somite formation. Dev Biol 202, 85-102.

Liu, C.F., Lefebvre, V., 2015. The transcription factors SOX9 and SOX5/SOX6 cooperate genome-wide through super-enhancers to drive chondrogenesis. Nucleic Acids Res 43, 8183-8203.

Long, F., 2011. Building strong bones: molecular regulation of the osteoblast lineage. Nat Rev Mol Cell Biol 13, 27-38.

Long, F., Ornitz, D.M., 2013. Development of the endochondral skeleton. Cold Spring Harb Perspect Biol 5, a008334.

Long, F., Zhang, X.M., Karp, S., Yang, Y., McMahon, A.P., 2001. Genetic manipulation of hedgehog signaling in the endochondral skeleton reveals a direct role in the regulation of chondrocyte proliferation. Development 128, 5099-5108.

Lu, P., Yu, Y., Perdue, Y., Werb, Z., 2008. The apical ectodermal ridge is a timer for generating distal limb progenitors. Development 135, 1395-1405.

Maes, C., Kobayashi, T., Selig, M.K., Torrekens, S., Roth, S.I., Mackem, S., Carmeliet, G., Kronenberg, H.M., 2010. Osteoblast precursors, but not mature osteoblasts, move into developing and fractured bones along with invading blood vessels. Dev Cell 19, 329-344.

Maiese, K., 2009. Forkhead transcription factors : vital elements in biology and medicine. Springer Science+Business Media ;Landes Bioscience, New York, Austin, Tex.

Maini, P.K., Baker, R.E., Schnell, S., 2015. Rethinking Models of Pattern Formation in Somitogenesis. Cell Syst 1, 248-249.

Mansour, S., Brice, G.W., Jeffery, S., Mortimer, P., 1993. Lymphedema-Distichiasis Syndrome.

Matsui, Y., Alini, M., Webber, C., Poole, A.R., 1991. Characterization of aggregating proteoglycans from the proliferative, maturing, hypertrophic, and calcifying zones of the cartilaginous physis. J Bone Joint Surg Am 73, 1064-1074.

McGrew, M.J., Dale, J.K., Fraboulet, S., Pourquie, O., 1998. The lunatic fringe gene is a target of the molecular clock linked to somite segmentation in avian embryos. Curr Biol 8, 979-982.

Mears, A.J., Jordan, T., Mirzayans, F., Dubois, S., Kume, T., Parlee, M., Ritch, R., Koop, B., Kuo, W.L., Collins, C., Marshall, J., Gould, D.B., Pearce, W., Carlsson, P., Enerback, S., Morissette, J., Bhattacharya, S., Hogan, B., Raymond, V., Walter, M.A., 1998. Mutations of the forkhead/winged-helix gene, FKHL7, in patients with Axenfeld-Rieger anomaly. Am J Hum Genet 63, 1316-1328.

Meeker, N.D., Hutchinson, S.A., Ho, L., Trede, N.S., 2007. Method for isolation of PCR-ready genomic DNA from zebrafish tissues. Biotechniques 43, 610, 612, 614.

Mellor, R.H., Brice, G., Stanton, A.W., French, J., Smith, A., Jeffery, S., Levick, J.R., Burnand, K.G., Mortimer, P.S., Lymphoedema Research, C., 2007. Mutations in FOXC2 are strongly associated with primary valve failure in veins of the lower limb. Circulation 115, 1912-1920.

Meyer, M.B., Benkusky, N.A., Sen, B., Rubin, J., Pike, J.W., 2016. Epigenetic Plasticity Drives Adipogenic and Osteogenic Differentiation of Marrow-derived Mesenchymal Stem Cells. J Biol Chem 291, 17829-17847.

Meyer-Marcotty, P., Weisschuh, N., Dressler, P., Hartmann, J., Stellzig-Eisenhauer, A., 2008. Morphology of the sella turcica in Axenfeld-Rieger syndrome with PITX2 mutation. J Oral Pathol Med 37, 504-510.

Mirzayans, F., Gould, D.B., Heon, E., Billingsley, G.D., Cheung, J.C., Mears, A.J., Walter, M.A., 2000. Axenfeld-Rieger syndrome resulting from mutation of the FKHL7 gene on chromosome 6p25. Eur J Hum Genet 8, 71-74.

Mirzayans, F., Lavy, R., Penner-Chea, J., Berry, F.B., 2012. Initiation of early osteoblast differentiation events through the direct transcriptional regulation of Msx2 by FOXC1. PLoS One 7, e49095.

Mise, T., Iijima, M., Inohaya, K., Kudo, A., Wada, H., 2008. Function of Pax1 and Pax9 in the sclerotome of medaka fish. Genesis 46, 185-192.

Morales, A.V., Yasuda, Y., Ish-Horowicz, D., 2002. Periodic Lunatic fringe expression is controlled during segmentation by a cyclic transcriptional enhancer responsive to notch signaling. Dev Cell 3, 63-74.

Moreno, T.A., Kintner, C., 2004. Regulation of segmental patterning by retinoic acid signaling during Xenopus somitogenesis. Dev Cell 6, 205-218.

Morimoto, M., Sasaki, N., Oginuma, M., Kiso, M., Igarashi, K., Aizaki, K., Kanno, J., Saga, Y., 2007. The negative regulation of Mesp2 by mouse Ripply2 is required to establish the rostro-caudal patterning within a somite. Development 134, 1561-1569.

Morimoto, M., Takahashi, Y., Endo, M., Saga, Y., 2005. The Mesp2 transcription factor establishes segmental borders by suppressing Notch activity. Nature 435, 354-359.

Mortemousque, B., Amati-Bonneau, P., Couture, F., Graffan, R., Dubois, S., Colin, J., Bonneau, D., Morissette, J., Lacombe, D., Raymond, V., 2004. Axenfeld-Rieger anomaly: a novel mutation in the forkhead box C1 (FOXC1) gene in a 4-generation family. Arch Ophthalmol 122, 1527-1533.

Motojima, M., Tanimoto, S., Ohtsuka, M., Matsusaka, T., Kume, T., Abe, K., 2016. Characterization of Kidney and Skeleton Phenotypes of Mice Double Heterozygous for Foxc1 and Foxc2. Cells Tissues Organs 201, 380-389.

Murakami, U., Kameyama, Y., Nogami, H., 1963. Malformation of the Extremity in the Mouse Foetus Caused by X-Radiation of the Mother during Pregnancy. J Embryol Exp Morphol 11, 549-569.

Murphy, T.C., Saleem, R.A., Footz, T., Ritch, R., McGillivray, B., Walter, M.A., 2004. The wing 2 region of the FOXC1 forkhead domain is necessary for normal DNA-binding and transactivation functions. Invest Ophthalmol Vis Sci 45, 2531-2538.

Naski, M.C., Colvin, J.S., Coffin, J.D., Ornitz, D.M., 1998. Repression of hedgehog signaling and BMP4 expression in growth plate cartilage by fibroblast growth factor receptor 3. Development 125, 4977-4988.

Niederreither, K., Abu-Abed, S., Schuhbaur, B., Petkovich, M., Chambon, P., Dolle, P., 2002a. Genetic evidence that oxidative derivatives of retinoic acid are not involved in retinoid signaling during mouse development. Nat Genet 31, 84-88.

Niederreither, K., Fraulob, V., Garnier, J.M., Chambon, P., Dolle, P., 2002b. Differential expression of retinoic acid-synthesizing (RALDH) enzymes during fetal development and organ differentiation in the mouse. Mech Dev 110, 165-171.

Nishimura, D.Y., Searby, C.C., Alward, W.L., Walton, D., Craig, J.E., Mackey, D.A., Kawase, K., Kanis, A.B., Patil, S.R., Stone, E.M., Sheffield, V.C., 2001. A spectrum of FOXC1 mutations suggests gene dosage as a mechanism for developmental defects of the anterior chamber of the eye. Am J Hum Genet 68, 364-372.

Nishimura, D.Y., Swiderski, R.E., Alward, W.L., Searby, C.C., Patil, S.R., Bennet, S.R., Kanis, A.B., Gastier, J.M., Stone, E.M., Sheffield, V.C., 1998a. The forkhead transcription factor gene FKHL7 is responsible for glaucoma phenotypes which map to 6p25. Nature Genetics 19, 140-147.

Noden, D.M., 1991. Cell movements and control of patterned tissue assembly during craniofacial development. J Craniofac Genet Dev Biol 11, 192-213.

O'Rahilly, R., Muller, F., Meyer, D.B., 1980. The human vertebral column at the end of the embryonic period proper. 1. The column as a whole. J Anat 131, 565-575.

Oberlender, S.A., Tuan, R.S., 1994. Spatiotemporal profile of N-cadherin expression in the developing limb mesenchyme. Cell Adhes Commun 2, 521-537.

Oginuma, M., Niwa, Y., Chapman, D.L., Saga, Y., 2008. Mesp2 and Tbx6 cooperatively create periodic patterns coupled with the clock machinery during mouse somitogenesis. Development 135, 2555-2562.

Ogura, Y., Yabuki, S., Iida, A., Kou, I., Nakajima, M., Kano, H., Shiina, M., Kikuchi, S., Toyama, Y., Ogata, K., Nakamura, M., Matsumoto, M., Ikegawa, S., 2013. FOXC2

mutations in familial and sporadic spinal extradural arachnoid cyst. PLoS One 8, e80548.

Oh, C.D., Maity, S.N., Lu, J.F., Zhang, J., Liang, S., Coustry, F., de Crombrugghe, B., Yasuda, H., 2010. Identification of SOX9 interaction sites in the genome of chondrocytes. PLoS One 5, e10113.

Ohba, S., He, X., Hojo, H., McMahon, A.P., 2015. Distinct Transcriptional Programs Underlie Sox9 Regulation of the Mammalian Chondrocyte. Cell Rep 12, 229-243.

Oka, C., Nakano, T., Wakeham, A., de la Pompa, J.L., Mori, C., Sakai, T., Okazaki, S., Kawaichi, M., Shiota, K., Mak, T.W., Honjo, T., 1995. Disruption of the mouse RBP-J kappa gene results in early embryonic death. Development 121, 3291-3301.

Olsen, B.R., Reginato, A.M., Wang, W., 2000. Bone development. Annu Rev Cell Dev Biol 16, 191-220.

Ordahl, C., 1993. Myogenic lineages within the developing somite, in: Bernfield, M. (Ed.), Molecular basis of morphogenesis. Wiley-Liss, New York, pp. xvi, 276 p.

Ordahl, C.P., Le Douarin, N.M., 1992. Two myogenic lineages within the developing somite. Development 114, 339-353.

Ornitz, D.M., 2005. FGF signaling in the developing endochondral skeleton. Cytokine Growth Factor Rev 16, 205-213.

Ornitz, D.M., Marie, P.J., 2002. FGF signaling pathways in endochondral and intramembranous bone development and human genetic disease. Genes Dev 16, 1446-1465.

Ostrovsky, D., Sanger, J.W., Lash, J.W., 1988. Somitogenesis in the mouse embryo. Cell Differ 23, 17-25.

Ozeki, H., Shirai, S., Ikeda, K., Ogura, Y., 1999. Anomalies associated with Axenfeld-Rieger syndrome. Graefes Arch Clin Exp Ophthalmol 237, 730-734.

Palmeirim, I., Dubrulle, J., Henrique, D., Ish-Horowicz, D., Pourquie, O., 1998. Uncoupling segmentation and somitogenesis in the chick presomitic mesoderm. Dev Genet 23, 77-85.

Palmeirim, I., Henrique, D., Ish-Horowicz, D., Pourquie, O., 1997. Avian hairy gene expression identifies a molecular clock linked to vertebrate segmentation and somitogenesis. Cell 91, 639-648.

Park, S.J., Gadi, J., Cho, K.W., Kim, K.J., Kim, S.H., Jung, H.S., Lim, S.K., 2011. The forkhead transcription factor Foxc2 promotes osteoblastogenesis via up-regulation of integrin beta1 expression. Bone 49, 428-438.

Peinado, H., Ballestar, E., Esteller, M., Cano, A., 2004. Snail mediates E-cadherin repression by the recruitment of the Sin3A/histone deacetylase 1 (HDAC1)/HDAC2 complex. Mol Cell Biol 24, 306-319.

Petrova, T.V., Karpanen, T., Norrmen, C., Mellor, R., Tamakoshi, T., Finegold, D., Ferrell, R., Kerjaschki, D., Mortimer, P., Yla-Herttuala, S., Miura, N., Alitalo, K., 2004. Defective valves and abnormal mural cell recruitment underlie lymphatic vascular failure in lymphedema distichiasis. Nat Med 10, 974-981.

Pierrou, S., Hellqvist, M., Samuelsson, L., Enerback, S., Carlsson, P., 1994. Cloning and characterization of seven human forkhead proteins: binding site specificity and DNA bending. EMBO J 13, 5002-5012.

Pourquie, O., 2003. Vertebrate somitogenesis: a novel paradigm for animal segmentation? Int J Dev Biol 47, 597-603.

Pourquie, O., Coltey, M., Teillet, M.A., Ordahl, C., Le Douarin, N.M., 1993. Control of dorsoventral patterning of somitic derivatives by notochord and floor plate. Proc Natl Acad Sci U S A 90, 5242-5246.

Pourquie, O., Tam, P.P., 2001. A nomenclature for prospective somites and phases of cyclic gene expression in the presomitic mesoderm. Dev Cell 1, 619-620.

Radice, G.L., Rayburn, H., Matsunami, H., Knudsen, K.A., Takeichi, M., Hynes, R.O., 1997. Developmental defects in mouse embryos lacking N-cadherin. Dev Biol 181, 64-78.

Rawls, A., Fisher, R.E., 2009. The genetics and development of scoliosis, 1st ed. Springer, New York.

Rice, D.P., Rice, R., 2008. Locate, condense, differentiate, grow and confront: developmental mechanisms controlling intramembranous bone and suture formation and function. Front Oral Biol 12, 22-40.

Rice, R., Rice, D.P., Olsen, B.R., Thesleff, I., 2003. Progression of calvarial bone development requires Foxc1 regulation of Msx2 and Alx4. Dev Biol 262, 75-87.

Ridderstrale, M., Carlsson, E., Klannemark, M., Cederberg, A., Kosters, C., Tornqvist, H., Storgaard, H., Vaag, A., Enerback, S., Groop, L., 2002. FOXC2 mRNA Expression and a 5' untranslated region polymorphism of the gene are associated with insulin resistance. Diabetes 51, 3554-3560.

Rodrigo, I., Hill, R.E., Balling, R., Munsterberg, A., Imai, K., 2003. Pax1 and Pax9 activate Bapx1 to induce chondrogenic differentiation in the sclerotome. Development 130, 473-482.

Rosbotham, J.L., Brice, G.W., Child, A.H., Nunan, T.O., Mortimer, P.S., Burnand, K.G., 2000. Distichiasis-lymphoedema: clinical features, venous function and lymphoscintigraphy. Br J Dermatol 142, 148-152.

Roux, K.J., Kim, D.I., Raida, M., Burke, B., 2012. A promiscuous biotin ligase fusion protein identifies proximal and interacting proteins in mammalian cells. J Cell Biol 196, 801-810.

Saga, Y., 2007. Segmental border is defined by the key transcription factor Mesp2, by means of the suppression of Notch activity. Developmental dynamics : an official publication of the American Association of Anatomists 236, 1450-1455.

Saga, Y., Hata, N., Koseki, H., Taketo, M.M., 1997. Mesp2: a novel mouse gene expressed in the presegmented mesoderm and essential for segmentation initiation. Genes Dev 11, 1827-1839.

Saga, Y., Takahashi, Y., 2008. Mesp-family genes are required for segmental patterning and segmental border formation. Adv Exp Med Biol 638, 113-123.

Saga, Y., Takeda, H., 2001. The making of the somite: molecular events in vertebrate segmentation. Nat Rev Genet 2, 835-845.

Sakai, Y., Meno, C., Fujii, H., Nishino, J., Shiratori, H., Saijoh, Y., Rossant, J., Hamada, H., 2001. The retinoic acid-inactivating enzyme CYP26 is essential for establishing an uneven distribution of retinoic acid along the anterio-posterior axis within the mouse embryo. Genes Dev 15, 213-225.

Sargent, C., Bauer, J., Khalil, M., Filmore, P., Bernas, M., Witte, M., Pearson, M.P., Erickson, R.P., 2014. A five generation family with a novel mutation in FOXC2 and lymphedema worsening to hydrops in the youngest generation. Am J Med Genet A 164A, 2802-2807.

Sawada, A., Shinya, M., Jiang, Y.J., Kawakami, A., Kuroiwa, A., Takeda, H., 2001. Fgf/MAPK signalling is a crucial positional cue in somite boundary formation. Development 128, 4873-4880.

Schier, A.F., Neuhauss, S.C., Harvey, M., Malicki, J., Solnica-Krezel, L., Stainier, D.Y., Zwartkruis, F., Abdelilah, S., Stemple, D.L., Rangini, Z., Yang, H., Driever, W., 1996. Mutations affecting the development of the embryonic zebrafish brain. Development 123, 165-178.

Schipani, E., Kruse, K., Juppner, H., 1995. A constitutively active mutant PTH-PTHrP receptor in Jansen-type metaphyseal chondrodysplasia. Science 268, 98-100.

Schipani, E., Langman, C.B., Parfitt, A.M., Jensen, G.S., Kikuchi, S., Kooh, S.W., Cole, W.G., Juppner, H., 1996. Constitutively activated receptors for parathyroid hormone and parathyroid hormone-related peptide in Jansen's metaphyseal chondrodysplasia. N Engl J Med 335, 708-714.

Schipani, E., Lanske, B., Hunzelman, J., Luz, A., Kovacs, C.S., Lee, K., Pirro, A., Kronenberg, H.M., Juppner, H., 1997. Targeted expression of constitutively active receptors for parathyroid hormone and parathyroid hormone-related peptide delays endochondral bone formation and rescues mice that lack parathyroid hormone-related peptide. Proc Natl Acad Sci U S A 94, 13689-13694.

Schmid, T.M., Linsenmayer, T.F., 1985. Immunohistochemical localization of short chain cartilage collagen (type X) in avian tissues. J Cell Biol 100, 598-605.

Schoenwolf, G.C., Larsen, W.J., 2009. Larsen's human embryology, 4th ed. Churchill Livingstone/Elsevier, Philadelphia.

Schuster-Gossler, K., Harris, B., Johnson, K.R., Serth, J., Gossler, A., 2009. Notch signalling in the paraxial mesoderm is most sensitive to reduced Pofut1 levels during early mouse development. BMC Dev Biol 9, 6.

Seo, S., Kume, T., 2006. Forkhead transcription factors, Foxc1 and Foxc2, are required for the morphogenesis of the cardiac outflow tract. Dev Biol 296, 421-436.

Shields, M.B., Buckley, E., Klintworth, G.K., Thresher, R., 1985. Axenfeld-Rieger syndrome. A spectrum of developmental disorders. Surv Ophthalmol 29, 387-409.

Shifley, E.T., Cole, S.E., 2008. Lunatic fringe protein processing by proprotein convertases may contribute to the short protein half-life in the segmentation clock. Biochim Biophys Acta 1783, 2384-2390.

Shifley, E.T., Vanhorn, K.M., Perez-Balaguer, A., Franklin, J.D., Weinstein, M., Cole, S.E., 2008. Oscillatory lunatic fringe activity is crucial for segmentation of the anterior but not posterior skeleton. Development 135, 899-908.

Sholto-Douglas-Vernon, C., Bell, R., Brice, G., Mansour, S., Sarfarazi, M., Child, A.H., Smith, A., Mellor, R., Burnand, K., Mortimer, P., Jeffery, S., 2005. Lymphoedema-distichiasis and FOXC2: unreported mutations, de novo mutation estimate, families without coding mutations. Hum Genet 117, 238-242.

Siegenthaler, J.A., Choe, Y., Patterson, K.P., Hsieh, I., Li, D., Jaminet, S.C., Daneman, R., Kume, T., Huang, E.J., Pleasure, S.J., 2013. Foxc1 is required by pericytes during fetal brain angiogenesis. Biol Open 2, 647-659.

Sieger, D., Tautz, D., Gajewski, M., 2003. The role of Suppressor of Hairless in Notch mediated signalling during zebrafish somitogenesis. Mech Dev 120, 1083-1094.

Sirbu, I.O., Duester, G., 2006. Retinoic-acid signalling in node ectoderm and posterior neural plate directs left-right patterning of somitic mesoderm. Nat Cell Biol 8, 271-277.

Skarie, J.M., Link, B.A., 2009. FoxC1 is essential for vascular basement membrane integrity and hyaloid vessel morphogenesis. Invest Ophthalmol Vis Sci 50, 5026-5034.

Smits, P., Li, P., Mandel, J., Zhang, Z., Deng, J.M., Behringer, R.R., de Crombrugghe, B., Lefebvre, V., 2001. The transcription factors L-Sox5 and Sox6 are essential for cartilage formation. Dev Cell 1, 277-290.

Sock, E., Pagon, R.A., Keymolen, K., Lissens, W., Wegner, M., Scherer, G., 2003. Loss of DNA-dependent dimerization of the transcription factor SOX9 as a cause for campomelic dysplasia. Hum Mol Genet 12, 1439-1447.

Soegiarto, D.W., Kiachopoulos, S., Schipani, E., Juppner, H., Erben, R.G., Lanske, B., 2001. Partial rescue of PTH/PTHrP receptor knockout mice by targeted expression of the Jansen transgene. Endocrinology 142, 5303-5310.

St-Jacques, B., Hammerschmidt, M., McMahon, A.P., 1999. Indian hedgehog signaling regulates proliferation and differentiation of chondrocytes and is essential for bone formation. Genes Dev 13, 2072-2086.

Stadler, H.S., Higgins, K.M., Capecchi, M.R., 2001. Loss of Eph-receptor expression correlates with loss of cell adhesion and chondrogenic capacity in Hoxa13 mutant limbs. Development 128, 4177-4188.

Stauber, M., Sachidanandan, C., Morgenstern, C., Ish-Horowicz, D., 2009. Differential axial requirements for lunatic fringe and Hes7 transcription during mouse somitogenesis. PLoS One 4, e7996.

Stickens, D., Behonick, D.J., Ortega, N., Heyer, B., Hartenstein, B., Yu, Y., Fosang, A.J., Schorpp-Kistner, M., Angel, P., Werb, Z., 2004. Altered endochondral bone development in matrix metalloproteinase 13-deficient mice. Development 131, 5883-5895.

Strungaru, M.H., Dinu, I., Walter, M.A., 2007. Genotype-phenotype correlations in Axenfeld-Rieger malformation and glaucoma patients with FOXC1 and PITX2 mutations. Invest Ophthalmol Vis Sci 48, 228-237.

Sun, J., Ishii, M., Ting, M.C., Maxson, R., 2013. Foxc1 controls the growth of the murine frontal bone rudiment by direct regulation of a Bmp response threshold of Msx2. Development 140, 1034-1044.

Suzuki, T., Takahashi, K., Kuwahara, S., Wada, Y., Abe, T., Tamai, M., 2001. A novel (Pro79Thr) mutation in the FKHL7 gene in a Japanese family with Axenfeld-Rieger syndrome. Am J Ophthalmol 132, 572-575.

Swiatek, P.J., Lindsell, C.E., del Amo, F.F., Weinmaster, G., Gridley, T., 1994. Notch1 is essential for postimplantation development in mice. Genes Dev 8, 707-719.

Takahashi, J., Ohbayashi, A., Oginuma, M., Saito, D., Mochizuki, A., Saga, Y., Takada, S., 2010. Analysis of Ripply1/2-deficient mouse embryos reveals a mechanism underlying the rostro-caudal patterning within a somite. Dev Biol 342, 134-145.

Takahashi, Y., Koizumi, K., Takagi, A., Kitajima, S., Inoue, T., Koseki, H., Saga, Y., 2000. Mesp2 initiates somite segmentation through the Notch signalling pathway. Nat Genet 25, 390-396.

Takemoto, M., He, L., Norlin, J., Patrakka, J., Xiao, Z., Petrova, T., Bondjers, C., Asp, J., Wallgard, E., Sun, Y., Samuelsson, T., Mostad, P., Lundin, S., Miura, N., Sado, Y., Alitalo, K., Quaggin, S.E., Tryggvason, K., Betsholtz, C., 2006. Large-scale identification of genes implicated in kidney glomerulus development and function. EMBO J 25, 1160-1174.

Tam, P.P., Tan, S.S., 1992. The somitogenetic potential of cells in the primitive streak and the tail bud of the organogenesis-stage mouse embryo. Development 115, 703-715.

Tam, P.P., Trainor, P.A., 1994. Specification and segmentation of the paraxial mesoderm. Anat Embryol (Berl) 189, 275-305.

Tavella, S., Raffo, P., Tacchetti, C., Cancedda, R., Castagnola, P., 1994. N-CAM and N-cadherin expression during in vitro chondrogenesis. Exp Cell Res 215, 354-362.

Tavian, D., Missaglia, S., Maltese, P.E., Michelini, S., Fiorentino, A., Ricci, M., Serrani, R., Walter, M.A., Bertelli, M., 2016. FOXC2 disease-mutations identified in lymphedema-distichiasis patients cause both loss and gain of protein function. Oncotarget 7, 54228-54239.

Therapontos, C., Vargesson, N., 2010. Zebrafish notch signalling pathway mutants exhibit trunk vessel patterning anomalies that are secondary to somite misregulation. Dev Dyn 239, 2761-2768.

Thisse, C., and Thisse, B. , 2005. High Throughput Expression Analysis of ZF-Models Consortium Clones. . ZFIN Direct Data Submission.

Thorogood, P.V., Hinchliffe, J.R., 1975. An analysis of the condensation process during chondrogenesis in the embryonic chick hind limb. J Embryol Exp Morphol 33, 581-606.

Topczewska, J.M., Topczewski, J., Shostak, A., Kume, T., Solnica-Krezel, L., Hogan, B.L., 2001a. The winged helix transcription factor Foxc1a is essential for somitogenesis in zebrafish. Genes Dev 15, 2483-2493.

Topczewska, J.M., Topczewski, J., Solnica-Krezel, L., Hogan, B.L., 2001b. Sequence and expression of zebrafish foxc1a and foxc1b, encoding conserved forkhead/winged helix transcription factors. Mech Dev 100, 343-347.

Tumer, Z., Bach-Holm, D., 2009. Axenfeld-Rieger syndrome and spectrum of PITX2 and FOXC1 mutations. Eur J Hum Genet 17, 1527-1539.

van Dongen, M.J., Cederberg, A., Carlsson, P., Enerback, S., Wikstrom, M., 2000. Solution structure and dynamics of the DNA-binding domain of the adipocyte-transcription factor FREAC-11. J Mol Biol 296, 351-359.

van Eeden, F.J., Granato, M., Schach, U., Brand, M., Furutani-Seiki, M., Haffter, P., Hammerschmidt, M., Heisenberg, C.P., Jiang, Y.J., Kane, D.A., Kelsh, R.N., Mullins, M.C., Odenthal, J., Warga, R.M., Allende, M.L., Weinberg, E.S., Nusslein-Volhard, C., 1996. Mutations affecting somite formation and patterning in the zebrafish, Danio rerio. Development 123, 153-164.

van Steensel, M.A., Damstra, R.J., Heitink, M.V., Bladergroen, R.S., Veraart, J., Steijlen, P.M., van Geel, M., 2009. Novel missense mutations in the FOXC2 gene alter transcriptional activity. Hum Mutat 30, E1002-1009.

Vastenhouw, N.L., Schier, A.F., 2012. Bivalent histone modifications in early embryogenesis. Curr Opin Cell Biol 24, 374-386.

Vega, R.B., Matsuda, K., Oh, J., Barbosa, A.C., Yang, X., Meadows, E., McAnally, J., Pomajzl, C., Shelton, J.M., Richardson, J.A., Karsenty, G., Olson, E.N., 2004. Histone deacetylase 4 controls chondrocyte hypertrophy during skeletogenesis. Cell 119, 555-566.

Veldman, M.B., Lin, S., 2012. Etsrp/Etv2 is directly regulated by Foxc1a/b in the zebrafish angioblast. Circ Res 110, 220-229.

Vermot, J., Pourquie, O., 2005. Retinoic acid coordinates somitogenesis and left-right patterning in vertebrate embryos. Nature 435, 215-220.

Vortkamp, A., Lee, K., Lanske, B., Segre, G.V., Kronenberg, H.M., Tabin, C.J., 1996. Regulation of rate of cartilage differentiation by Indian hedgehog and PTH-related protein. Science 273, 613-622.

Wada, N., Kimura, I., Tanaka, H., Ide, H., Nohno, T., 1998. Glycosylphosphatidylinositol-anchored cell surface proteins regulate position-specific cell affinity in the limb bud. Dev Biol 202, 244-252.

Wagner, T., Wirth, J., Meyer, J., Zabel, B., Held, M., Zimmer, J., Pasantes, J., Bricarelli, F.D., Keutel, J., Hustert, E., Wolf, U., Tommerup, N., Schempp, W., Scherer, G., 1994. Autosomal sex reversal and campomelic dysplasia are caused by mutations in and around the SRY-related gene SOX9. Cell 79, 1111-1120.

Wahl, M.B., Deng, C., Lewandoski, M., Pourquie, O., 2007. FGF signaling acts upstream of the NOTCH and WNT signaling pathways to control segmentation clock oscillations in mouse somitogenesis. Development 134, 4033-4041.

Wang, W.G., Lou, S.Q., Ju, X.D., Xia, K., Xia, J.H., 2003. In vitro chondrogenesis of human bone marrow-derived mesenchymal progenitor cells in monolayer culture: activation by transfection with TGF-beta2. Tissue Cell 35, 69-77.

Weigelt, J., Climent, I., Dahlman-Wright, K., Wikstrom, M., 2001. Solution structure of the DNA binding domain of the human forkhead transcription factor AFX (FOXO4). Biochemistry 40, 5861-5869.

Weir, E.C., Philbrick, W.M., Amling, M., Neff, L.A., Baron, R., Broadus, A.E., 1996. Targeted overexpression of parathyroid hormone-related peptide in chondrocytes causes chondrodysplasia and delayed endochondral bone formation. Proc Natl Acad Sci U S A 93, 10240-10245.

Whittock, N.V., Sparrow, D.B., Wouters, M.A., Sillence, D., Ellard, S., Dunwoodie, S.L., Turnpenny, P.D., 2004. Mutated MESP2 causes spondylocostal dysostosis in humans. American journal of human genetics 74, 1249-1254.

Winnier, G.E., Hargett, L., Hogan, B.L., 1997. The winged helix transcription factor MFH1 is required for proliferation and patterning of paraxial mesoderm in the mouse embryo. Genes Dev 11, 926-940.

Winnier, G.E., Kume, T., Deng, K., Rogers, R., Bundy, J., Raines, C., Walter, M.A., Hogan, B.L., Conway, S.J., 1999. Roles for the winged helix transcription factors MF1 and MFH1 in cardiovascular development revealed by nonallelic noncomplementation of null alleles. Dev Biol 213, 418-431.

Wood, A., Thorogood, P., 1994. Patterns of cell behaviour underlying somitogenesis and notochord formation in intact vertebrate embryos. Dev Dyn 201, 151-167.

Yabe, T., Hoshijima, K., Yamamoto, T., Takada, S., 2016. Quadruple zebrafish mutant reveals different roles of Mesp genes in somite segmentation between mouse and zebrafish. Development 143, 2842-2852.

Yagi, T., Tokunaga, T., Furuta, Y., Nada, S., Yoshida, M., Tsukada, T., Saga, Y., Takeda, N., Ikawa, Y., Aizawa, S., 1993. A novel ES cell line, TT2, with high germline-differentiating potency. Anal Biochem 214, 70-76.

Yang, L., Tsang, K.Y., Tang, H.C., Chan, D., Cheah, K.S., 2014. Hypertrophic chondrocytes can become osteoblasts and osteocytes in endochondral bone formation. Proc Natl Acad Sci U S A 111, 12097-12102.

Yasuhiko, Y., Haraguchi, S., Kitajima, S., Takahashi, Y., Kanno, J., Saga, Y., 2006. Tbx6-mediated Notch signaling controls somite-specific Mesp2 expression. Proc Natl Acad Sci U S A 103, 3651-3656.

Yoon, B.S., Lyons, K.M., 2004. Multiple functions of BMPs in chondrogenesis. J Cell Biochem 93, 93-103.

Yoshida, M., Hata, K., Takashima, R., Ono, K., Nakamura, E., Takahata, Y., Murakami, T., Iseki, S., Takano-Yamamoto, T., Nishimura, R., Yoneda, T., 2015. The transcription factor Foxc1 is necessary for Ihh-Gli2-regulated endochondral ossification. Nat Commun 6, 6653.

Yu, K., Xu, J., Liu, Z., Sosic, D., Shao, J., Olson, E.N., Towler, D.A., Ornitz, D.M., 2003. Conditional inactivation of FGF receptor 2 reveals an essential role for FGF signaling

in the regulation of osteoblast function and bone growth. Development 130, 3063-3074.

Yu, Y., Al-Mansoori, L., Opas, M., 2015. Optimized osteogenic differentiation protocol from R1 mouse embryonic stem cells in vitro. Differentiation 89, 1-10.

Zhao, W., Ajima, R., Ninomiya, Y., Saga, Y., 2015. Segmental border is defined by Ripply2-mediated Tbx6 repression independent of Mesp2. Dev Biol 400, 105-117.

Zhu, L.L., Lv, Y.N., Chen, H.D., Gao, X.H., 2014. A Chinese pedigree of lymphoedema-distichiasis syndrome with a novel mutation in the FOXC2 gene. Clin Exp Dermatol 39, 731-733.